DESIGN AND PERFORMANCE EVALUATION OF 2D LFMCW FDA

A THESIS SUBMITTED TO
THE GRADUATE SCHOOL OF NATURAL AND APPLIED SCIENCES
OF
MIDDLE EAST TECHNICAL UNIVERSITY

BY

SAVAŞ KARADAĞ

IN PARTIAL FULFILLMENT OF THE REQUIREMENTS
FOR
THE DEGREE OF DOCTOR OF PHILOSOPHY
IN
ELECTRICAL AND ELECTRONIC ENGINEERING

SEPTEMBER 2021

Approval of the thesis:

DESIGN AND PERFORMANCE EVALUATION OF 2D LFMCW FDA
submitted by **SAVAŞ KARADAĞ** in partial fulfillment of the requirements for the degree of **Doctor of Philosophy** i**n Electrical and Electronic Engineering, Middle East Technical University** by,

Prof. Dr. Halil Kalıpçılar
Dean, Graduate School of **Natural and Applied Sciences** _____

Prof. Dr. İlkay Ulusoy
Head of the Department, **Electrical and Electronic Eng.** _____

Prof. Dr. Şimşek Demir
Supervisor, **Electrical and Electronic Eng. Dept.** _____

Examining Committee Members:

Prof. Dr. Seyit Sencer Koç
Electrical and Electronic Engineering, METU _____

Prof. Dr. Şimşek Demir
Electrical and Electronic Engineering, METU _____

Prof. Dr. Gönül Turhan Sayan
Electrical and Electronic Engineering, METU _____

Prof. Dr. Asım Egemen Yılmaz
Electrical and Electronic Engineering, Ankara University _____

Prof. Dr. Vakur B. Ertürk
Electrical and Electronic Engineering, Bilkent University _____

Date: 07.09.2021

I hereby declare that all information in this document has been obtained and presented in accordance with academic rules and ethical conduct. I also declare that, as required by these rules and conduct, I have fully cited and referenced all material and results that are not original to this work.

Name, Last name : Savaş Karadağ

Signature :

ABSTRACT

DESIGN AND PERFORMANCE EVALUATION OF 2D LFMCW FDA

Karadağ, Savaş
Doctor of Philosophy, Electrical and Electronic Engineering
Supervisor : Prof. Dr. Şimşek Demir

September 2021, 171 pages

Waveform diversity is a highly desired property for radars because of its numerous benefits. Frequency diversity is one type of the waveform diversity. Total radiation pattern of transmitting antenna elements that are operating at slightly different center frequencies has peaks and nulls depending on the summation of the radiated fields, which can be constructive or destructive with respect to location and time. LFM chirp fed antenna elements with increasing true time delays will give rise to frequency diversity, thus, self-scanning beam patterns. This is named as LFMCW based FDA in the literature.

In this thesis, a direction finding method with LFMCW based linear FDA is presented and evaluated. Furthermore, comparison with a proven MIMO example that focuses on advantages of spatially modulated array takes place. It is shown in this study that one can obtain comparable performance by using much simpler LFMCW–FDA implementation than state of the art MIMO implementations which are relatively more complex in structure.

Waveform diversity properties and application methods of LFMCW-FDA are both analytically and experimentally proven for radar implementation by [1]–[5]. All of them utilized the linear array until now. In this study, a novel implementation with a

planar antenna array is introduced. Migration to planar array makes 3D scanning possible with this technic. The proposed structure is evaluated by simulations of a realistic radar example. Finally, the target RCS characteristic of the planar array is investigated and compared with the equivalent PA radar.

Keywords: Frequency Diverse Array, Phased Array, LFMCW, Radar

Cross Section.

ÖZ

İKİ BOYUTLU DOĞRUSAL KİPLEMELİ AYRIK FREKANS ANTEN DİZİSİ TASARIMI VE PERFORMANS DEĞERLENDİRİLMESİ

Karadağ, Savaş
Doktora, Elektrik ve Elektronik Mühendisliği
Tez Yöneticisi: Prof. Dr. Şimşek Demir

Eylül 2021, 171 sayfa

Dalga şekli çeşitlendirilmesi birçok faydası sebebiyle radar uygulamalarında sık sık istenen bir tekniktir. Dalga çeşitlendirme tekniklerinden biri de frekans çeşitlendirme yöntemidir. Merkez frekansları çok hafif farklı olan sinyallerin kullanıldığı antenlerin oluşturduğu dizilerinin toplam ışıma örüntüsünde gönderilen sinyallerin toplam girişim fazlarına bağlı olarak tepeler ve vadiler oluşur. Dizi antenlerinin arasında frekans çeşitliliği yaratabilmek için farklı teknikler kullanılabilir. Doğrusal frekans modülasyonuna sahip işaret, gerçek zamanlı gecikme yolları vasıtasıyla bir anten dizisi beslendiğinde elemanlar arası frekans farkı, dolayısıyla kendiliğinden uzayı tarayan hüzmeler, elde edilebilir. Bu yöntem literatürde doğrusal frekans modülasyonlu devamlı dalgaya dayalı ayrık frekans dizisi (LFMCW-FDA) olarak adlandırılır.

Bu çalışma kapsamında LFMCW-FDA mantığıyla kurulmuş doğrusal anten dizisi kullanılarak yeni bir yön bulma (DF) metodu sunulmakta ve değerlendirilmektedir. Bunun da ötesinde, literatürdeki uzaysal modülasyonun avantajlarına odaklanılmaktatır; işlevselliği kanıtlanmış olan çoklu giriş-çoklu çıkış anten dizisi (MIMO) örneği ile karşılaştırmalar yer almaktadır. Bu çalışmada uygulaması çok daha kolay olan LFMCW-FDA tekniğinden, en gelişmiş yöntemlerden olan MIMO uygulamasıyla denk performansa erişilebileceği gösterilmiştir.

LFMCW-FDA yöntemi hem analitik olarak hem deneysel olarak radar uygulamaları için kanıtlanmış bir tekniktir [1]–[5]. Şimdiye kadar bu örneklerin her biri doğrusal anten dizilerinden faydalanmaktadır. Bu çalışmalarda gösterilen avantajlar uygulama kolaylığı, çoklu yansıma koşulları altında etkinliği ve hedef kesit alanın daha az dalgalanmasıdır. Literatüre başka bir katkı olarak, yeni bir LFMCW-FDA yönteminden faydalanan düzlemsel anten dizisi sunulmaktadır. Bu gelişme ile üç boyutlu tarama mümkün kılınmaktadır. Bu yeni yöntem gerçekçi radar senaryoları ile değerlendirilmektedir. Son olarak bu radar kullanılarak hedef radar kesit alanının karakteristik özellikleri araştırılmış ve eş değer nitelikteki faz dizili radarla elde edilmiş değerler ile karşılaştırılmıştır.

Anahtar Kelimeler: Ayrık Frekanslı Dizi, Faz Dizili Anten, LFMCW, Radar Kesit Alanı.

To my brother Abdullah Sapmaz

ACKNOWLEDGMENTS

I would like to express my gratitude to my advisors Prof. Simsek Demir in the first place for their guidance, support and encouragement during the course of my thesis work.

In addition, I am thankful to members of my thesis monitoring committee Prof. Sencer Koç and Prof. Dr. Asım Egemen Yılmaz as well as to Prof. Altunkan Hızal and Dr. Çağrı Çetintepe for their fruitful comments and discussions during my committees, and for guiding me throughout my research.

I would never be more grateful to my dear wife Baran, for her endless encouragement throughout this study. It would not be possible to continue without her everlasting love and support. Her name should be on this thesis as much as mine. Indeed, I also need to thank to remaining family members/cats Şinasi, Şemsi and Behlül for theır companionship.

I would like to express my deepest gratitude to my parents and my brother especially for their endless support during my whole education that makes possible to pursue this Ph.D.

My sincere thanks go to all my friends who made this journey more joyful. As a sign of appreciation, I would like to name them on this page: Ali Özgün, Alper Özkök, Arsen Turhaner, Aslı Yıldırım, Berk Başar, Çağrı Akkaya, Damla Ceylan, Damla Alptekin, Delal Bulut, Diloş Yıldırım, Dilek and Dilay Kafes, Emre Başpınar, Emre Kafes, Enis Kobal, Eylem Karadağ, Ferhat Aydoğan, Feza Mutlu, İlker Comart, Linda, Merve Boysan, Muhammet Özgür, Murat Akpınar, Özgür Bulut, Selmin Eren, Serpil Albay, Semih Uyar, Sezgi Aytekin, Zilan Yıldırım and all Yıldırım family.

TABLE OF CONTENTS

LIST OF TABLES

TABLES

LIST OF FIGURES

LIST OF ABBREVIATIONS

ABBREVIATIONS

AM	Amplitude Modulation
AoA	Angle of Arrival
CDS	Cumulative Detection Step
CTI	Coherent Integration Time
DBF	Digital Beam Forming
DCR	Direct Conversion Receiver
DDS	Direct Digital Synthesizer
ESA	Electronically Steered Array
FBW	Frequency Bandwidth
FDA	Frequency Diverse Array
FD	Frequency Domain
FM	Frequency Modulation
FRT	Frame Time
FT	Fourier Transform
LFM	Linear Frequency Modulation
LFMCW	Linear Frequency Modulated Continuous Wave
LO	Local Oscillator
LPF	Low-pass Filter
PA	Phased Array

PM	Phase Modulation
PRI	Pulse Repetition Interval
RX	Receiver
RCS	Radar Cross-Section
SC	Spectral Component
SNR	Signal to Noise Ratio
SW I	Swerling Type One
TD	Time Domain
TTD	True Time Delay
TX	Transmitter
WA	Wavelength Array
WDA	Waveform Diverse Array

CHAPTER 1

INTRODUCTION

There are various types of waveform diversity which achieve electrical steering of the radiation pattern [6], [7]. Phase array is one of the most common type that uses phase differences between antenna excitation signal to control the beam steering. Spatial diversity is another type that uses different propagation paths by using different transmitting or receiving antennas. It can be, for example, different base stations for mobile communication, or, electrically small displacement of the array elements. When the same signal transmission is repeated again at different times to get rid of the noise and decrease the bit error and false alarm probability, it is named as time diversity.

Another type of diversity is frequency diversity which is the core of this study. In this diversity, each transmitting antenna element operates at a different frequency, therefore, overall beam pattern changes with time and the position of the observer because signals with slightly different center frequencies can be destructive or constructive with respect to the location and the time. Scanning behavior of the FDA is different from the conventional phased arrays. Whereas beam is controlled by phase shifters in PA, radiation pattern changes with respect to time in FDA. Phased arrays can be directed to stable angle and they illuminate this angular section independent from the distance. On the other hand, maxima on the FDA radiation patterns depend on also the distance. Therefore, it is possible to focus on a specific point without wasting the energy to illuminate the whole angular section. Moreover, that is advantageous to securely communicate with the ally and to increase the efficiency of wireless power transmission power transmission [8], [9]. In addition, its S-shaped range-angle dependent beam patterns could be useful for suppressing

the interferences from various locations [10]. Focusing on a single location makes target tracking with FDA more robust, because interferences due to other targets along same angle could be suppressed by virtue of the S-shaped patterns.

Continuous scanning of the field of view (FOV) is one of the distinctive characteristics of FDA [11]. FDA scans the whole space throughout only one scanning period, $1/\Delta f$. However, conventional PA radars need to be controlled by phase shifters that decelerates the space scanning. Implementation of the faster scanning is possible with the FDA that is another advantage. Because target displacement would be less during the target detection process [12].

A basic implementation of the FDA is to use different signal sources for each transmitting element with different center frequencies. Therefore, the phase shifters, which cost a lot and bring implementation complexity, become redundant in FDA. As a result of that, realization of FDA is cost-effective and undemanding. A value added by FDA is illustrated in target RCS characteristics, RCS fluctuation with FDA is smoother than the obtained with the conventional PAs [1]. Its immunity against multipath signals is another benefit of FDA usage [2]. On the other hand, this rather novel topic have different challenges from the conventional methods. Because of the range-angle ambiguity, space time adaptive processing (STAP) is necessary in this application. There are many studies, which focus on the solution for the range-angle ambiguity. Beam scanning property is controlled by radar parameters such as frequency offset types and amount, which is still hot topic for FDA researchers.

A classical implementation of the FDA is to use different signal sources for each transmitting element with different center frequencies. Another possibility is to build separate up-converter circuits for each transmitting antenna by using a different IF signal to obtain the frequency diversity in the RF output signal [13], [14] and [11]. These two options are widely used methods to create frequency diversity in the transmitter. Need of many circuit components for separate transmitter for each element and, so, complexities in the implementation could be drawbacks even though it is less complex than the conventional PAs. A simpler and reliable method

of realization was proposed by [11] in order to get rid of need for the separate transmitter before each antenna element. This approach has been investigated by different researchers with respect to various aspects. By using single LFM chirp on each antenna with different true time delays, time diversity among transmitted signals is created that causes the frequency diversity because frequency of the chirp is changing with respect to the time linearly. This method is called as LFMCW based FDA, whereas other one will be called as classical FDA throughout this report. Some valuable studies in the literature have already shown that the LFMCW based FDA can be effectively usable and has many advantages such as low-cost implementation, superiorities in the presence of multipath effects over PA and performance in terms of the target RCS characteristic, etc. [3]. However, there are still open points that can be studied to make the LFMCW based FDA state of art technology.

In this study, DF method for LFMCW based linear FDA is reviewed, discussed and evaluated. Angle resolution is decided in time domain, whereas range is determined in frequency domain. Abilities and limitations of the proposed method will be discussed and explained with numerical examples. This DF method is based on the idea that is proposed in [5] by Dr. Eker. To extend the scope of his study, impact of instantaneous FDA bandwidth over aperture on the range resolution is derived explicitly and taken into consideration during DF examples. Furthermore, radar images in the presence of 5 targets are presented, that is obtained by taking FFT of the time domain samples within a sliding window with weighting coefficients derived from $sinc$ function's main lobe. Therefore, performance of the LFMCW-FDA radar is shown by numerical examples that confirms the aforementioned resolution approaches. Furthermore, it is shown that utilization of LFM pulses instead of CW signals could be a remedy for the range-angle ambiguity in FDA radars.

FDAs are capable to scan automatically the field of view (FOV), this means that FDA has inherently spatially modulated beam steering behavior. Studies on spatial modulation in radars show that they can resolve multiple targets better that the radars with the fixed radiation pattern during pulse period [38, 39]. Similarities between the

spatially modulated MIMO array and LFMCW-FDA are investigated in this study. It is revealed that the proposed MIMO, which utilizes waveform diversity, is equivalent to the LFM based FDA, when MIMO uses LFM radar signal with linear spatial modulation schemes. The advantage of resolving multiple targets is presented with numerical examples in this thesis. Range resolution is mainly determined by the bandwidth of the LFM pulse and the increments in true time delays, whereas angle resolution is determined by array size and excitation type. Radar performance is evaluated in the presence of 5 targets located on X shape. Numerical examples prove that LFMCW-FDA achieves the objective of distinguishing different targets within single pulse.

There are many studies on FDA in the literature, that have been analytically and experimentally proved the promising performance of linear antenna array based on LFMCW-FDA, [1], [2], [4], [11]. With linear array, only 2D scan is possible. Throughout this study, we introduce and evaluate a novel planar array that makes 3D scanning possible. Although, there are a few examples of 2D FDA in the literature, first example of 2D LFMCW FDA is given here as a main contribution to FDA literature. Critical design steps for the planar array are presented, in order to have properly scanning behavior. It is possible to scan whole space, which is defined by $\theta \sim 38^o \rightarrow 143^o$ and $\phi \sim 30^o \rightarrow 134^o$ within only a single LFM chirp, that is swept in 1ms for the given example in this study. That is illustrated by the coverage diagrams as well. The scanning behavior of the novel array is similar to raster scan. Migration of the advantages of the LFMCW-FDA from linear array to 2D array would make this method more comprehensive and closer to be state of art technology. Moreover, fast scanning feature of the proposed array is another efficacious yield when it is used in radar applications. Therefore, radar implementation with the proposed 2D array deployed as a transmitter is given in Chapter 4. Angle of arrival (AoA) is determined by phased array receiver in the given structure, while range of the target is determined from frequency domain. By using 8x5 elements array, 1.5m range resolution is obtained. Degradation in range resolution is observed due to the frequency diversity over aperture that makes

spectral components of reflected signal spread over wider frequency bandwidth than the classical LFM radars. On the other hand, there many advantages to use FDA, such as fast and self-scanning beam pattern, immunity to multipath, smoother target RCS with respect to incidence angle and low cost implementation of the LFMCW-FDA. Radar example shows benefits of the proposed system by comparing it with the equivalent phased array radar. Even though SNR is lower in FDA, fast detection with FDA stands out. That could be an advantage for short range high SNR radar applications. The target displacement during detection in LFMCW based FDA would be significantly smaller than the state of art competitor.

Target radar cross-section (RCS) is defined by that how much of the incident is reflected from it. Target RCS characteristic is related with the used radar system. Due to complexity of a target shape, surface and material, summation of the scattered fields from the complex surface of the target can be destructive or constructive with different angle of incidence. In other words, as the target rotates around its center, the total reflected field may fluctuate rapidly. It may be even zero for certain angles, that makes the detection of the target impossible. The linear FDA is already shown to have some superiorities over the state of art PA in [1], [2] in terms of multipath characteristics and the target RCS characteristics.

In this thesis, target RCS characteristic is investigated for the novel 2D LFMCW-FDA. In order to determine RCS, reflected field from a group of the point scatterer is assumed to be captured by an omni-directional antenna at origin. Dumbbell, which is composed of a pair of scatterers, is considered as target. So, overall RCS is investigated and illustrated for different bandwidth usages. As the bandwidth of chirp increases, smoother RCS change with respect to aspect angle is obtained. That shows increasing frequency diversity provides less zero RCS angle and smoother variation with the 2D LFMCW FDA.

1.1 Literature Review

In this part of thesis, the literature of FDA concept is reviewed. Due to high volume of research on this topic, it is not possible to include every valuable work to this section. The main intention to summarize the important accomplishments related to this work in this section. Furthermore, a capability of reshaping the radiation pattern and changing direction of maximum radiation direction is strongly desired for great numbers of applications such as radars, the communication [5].

FDA is proposed in [14] for the first time. Two patents are obtained by the authors later based on the FDA [15], [16] that contain FDA design using multiple waveform generator and a single waveform generator respectively. The array structure in [14] with separate frequency, amplitude and phase control on each spatial channel is illustrated in the Figure 1.1. Range dependent pattern due to slightly different center frequency at each antenna element takes place with classical phased array control blocks for amplitude and phase. Aperture tapering and beam steering are done by amplitude weighting and phase shifters respectively. It is claimed that the novel FDA concept provide resistance to multipath, while it permits more flexible beam formations. Moreover, each element can be considered as different spatial elements of the synthetic aperture radar (SAR). Because, each channel provides sufficient bandwidth transmission so that a requirement for long integration times in small apertures can be overcome. This work is expanded in [17] with implementations of the various scenarios. Therefore, range dependent behavior of the FDA is proved by different experiments.

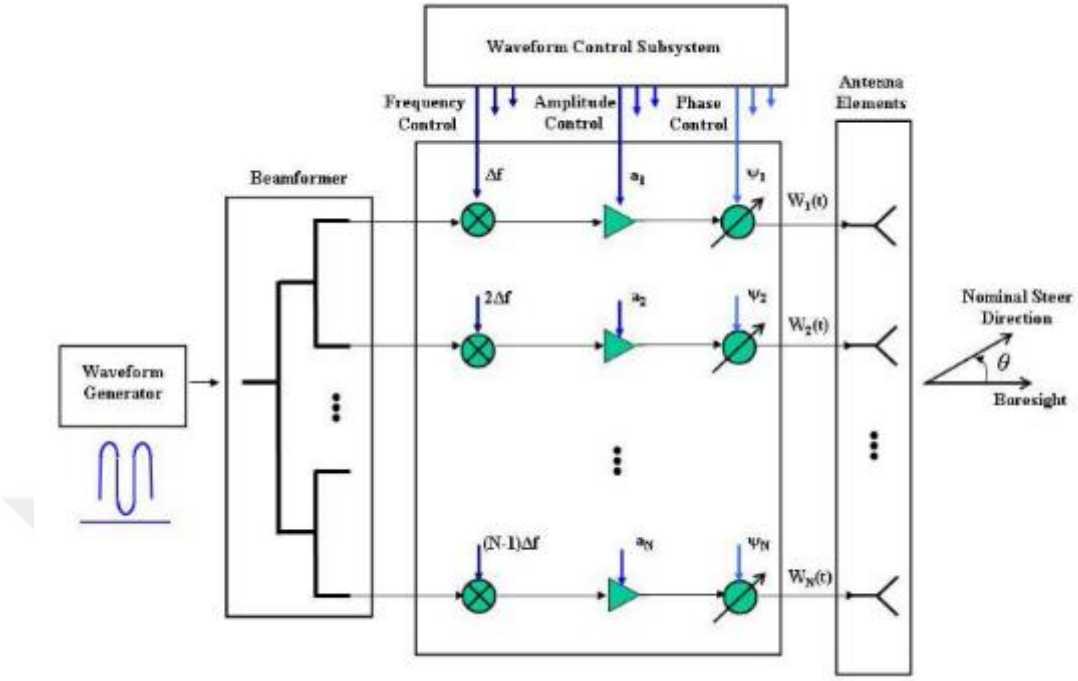

Figure 1.1. Hardware Implementation of the FDA in [14]

Another implementation is introduced in [11], that is comprised of much simpler circuitry i.e. two signal sources, multiple mixers and interconnections. Continuous scanning in range and angle is illustrated without deploying phase shifters. This study focuses on discovering the details of periodicity in time, range and angle by using a binominal distribution array. Figure 1.2 (a) shows the FDA hardware, that is equivalent to conventional systems when frequency diversity step (Δf) is zero. Same figure also illustrates the radiation pattern at different time instants. Periodicity in range, angle and time graphs are given for each variable, while other two stay constant.

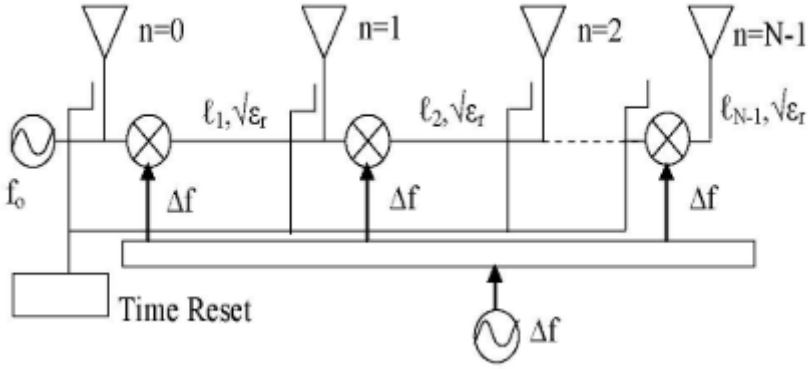

(a) Hardware

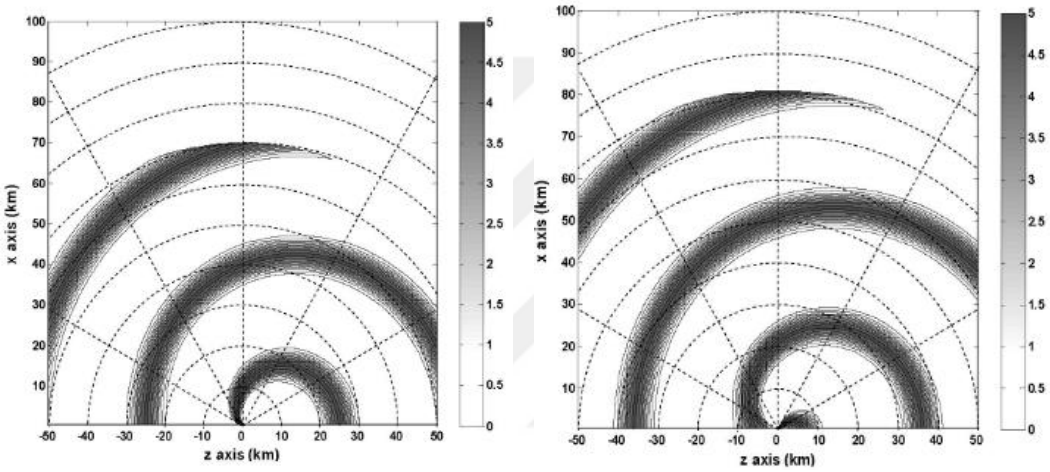

(b) $t = 233\mu s$ (c) $t = 270\mu s$

Figure 1.2. Implementation of the FDA in [11], (a) Hardware, (b) & (c) Range dependent radiation patterns at different times

Cross-range resolution can be improved by widening the angular data collection range in synthetic aperture radars (SAR) [18]. On the other, it requires longer measurement duration and it may cause *target smearing* for moving targets and not well controlled platform movements. The authors of [18]–[20] propose FDA based SAR setup to exploit the bended radiation pattern to focus on the FOV. The Figure 1.3 shows the pattern lines and displacement of the SAR during data collection. By using FDA, they show that within same distance of data acquisition, better resolution can be obtained by FDA. Furthermore, dynamic frequency shift selection is proposed to optimize the data collection within same length. Beside many other benefits, LFM usage is regarded as range resolution improving factor as pulse compression method

with match filtering on the receiver side. Moreover, planar FDA SAR, which is capable to accomplish strip-mapping, is introduced with numerical examples in [20].

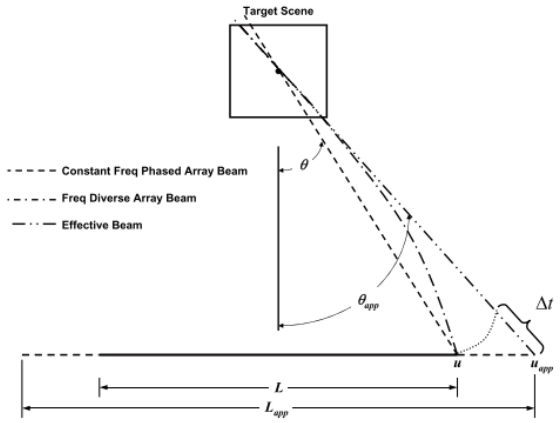

Figure 1.3. Bended and straight radiation lines of FDA and PA-SAR in [18]–[20]

The authors of [21], [22] present the full wave simulations to show beam patterns of FDA. They show that the scanning period T_{scan}, which is periodicity in time, is $\frac{1}{\Delta f}$ where Δf is frequency diversity step. The expended studies are reported in [23] as a dissertation later. Pulsed radar implementation is discussed by steering the beam to fixed angle rather than continuous scanning. The authors introduce a relevant FDA beamformer to control the envelope of each signal with rectangular pulse. Therefore, transmitted signal becomes zero for any other angle than the angular section that coincides with pulse timings. It is proposed that selecting pulse repetition interval (PRI) same as T_{scan} provide beam steering to the given angle. Figure 1.4 illustrates the PRI , sketch of pulse with element frequencies and resulting simulated radiation pattern of the pulsed FDA.

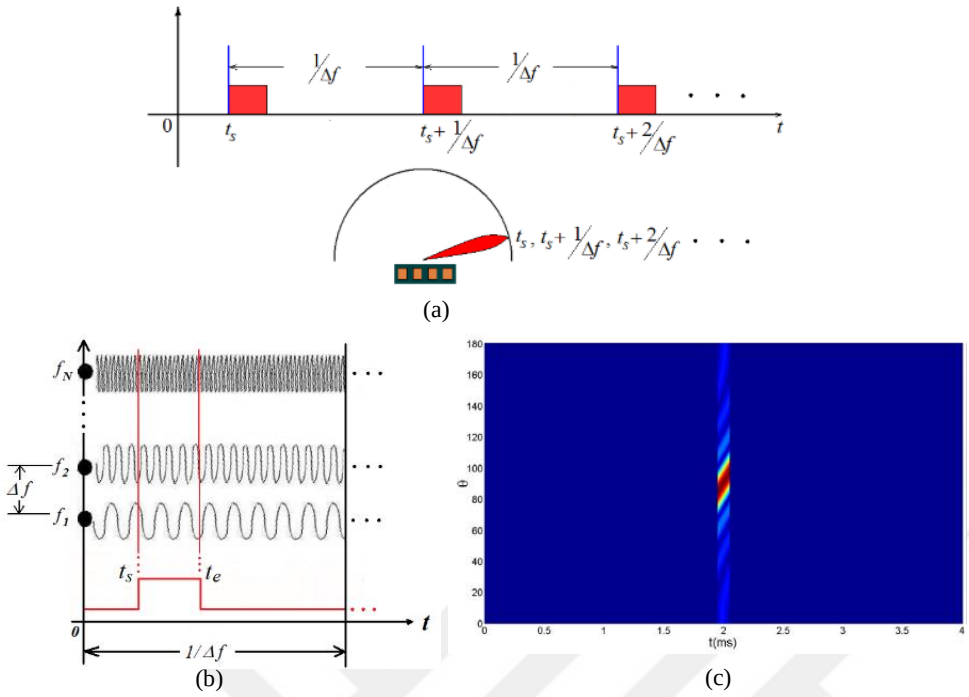

Figure 1.4. Implementation of the pulsed FDA in [23], (a) Pulse Waveform, (b)Pulse with CW signals (c) Resulting Radiation Pattern

Different LFM pulses are used on each element in [24]. Each chirp starts from slightly different frequencies, so waveform diversity provides the time-varying beamforming. It shows the characterization of the chirp in order to obtain practical energy spreading by carefully arranging the non-linear relationship between spatial and electrical angles with proper parameters. It shows the linear beam scanning by using both phase and frequency shifts. It also defines the ambiguity function based on the matched filtering, and illustrates the performance of the AoA and the range estimations with different target cases.

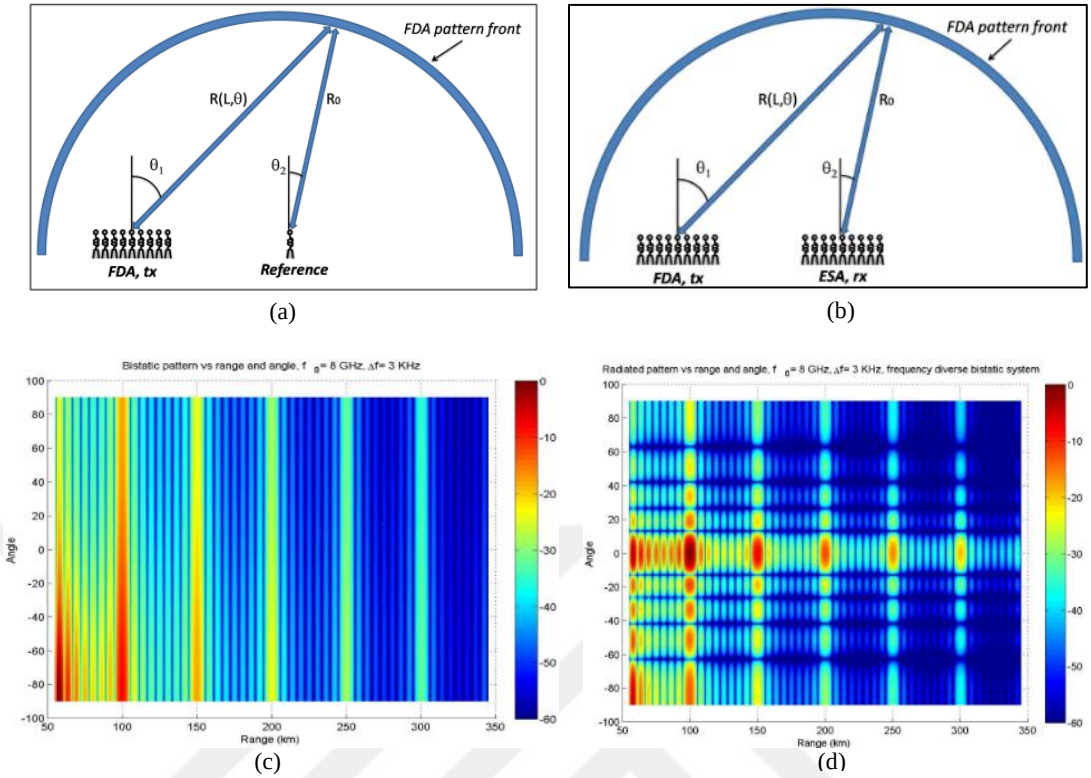

Figure 1.5. Implementation of the FDA with WA in [25]–[28], WA antenna distributions with omnidirectional RX (a) and phased array RX (b). Two way patterns with omnidirectional RX (c) and ESA RX (d)

The frequency diverse bistatic system (FDBS) is first introduced in [25], later is detailed by the authors of [25]–[28]. A regular FDA has well-known range angle time dependent radiation pattern. A reference point away from the transmitter array is selected in order to eliminate or lessen the S shaped radiation pattern in the FDA, which is named as *wavelength array* (WA). The displacement between the array elements and the reference point is given as $L\lambda_k$, that is multiple of instantaneous wavelength of the signal on the corresponding element. The Figure 1.5 (a) shows the proposed placement. With such placement of the array, angle dependency of the obtained radiation pattern is eliminated. The resulting pattern on the Figure 1.5 (c) shows the range and time dependent pattern with lessened effect of angle. Angular dependency is controlled by utilizing the ESA RX, so that two-way pattern can be steered to the desired angle by the conventional phased array or MIMO setup.

Furthermore, frequency diverse MIMO techniques are discussed in [27] based on the aforementioned method. Different radiation patterns are obtained by applying nonlinear frequency shift with FDBS as well. Cross-correlation calculations are given in order to illustrate the properties of the multi-dimensional ambiguity function of Δt, ΔR, $\Delta \theta$, and $f_{doppler}$.

FDA is implemented with various combinations of circuit components. It can be realized by deploying multiple waveform generators or multiple mixers which may cost reasonably high. The authors of [4], [5] occupies their selves with trying to find out simple and plain FDA implementation. They introduce a novel method of linearly frequency modulated continuous-wave (LFMCW) based FDA. That exploits the same chirp on each element by inserting true time delay between consecutive elements as it can be seen in the Figure 1.6 (a). Therefore, each chirp starts at different time instant and the instantaneous frequencies are different over the array aperture. This makes the proposed system totally different from the frequency scanning array (FSA). The frequency slope of the chirp, start-stop frequencies and the duration of chirp can control frequency shift during the operation, also measure of the TTDs during implementation.

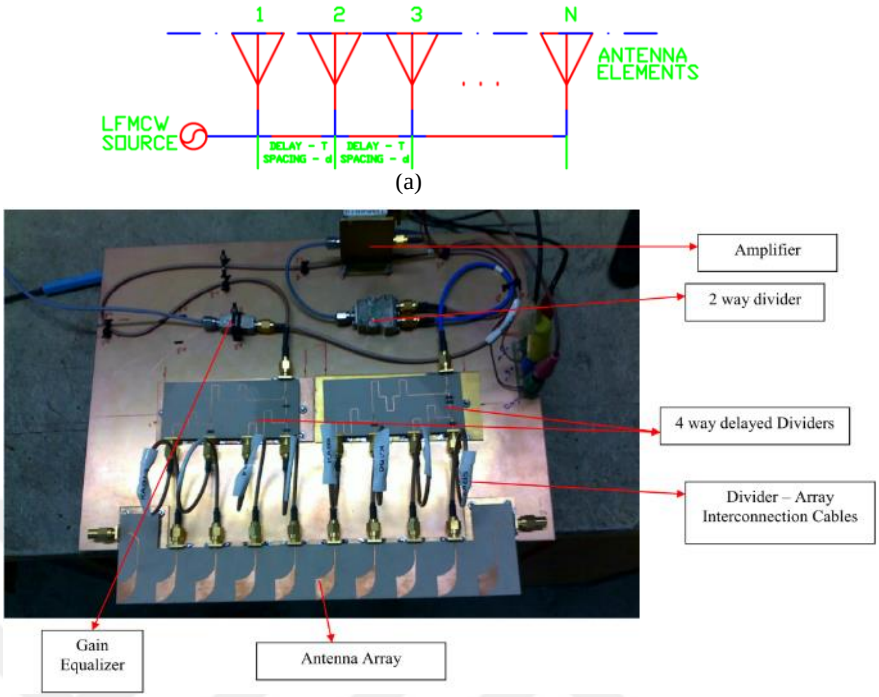

Figure 1.6. Implementation of the FDA with single LFMCW source in [4], [5], (a) basic schematic of the LFMCW-FDA and (b) the test setup

Above figure shows the fabricated array and the feed network on the setup. Vivaldi antenna elements make possible to conduct experiments within the wide bandwidth. TTDs gives $0.55nsec$ delay. Effects of center frequency, frequency slope and the bandwidth are showed and confirm the analytical approach experimentally throughout these studies. Some discrepancies are observed and explained with the non-linearity in control of the VCO and frequency response of the antenna elements. Furthermore, radar application examples with different target combinations are simulated. Angle resolution is derived from the time domain signal and showed the dependency on the AoA. The low frequency envelope of the field reflected back from a target is illustrated. Then, the range resolution is decided by considering the shortened useful pulse width by the FDA envelope. That approach is the basis of the DF method discussed in this study as well.

Three FDA receiver constructions are presented in [29] as an extended study of [30]. These receivers are composed of filter chains, band limited coherent FDA receiver contains different narrow band filters on each RX antenna. One antenna captures only one spectral component of the proposed linear classical FDA transmitter. Phase and amplitude of each spectral component are controlled independently. *Full-band pseudo-coherent FDA receiver* deploy wideband filter however single receiver unit changes phase and amplitude of only single spectral component. In the last receiver, f*ull-band coherent FDA receiver*, each RX unit takes all TX spectrum, but it handles all components separately to direct the two-way radiation pattern on the target. Although, it has the most complex implementation among them, the authors verify the usefulness of the method as a radar system. During they are expending their study towards a planar FDA receiver, the first two-dimensional FDA structure is proposed in these companion studies [30], [31]. Planar array with $9x9$ elements is located on $xy-plane$ with half-wavelength spacing. Excitation of array has prerequisite of which frequency shift along one axis must be much greater than the other axis. 4D radiation patterns are illustrated for different frequency shift cases such as $\Delta f_x = \pm 1kHz$ with $\Delta f_y = \pm 10kHz$ and $\Delta f_x = \pm 10kHz$ with $\Delta f_y = \pm 1kHz$. Even though this big step taken by this study, it does not encompass the definition of the critical parameters that controls the radiation pattern for practical radar. By utilization of f*ull-band coherent FDA receiver* as explained for linear array, "extremely unique patterns" are obtained. The 3D null steering and null steering in the range are presented as advantageous possibilities.

(a)

(b)

(c)

Figure 1.7. Measurement setup of the FDA in [3], (a) LFMCW-FDA link measurement over ground plane and (b) radar measurements with two corner reflector targets

The authors of [1]–[3] focus on some of the promising advantages of the FDA concept. Radar may have some blind spot due to multipath especially on the ground plane with low grazing angles. In addition, fading effects may occur due to multiple wave components in a communication link. It shows that the power fluctuation in the summation of the multiple waves can be decorrelated by the frequency diversity. Analytical background on FDA under multipath effects over the ground is derived for communication link, which shows the better results than the conventional phased array. Moreover, it is claimed and discussed that FDA could be remedy for the radar

cross-section fluctuation with respect to aspect angle. The expectations of smoother RCS fluctuation and less blind look angle are confirmed with derivations. The essential contribution is the proclamation of the first experimental LFMCW FDA multipath communication link and the radar application. Whereas RCS fluctuation is around 12.5/6.8dB in the PA measurement, it is obtained as 3.3/2.2dB with the center frequencies 6.00/7.84GHz respectively. The authors prove the claimed advantages of the FDA by revealing the outstanding results.

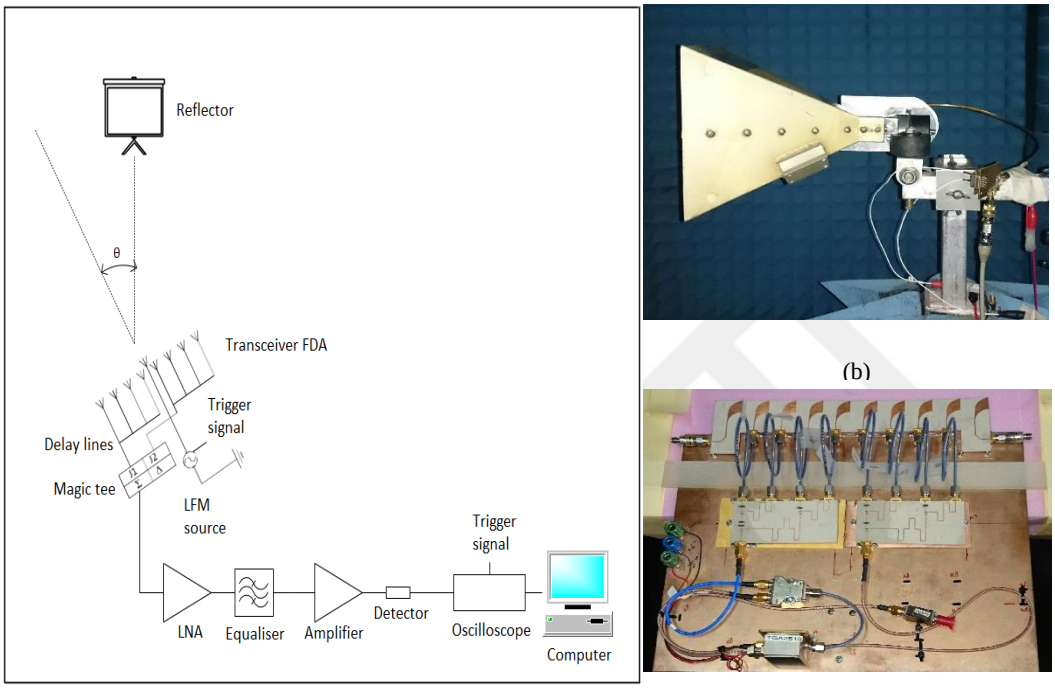

Figure 1.8. Measurement setup of the FDA in [32], [33] (a) LFMCW-FDA radar diagram (b) LFM TX wideband horn antenna (c) FDA RX with feed network and Magic-T

Monopulse direction finding application with LFMCW-FDA is proposed in [32], [33]. The proposed method is claimed to find the angular position of a target within a single LFM pulse. The setup is comprised of a single wideband horn transmitter antenna, eight-element FDA receiver that is composed of two sub arrays and the related feed network elements. As same setup is used as in the previous LFMCW-

FDA implementations. One sub array consists of four Vivaldi antenna array and the TTD lines fabricated on PCB. Outputs of them are connected to magic-T, which gives $\sum$ and Δ of the input signals. Thus, the authors utilize the difference between the beam patterns that are reconstructed by Magic-T. Then, problem is simplified to amplitude comparison DF with the resulting waveforms. However, the relationship between angle and time is carefully taken care for better AoA estimation. DF examples for various cases with different center frequencies, bandwidths and angular position of the target are conducted to validate the analytical approach experimentally. The accuracy of the AoA estimation is obtained within $\pm 2^{o}$ by the proposed setup.

The authors of [34] introduce the narrow band wide angle scanning circular FDA placed equiangular spacing. The criteria for parameters are explained with analytical details. Derivations from a single circular array are extended to double circular FDA for proper space scanning. After supporting the findings with analytical interpretations, they show the simulation results with beneficial beam steering capability. Also, match filtering implementation for direction finding is considered. It is stated that the ability of the beam steering and beam shaping can be improved further by adding more CFDA into the system. The idea of CFDA is extended by the authors of [35] by using concentric CFDA (CCFDA) which contains three circular subarrays. They have shown its beam steering abilities with the periodicity in time. They obtain the spatially steerable smoot elliptical beam patterns.

Range and angle measurement method is proposed by using a linear pulsed FDA radar in [36]. Same antenna array is used for FDA in transmitting mode, whereas it is utilized as PA in receiving mode to estimate the AoA by using the digital beamforming. Decreasing and increasing frequency shift over linear FDA elements effectuate the radiation patterns that are mirrored. Therefore, FDA build-up time for a radial location would be different for positive and negative frequency shift as well as an angular position. Ability to use two tone signals that contain both decreasing and increasing frequency shift version of FDA is proposed for decreasing the

measurement time significantly. It proposes to exploit the pulse compression with 300 random polyphase code which same for all transmitter by using matched filter on the receiver side. Numerical example illustrates the improvement in the range resolution with pulse compression. Simulation result of a case with two targets along same angle with 3km and 20 km radial distance shows the functionality of the method. In the experiment setup, seven coherent DDS are used to obtain two-tone signals by up-converting with same RF oscillator. Angular tilt is constructed by using cables with linearly increasing lengths. On the other hand, identical cables are used to combine the signals before mixing with the other side. Figure 1.9 shows the functionality of the proposed method by illustrating the different time between peaks with varying frequency shift. Even though, measurements are conducted in a pipeline setup rather than real radar scenario, they still prove the functional approach.

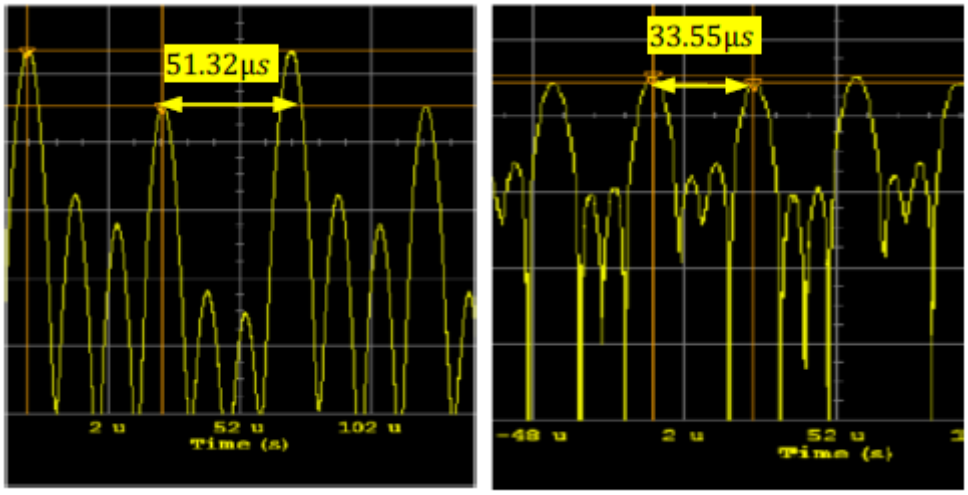

(a) $\Delta f = 10kHz$ (b) $\Delta f = 15kHz$

Figure 1.9. Peak Detector output waveform of the FDA radar example in [36]

Planar FDA also attracts wireless power transmission (WPT) researchers' attention, with its range dependent radiation patterns. The authors of [8] exploit planar FDA for WPT. FDA outperforms PA in this subject. Because PA transfers power along an angular section, whereas focusing energy on a certain position in space is achieved in this study.

We propose a novel FMCW based planar FDA in [12] which is basis of the Chapter 4 of this study. The planar array, which is placed on $xz-plane$, is discussed with field derivations, then usable radar example is presented and evaluated by comparing it with the equivalent PA example. The authors of [37] propose similar array geometry but using continuous wave signals with different frequency shifts along x and z axes instead of LFM signal. The array is composed of $18x4$ elements with frequency shifts $|\Delta f_x| = 1\backslash 3MHz$ and $|\Delta f_z| = 7MHz$ along x and z axes respectively. The resulting maximum radiation direction varies as in the Figure 1.10, which shows coverage diagram of the planar FDA. This study utilizes the uniformly distributed poly-phase codes that are randomly selected from $\{0, \pm\pi/2, \pi\}$. On the other hand, the receiver is phased array with digital beam forming capability. Furthermore, match filtering is used for pulse suppression which improves the range resolution to $6m$. Significant decrease in side lobes of the time domain signal is illustrated as well. Although, FDA suffers from low SNR due to inherit full scan property, it is claimed that the cumulative detection scheme in slow time could be remedy for it.

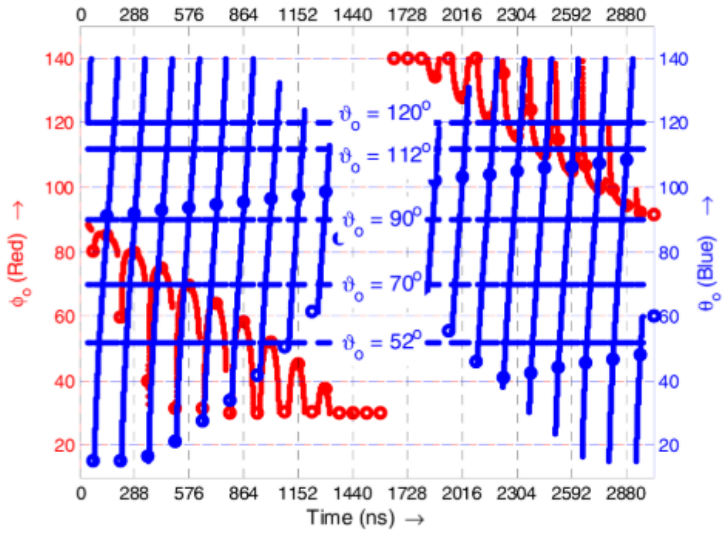

Figure 1.10. Coverage diagram of the planar FDA TX in [37]

Another planar FDA approach is presented in [38] as it can be seen on the Figure 1.11. This system is composed of hybrid planar TX array that is comprises of FDA

along azimuth and classical PA along elevation. The range periodicity ambiguity is removed by PA, whereas FDA removes the non-periodicity ambiguity. Effectiveness of this combination of the radar is validated by the simulations in this study.

The authors of [39] investigate the selection of the frequency shifts based adaptive 3D beamforming technique in planar FDA. Three beamforming approach are investigated and compared with each other. Matched filtering is utilized with different weighting coefficients in both transmitter and receiver. Classical and minimum variance distortionless response (MVDR) beamforming methods designed with constant frequency selection. However, the proposed frequency offset scheme (FOSS) strictly relies on the adaptively selected frequency shifts. However, they reveal that it does not require weighting for beamforming. Moreover, they obtain by using FOSS almost 20 dB higher signal to interference and noise ratio gain, which defines the gain ratio between desired and unwanted signal source, than others in simulations.

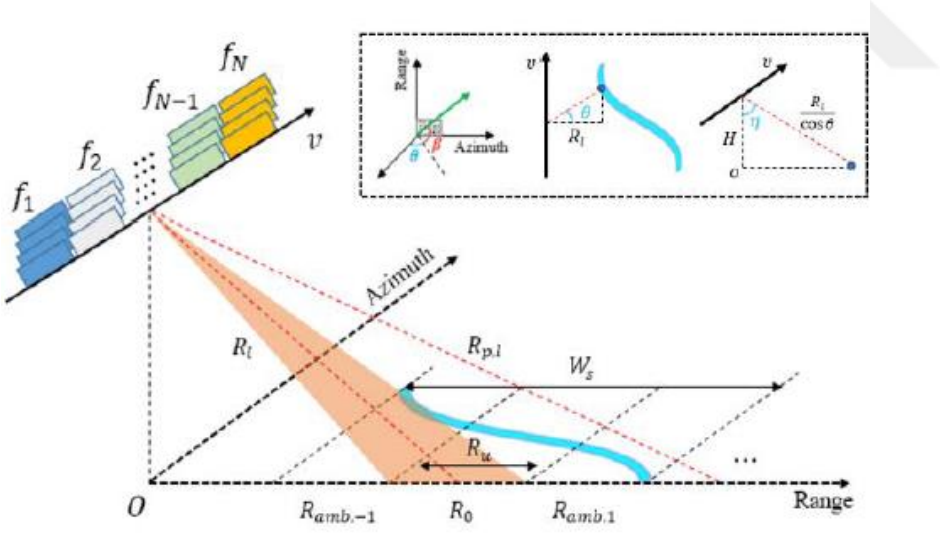

Figure 1.11. Planar side looking FDA-SAR system in [38]

1.2 Motivation

One of the main focuses of this study is to review and evaluate a DF method. Essential parameters such as angle resolution and range resolution will be reviewed by using a homodyne receiver that contains a single omnidirectional antenna. Aforementioned definitions are complying with the selected digital signal processing methods. Even though, it is possible to build a radar with better performance, promising performance is obtained by using low cost setup which can be implemented by PCB technologies and minimum number of IC parts. The proposed setup will be compared with the state of art MIMO example that may cost much more expensive.

A novel planar LFMCW based FDA would make use of the advantages of the FDA concept in 3D scanning radar. Also, that feature is highly demanded by common radar application. In this study, analysis of the transmitted field by the planar FDA that is similar to raster scan will be given in order to show comparable performance as the state of art PA concepts. In order to progress step by step, it is deployed only as transmitter of the radar example, whereas, PA is selected as the receiver of the radar.

Radar cross-section (RCS) is a useful parameter for radar applications that is defined by $\sigma = \lim_{R\to\infty} 4\pi R^2 \frac{|E^r|^2}{|E^t|^2}$. It is directly related with the reflected power from a target. Investigation of the RCS characteristic that obtained by planar array is another aim of this study. The target RCS may differ with respect to incidence angle. It may have nulls for certain angles, that makes the target invisible to radar. Therefore, such behaviors are not desired for security reasons and have high risks in surveillance applications. Moreover, it may be dangerous for the air traffic control (ATC) radars as well. Advantages of using LFMCW based linear FDA in the target RCS characteristics have already shown by the previous research and validated by measurements. It will be investigated again with the proposed planar array. Main

goal is to show that LFMCW based planar FDA has much less nulls in the RCS vs incidence angle graphs.

1.3 Summary of Works Done

First contribution done by this study is to review that reliable and easily implementable DF is possible with the LFMCW FDA, that is proposed also in [5]. That is detailed by explanation of the approach as a preparation for the comparison with the MIMO radar competitor. In order to fill the gaps in LFMCW based FDA literature, the novel planar array structure, that exploits advantages presented by its predecessors, is proposed. Moreover, this concept, which is discussed with details, is compared with the equivalent PA radar in a realistic scenario. Finally, immunity to RCS fluctuation of this system is formulized. Also, outperforming results are presented.

1.4 Organization

This report starts with the introduction chapter. In this chapter, very brief history of FDA is given. Then, how FDA concept is migrated to LFMCW based FDA is explained. Then, this chapter introduces the main contributions made by this study. A literature survey section follows the introduction with the summary of the valuable studies in the literature. The selected studies give readers an understanding about how the path of the research is developed and ends up with this study.

Despite of the presence of prior studies with the LFMCW based linear FDA, the total field transmitted and received back is derived again by starting from scratch in the Chapter 2. This chapter continues with review and explanations of the proposed direction finding method with the definitions of range and angle resolutions.

In the next chapter, design steps of the radar that proposed by [40], [41] take place, to reveal the similarities between the state of art MIMO concept and LFMCW based

FDA. This chapter is finalized with DF performance comparison of these two approaches.

In the Chapter 4, the novel LFMCW planar FDA method is presented. Firstly, realization of it is discussed and transmitted field derivations are given in time domain. Also radiation patterns are explained to show the covered space by it. Reflected fields that captured by the PA receiver are illustrated. Both comprise the radar that is evaluated in realistic scenario and compared with the given fully PA rival.

On account of the previous studies, which show the advantages of both LFMCW based and classical FDA, the target RCS characteristic has become a hot topic for LFMCW-FDA researchers. For the sake of the wholeness of the proposed planar array studies, this feature is investigated again for the novel method in the Chapter 5. Its performance is compared again with the PA competitor as in the previous sections.

In the last chapter of this study is composed of the conclusion and the possible future works that would make this concept closer to being the state of art.

CHAPTER 2

BACKGROUND ON LFMCW BASED FDA

Frequency diversity has been on the focus of the many researches for the last two decades. Implementation of the FDA is possible by deploying the transmitter as many as the number of the antenna elements in the array. Therefore, the frequency of the signal on any element can independently be controlled in order to have frequency diverse waveforms. Cost and complexity of the design and implementation would also scale up rapidly in the aftermath of the increasing number of the T/R modules. A Linear Frequency Modulated Continuous Wave (LFMCW) based Frequency Diverse Array (FDA) has been suggested as one of the possible FDA implementations in [5]. Various possible applications and implementation have been presented in [3]–[5], [32]. Those works have shown the promising results, that prove, the LFMCW-FDA is a worthwhile research topic and the feature of fast scanning of the space is one of the outstanding advantages of the FDA concept. Moreover, immunity to multipath effects and its outperforming the state of art radars in terms of the target RCS characteristic have been revealed in those studies. Some of the beneficial properties have not totally been unveiled in the literature yet.

In this chapter, the background of LFMCW based FDA will be reviewed and examined thoroughly in order to bring out some more capabilities of it. The direction finding performance of the LFMCW-FDA will be reviewed and discussed, after presenting the methods and formulations explicitly. Starting with the derivation of the transmitted electric field from an antenna to an observation point in space, properties of LFMCW-FDA radar will be investigated. In order to show the procedure for a target localization, the reflected signal will be derived and investigated to locate the possible targets.

2.1 Background on LFMCW FDA Radar

The classical Frequency Diverse Array (FDA) can be implemented with separate transmitter units whose RF sources are producing the different frequencies. The LFMCW based FDA utilizes a continuous wave pulse whose frequency changes linearly along the pulse duration. In order to create small frequency diversity steps along a linear transmitter antenna array, progressing true time delays are inserted along feed lines of antenna elements on the feed network of a linear antenna array. It can be realized by corporate feed network like in [3]–[5], [32] or a series fed network, therefore the frequency diversity can be actualized with a single LFMCW signal source. All transmitters can be fed by that signal via the carefully designed feed network, that significantly reduces the number of circuit elements such as mixer, amplifier, etc. As a result, the cost of transmitter can be significantly reduced.

2.1.1 Transmitted Electric Field by LFMCW-FDA

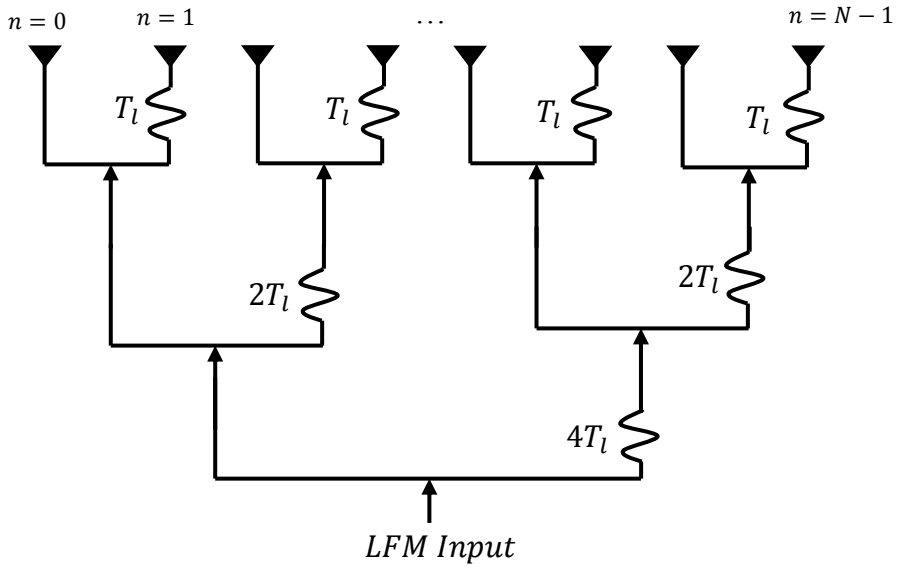

Figure 2.1. The corporate feed line with progressing true time delay lines of the transmitter array with $N = 8$

The transmitter structure of the radar proposed in this section is not different from the predecessor implementations of LFMCW-FDA in [3]–[5], [32]. The corporate feedline of the transmitter array can be seen on Figure 2.1. True time delay (TTD) lines are composed of the transmission lines that are longer than the lines at the opposite side of the power dividers' branches. The amount of delay of these TTD lines, relative to the straight lines, is given as "T_l" on the closest lines to the antennas. The relative delay on the upper hierarchical power divider stage is given as "T_l". Therefore, along the antenna elements, which are numbered from "0" to "$N-1$", the value of the time delays can be written as "nT_l".

$$\bar{E}_t(r,t) = \sum_{n=0}^{N-1} \frac{1}{r_n}\ s(t-t_n)\ \bar{\xi}_n(\theta,\phi,f_n)\ e^{j\left[w_0\,(t-t_n)+\frac{\mu}{2}(t-t_n)^2\right]} \qquad 2.1$$

The total transmitted electric field at a point $\boldsymbol{P(r_o, \vartheta_o, \varphi_o)}$ in Figure 2.2 due to the LFMCW-FDA transmitter can be written as in Eq-2.1. $s(t)$ is the baseband part of the RF signal. The baseband signal is assumed to be the rectangular pulse whose value is 1 during the pulse duration starting from 0 to pulse duration, τ, in time domain as in the Eq-2.2.

$$s(t) = \begin{cases} 1, & 0 \le t \le \tau \\ 0, & t < 0\ or\ \tau < t \end{cases} \qquad 2.2$$

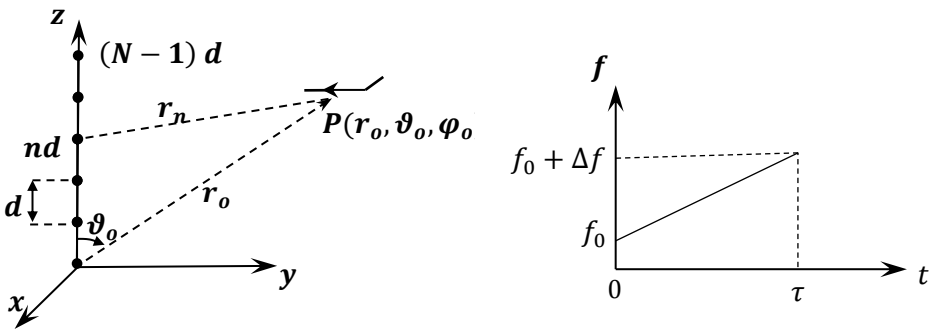

Figure 2.2. The Transmitter of Proposed Linear LFMCW based FDA and the frequency change of LFMCW pulse vs time

$\bar{\xi}_n(\theta, \phi, f_n)$ is the vector pattern of the n[th] single antenna element, that depends on the instantaneous frequency on the antenna and the design of antenna. The frequency of the input signal can be seen right hand side the Figure 2.2. That complex waveform can be written as formula $e^{j\left(w_0\, t+\frac{\mu_0}{2}t^2\right)}$, where w_0 is the angular frequency of the LFMCW pulse. Δf is the total frequency band of the LFMCW pulse. That value does not have to be the positive value. When implementing an LFMCW pulse with decreasing frequency, the total bandwidth can be defined as negative in order to make general formulas valid without deriving them again. In other words, negative value of it implies nothing but that the frequency sweeps with the negative slope over pulse. Radian slope on the frequency vs time graph is defined by $\mu = 2\,\pi\Delta f/\tau$, whereas the slope in terms of Hz/sec is given as $\mu_{\mathrm{f}} = \Delta f/\tau$.

$$t_n = \frac{r_n}{c} + n\,T_l \tag{2.3}$$

$$r_n = \begin{cases} r_0 - nd\cos\theta\,, & for\ phase\ terms \\ r_0\,, & for\ amplitude\ terms \end{cases} \tag{2.4}$$

For the far field observer, elementwise distance can be written as in the Eq-2.4 for phase related terms and amplitude related parts in derivations. Elementwise true time delay of the signal from source to the target is comprised of delay due to feed network and the propagation delay in free space.

$$Let \quad t' \triangleq t - \frac{r_0}{c} \tag{2.5}$$

The retarded time is defined by above equation. Because the total delay is much less than the pulse duration, one could write $s(t')$ instead of $s\left(t' - nT_l + \frac{nd\cos\theta}{c}\right)$, which is unit rectangular pulse. Element distance r_n is substituted by r_0 for amplitude terms and $r_0 - nd\cos\theta$ for phase terms. Element electric field density patters are assumed to be identical for all elements and constant over frequency band. With the given assumptions, the transmitted electric field can be written as in the Eq-2.6

$$\bar{E}_t(r,t) = \frac{1}{r_0}\ s(t')\ \bar{\xi}(\theta,\phi,f_0) \sum_{n=0}^{N-1} e^{j\left[w_0\left(t'-nT_l+\frac{nd\cos\theta}{c}\right)+\frac{\mu}{2}\left(t'-nT_l+\frac{nd\cos\theta}{c}\right)^2\right]} \tag{2.6}$$

After rearranging the above form, one could get the below equation.

$$\bar{E}_t(r,t) = \frac{1}{r_0}\ s(t')\ \bar{\xi}(\theta,\phi,f_0)\, e^{j\left[w_0 t'+\frac{\mu}{2}(t')^2\right]} \sum_{n=0}^{N-1} e^{-jn\left[w_0\left(T_l-\frac{d\cos\theta}{c}\right)+\mu\, t'\left(T_l-\frac{d\cos\theta}{c}\right)-\underbrace{n\frac{\mu}{2}\left(T_l-\frac{d\cos\theta}{c}\right)^2}_{too\ small}\right]} \tag{2.7}$$

Exponential of the term $jn^2\frac{\mu}{2}\left(T_l - \frac{d\cos\theta}{c}\right)^2$, which is in the order of $\frac{j\pi}{10^6}$, can be considered as 1. After omitting that term, summation could be calculated as the $digital - sinc$ function. The simplified total electric field at point P is found like in Eq-2.8 where Ψ is defined by Eq-2.9.

$$\bar{E}_t(r,t) \cong \frac{\bar{\xi}(\theta,\phi,f_0)}{r_0} s\left(t-\frac{r_0}{c}\right) e^{j\left(w_0 t'+\frac{\mu}{2}(t')^2-\frac{N-1}{2}\Psi\right)} \frac{\sin\left(N\Psi/2\right)}{\sin\left(\Psi/2\right)} \tag{2.8}$$

$$\Psi = (w_0 + \mu t')\left(T_l - \frac{d\cos\theta_0}{c}\right) \tag{2.9}$$

2.1.2 Properties of the Transmitted Field

$$\left.\frac{\sin\left(N\Psi/2\right)}{\sin\left(\Psi/2\right)}\right|_{t'=t_0} = N \tag{2.10}$$

The electric field at an observer's point has a peak value at specific time which can be found by Eq-2.8. Time of the maximum electric field, which is t_0, has a value that makes the $sinc$ function in Eq-2.8 maximum. Maximum value of the $sinc$ function is N when the retarded time equals to t_0, then the Eq-2.11 holds.

$$\Psi\,|_{t'=t_0} = (w_0 + \mu t_0)\left(T_l - \frac{d\cos\theta_0}{c}\right) = 2\pi p, \quad p \in \mathbb{Z} \tag{2.11}$$

$$t_0 = \frac{\tau}{\Delta f}\left(\frac{p}{\left(T_l - \frac{d\cos\theta_0}{c}\right)} - f_0\right), \quad p \in \mathbb{Z} \;\;\&\;\; 0 \le t_0 \le \tau \tag{2.12}$$

There are infinite number of solutions for t_0, which satisfies above equation. In addition to mathematical solution, one must consider the physical meaning of that equation. That maximum has to occur due to pulse transmitted from the array, that brings time limitation into the calculations. Firstly, propagation of the transmitted field takes time, which is roughly r_0/c , r_0 and c are the distance between the origin and the point of observation. If the constant retardation is subtracted from time, one may get retarded time, t'. Therefore, the maximum would occur between 0 and τ in terms of the retarded time. After having the physical restriction, the solution of the Eq-2.12 has an unique solution with well-defined transmitter parameters. More than one solution is also possible and valid that gives multiple peaks within the single pulse duration. Number of maxima in single pulse interval depends on various application parameters. However, that will be discussed on the section of a planar array implementation of the LFMCW-FDA. During the decision process of the array

parameters, this will be considered in order not have multiple valid solution for t_0 within pulse duration.

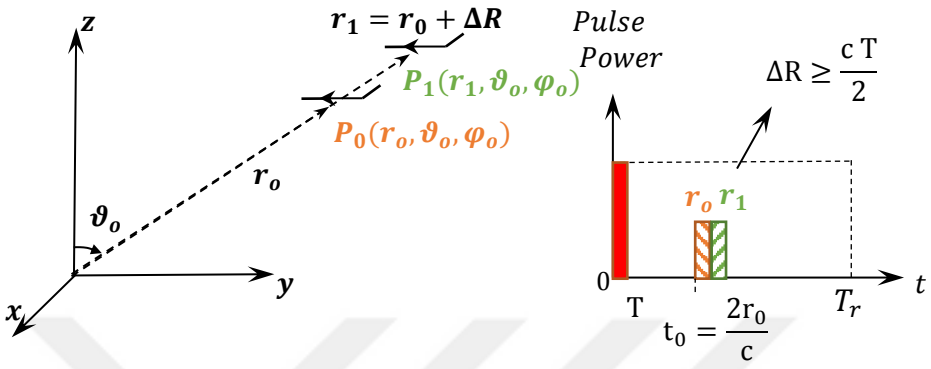

Figure 2.3. Range Resolution in Pulsed Radar

Range resolution is another property to be investigated, because it has vital role to distinguish different targets at the same angle. In order to distinguish different targets along an angle, conventional pulsed radars utilize the pulse width. This type of radar is out of scope of this work, however, very short introduction is important for continuity. A simple scheme is given as in the Figure 2.3. The most important parameter in the pulsed radars is pulse width for range resolution. The minimum range between two targets, ΔR, that can be resolved, is calculated as $\Delta R = cT/2$, where c is the velocity of light in free space. Another type of the radars may utilize the LFMCW pulse and phased array. In this type, all antenna elements radiate same frequency but different phases, which was determined to steer the main lobe demanded angle during throughout the LFM chirp. The LFM pulse duration can be longer than the pulsed radar. There is obvious difference between in determination of the range resolution.

The LFMCW-FDA radars are different from the conventional pulsed radars that send pulses with a very short period. Pulse, which is observed in LFMCW-FDA applications, can be examined by considering time domain field pattern at an

observation point. The time domain signal is shaped as $sinc$ function. Therefore, it roughly composes of a main lobe and side lobes. At that point, one may assume the pulse period as the null-to-null time duration. It can also be defined as -3dB or -6dB points with respect to the maximum value of the received voltage. However, the null-to-null time duration is considered as the pulse period for the further calculations.

$$\mathrm{N}\Psi\,|_{t'=t_0\mp\frac{T_{nn}}{2}} = \mathrm{N}\left(w_0+\mu\left(t_0\mp\frac{T_{nn}}{2}\right)\right)\left(T_l-\frac{d\cos\theta_0}{c}\right)=2\pi p\mp\pi,\quad p\in\mathbb{Z} \qquad 2.13$$

In Eq-2.13, the null-to-null time duration is given as T_{nn} and using above formula its value can approximately be written as in Eq-2.14. It is an approximation, because the maximum radiation direction, θ_0, does not stay unchanged. The effect of this change to T_{nn} value typically is limited, because T_l is much greater than $\frac{d\cos\theta_0}{c}$. Generally, the value of T_l is in the order of a couple of hundred of picoseconds, whereas the value of $\frac{d\cos\theta_0}{c}$ term is in the order of tens of picoseconds. This comparison is, of course, dependent on design of the array and signal determined by application.

$$T_{nn}\cong\frac{2\,\tau}{\mathrm{N}\,\Delta f\left(T_l-\frac{d\cos\theta_0}{c}\right)} \qquad 2.14$$

So-called pulse duration can be determined and changed with different parameters as it can be figured out in above equation. The more antenna elements in the array is present, the narrower main lobe in the time domain signal can be obtained. Moreover, increasing the frequency bandwidth of the LFM sweep makes the null-to-null time less. Furthermore, the length of delay lines is inversely proportional to T_{nn}. On the other hand, one can control that duration directly by changing the overall pulse duration value, τ.

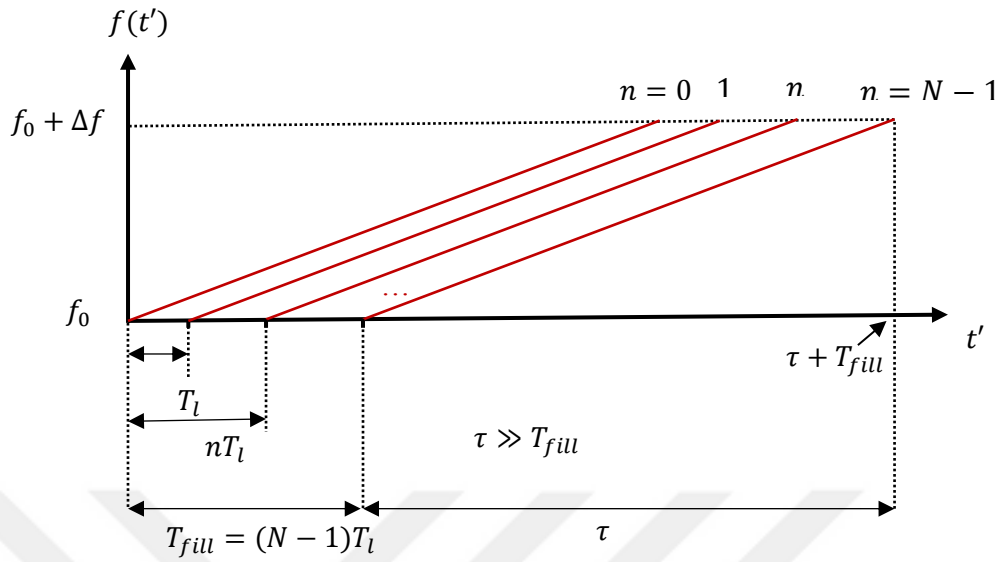

Figure 2.4. Frequencies of the LFMCW transmitter antennas with respect to retarded time

Instantaneous bandwidth of transmitted signal can be determined by a physical approach. Every antenna would radiate sine waves with different frequencies. As in the essence of FDA, every element has a small step of frequency difference to the adjacent elements, that is exactly intended by the design of LFMCW-FDA. Therefore, the instantaneous bandwidth can be calculated by subtracting the lowest frequency on the aperture from the highest frequency. For the sake of clarity, the instantaneous frequencies on each element have been given on the Figure 2.4 with respect to the retarded time. For an LFM pulse with positive slope in frequency vs time graph, the instantaneous bandwidth is "$\frac{\Delta f}{\tau} T_{fill}$", where $T_{fill} = (N-1)T_l$.

2.1.3 Simulation of the Transmitted Signal

Transmitted signal at a point has been calculated in previous subsection. In this subsection, the total electric field due to the array will be shown by simulations. Therefore, possible further manipulations will be investigated. Parameters have been

given on Table 2.1. N is the number of antenna elements within array. An isotropic antenna will be used as a single transmitter. Inter-element spacing between adjacent antennas is taken as half wavelength of the center frequency that is 10GHz. Therefore, the spacing is 1.5cm.

Table 2.1 Linear Transmitter Array Parameters

Parameter	*Value*	Parameters	*Value*
N	16	Δf	2.5%
$Antenna$	$Isotropic$	r	$[0, 100]\ km$
f_c	$10GHz$	d	$\frac{\lambda_c}{2}$
τ	$1\ ms$	θ	$\epsilon\ [0^0, 180^0]$
T_l	$4\ nsec$	ϕ	90^0

The distance from transmitter is assumed to be 1 km in order to observe transmitted field in terms of time. Moreover, the field of interest is reduced to the plane that is limited by $\theta\epsilon\ [0^0, 180^0]$ and $\phi = 90^0$ in order to show field strength on the plane.

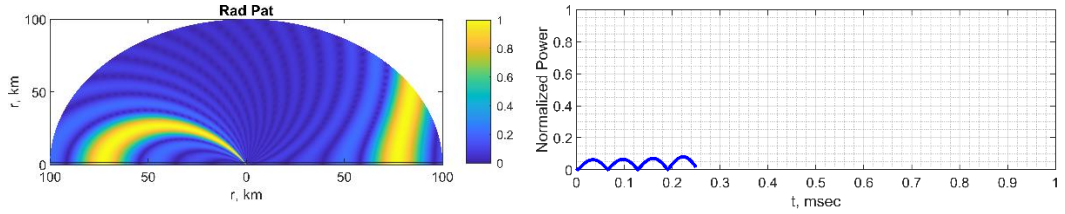

(a) $t = 0.25\,\tau$

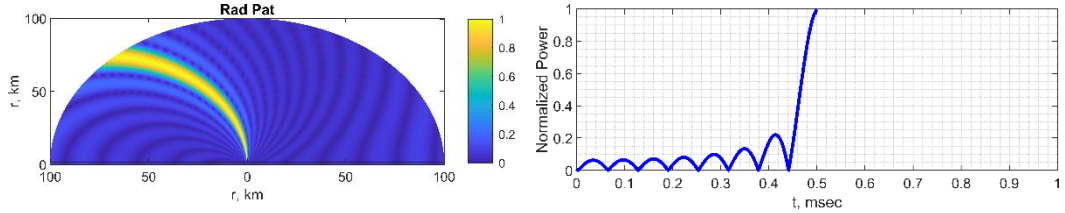

(b) $t = 0.50\,\tau$

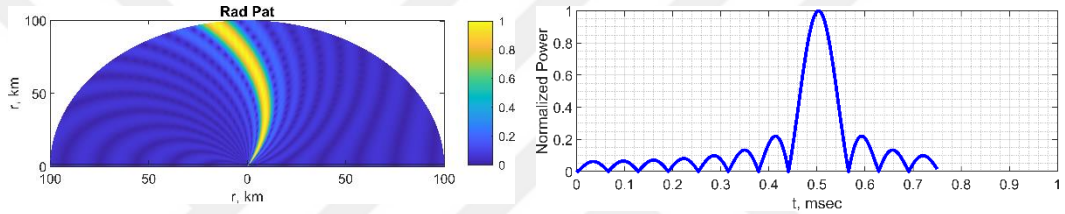

(c) $t = 0.75\,\tau$

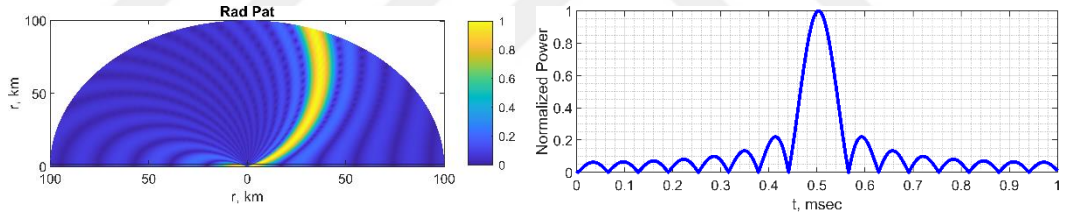

(d) $t = 1.00\,\tau$

Figure 2.5. Radiation Pattern and observed waveform with proposed linear LFMCW-FDA transmitter

The transmitted patterns are illustrated above figure on the azimuth plane defined above. The observer is located at $(r, \theta, \phi) = (1km, 90^o, 90^o)$, in order to obtain normalized power with respect to time. Spiral like radiation pattern is one of the FDA characteristic and observed here as well. It can be commonly called as S shape radiation pattern also, because they would seem like S, if rectangular plot used instead of polar plot. On the right hand side of the figure, normalized power pattern looks line absolute value of the $digital - sinc$ function, as it is found in the

previously. As pattern is changing with time, position and angle, space time adaptive processing (STAP) is necessary.

2.1.4 Received Field at the Origin that is reflected back from a point scatterer

There would be reflected signal in the presence of scatterers in the field of view. Detection of that field can be accomplished with an antenna or an array as the transmitter. A single receiver antenna will be considered in this part of the study.

$$\bar{E}_t(r,t) = \sum_{n=0}^{N-1} \frac{1}{r_n}\ s(t-t_n)\ \bar{\xi}_n(\theta,\phi,f_n)\ e^{j\left[w_0\,(t-t_n)+\frac{\mu}{2}(t-t_n)^2\right]} \qquad 2.15$$

$$t_n' = \frac{r_0}{c} + \frac{r_0}{c} + (n-1)\left(T_l - \frac{d\cos\theta_0}{c}\right) \qquad 2.16$$

Derivation of the received voltage can be started from the transmitted field as in the Eq-2.15. The total time delay of the reflected back from the scatterer at far field target that is transmitted signal from n^{th} element can be written as in the Eq-2.16. This term contains double way propagation delay, corresponding TTD in the transmitter's feed network and the phase delay value due to the spatial location.

$$v_{rx}(t) = A\sqrt{\sigma\, A_{eff}} \sum_{n=0}^{N-1} \frac{1}{r_n r_0}\ s(t-t_n')\ \xi_n(\theta,\phi,f_n)\ e^{j\left[w_0\,(t-t_n')+\frac{\mu}{2}(t-t_n')^2\right]} \qquad 2.17$$

$$t'' = t - \frac{2r_0}{c} \qquad 2.18$$

The field would be scattered from the target, whose radar cross section (RCS) is σ, with the term $\frac{\sqrt{\sigma}}{\sqrt{4\pi}\,R}$. Then, the field reflects back to the receiver antenna, which is assumed to be an omnidirectional antenna with the effective antenna aperture, A_{eff}. Therefore, one can finally write the received voltage on the RX terminal as in the Eq-2.17. The linear terms, which contain $1/\sqrt{4\pi}$ twice due to radiation and all efficiency related components, are represented by the term A in the derivations. The distance between the n^{th} element and the target is r_n that can be assumed to be r_0 for amplitude terms, whereas $r_0 - (n-1)\frac{d\cos\theta_0}{c}$ for the phase related terms. After substituting the Eq-2.16 into the Eq-2.15, one could obtain the Eq-2.19. Received voltage has high frequency term and also low frequency envelope whose shape is the $digital - sinc$ function as in the transmitted field derivation.

$$v_{rx}(t'') \cong A\sqrt{\sigma\, A_{eff}}\ \frac{\xi(\theta,\phi,f_0)}{r_0^2}\ \ s(t'')e^{j\left(w_0\, t'' + \frac{\mu}{2}(t'')^2 - \frac{N-1}{2}\Psi\right)}\frac{\sin\left(N\Psi/2\right)}{\sin\left(\Psi/2\right)} \qquad 2.19$$

$$\Psi = (w_0 + \mu t'')\left(T_l - \frac{d\cos\theta_0}{c}\right) \qquad 2.20$$

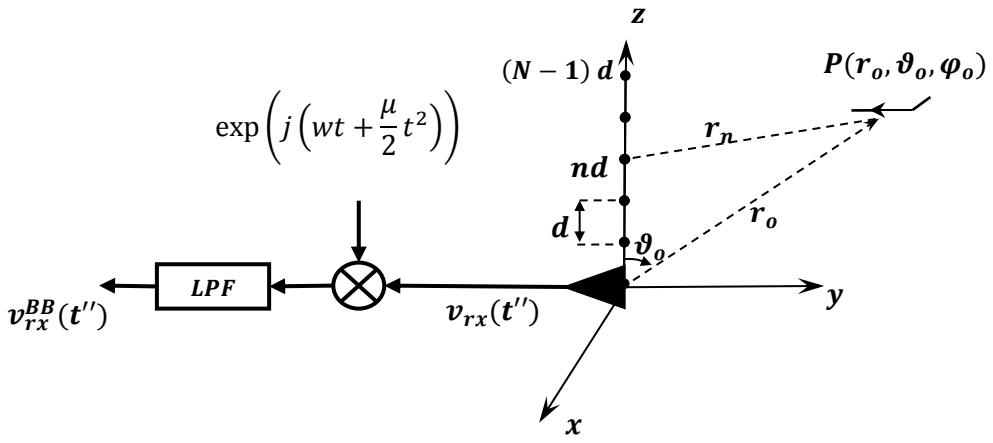

Figure 2.6. The Flow diagram of the receiver with the transmitter array

Baseband received signal will be derived in this part of the study for the further investigation on the target detection performance of the linear LFMCW-FDA radar. A direct conversion receiver (DCR) is being used to downconvert the received signal as basically illustruted on the Figure 2.6. This homodyne receiver is composed of only a mixer and a low-pass filter (LPF). Same local oscillator used in transmitter is also used in the RX to feed the LO input of the mixer. More realistic receiver must contain also a low noise amplifier (LNA), a band pass filter (BPF) and an intermediate frequency (IF) amplifier. However, these parts are assumed to be excluded for now in order to ease related derivations and illustruations. Moreover, their contribution to the system would be positive in a realistic scenerio. But continuing the receiver given on the Figure 2.6 is adequete to investigate the target detection capabilities of the proposed method.

$$v_{rx}^{BB}(t'') \cong A\sqrt{\sigma\, A_{eff}}\ \frac{\xi(\theta,\phi,f_0)}{r_0^2} \\ s(t'')e^{j\left(w_0\, t''+\frac{\mu}{2}(t'')^2-\left(wt+\frac{\mu}{2}t^2\right)-\frac{N-1}{2}\Psi\right)}\frac{\sin\left(N\Psi/2\right)}{\sin\left(\Psi/2\right)} \qquad 2.21$$

Assuming all conversion losses and path losses be zero, basebend received voltage can be written as in the Eq-2.21. Substituting the Eq-2.18 into the Eq-2.21, one could

find below expression. That shows the relation between the spectral components of the baseband signal and the target distance.

$$v_{rx}^{BB}(t) \cong A\sqrt{\sigma\, A_{eff}}\ \frac{\xi(\theta,\phi,f_0)}{r_0^2} \\ s\left(t-\frac{2r_0}{c}\right)\ e^{j\left(-w_0\frac{2r_0}{c}-\mu t\frac{2r_0}{c}+\frac{\mu}{2}\left(\frac{2r_0}{c}\right)^2-\frac{N-1}{2}\Psi\right)}\frac{\sin\left(N\Psi/2\right)}{\sin\left(\Psi/2\right)} \tag{2.22}$$

$$v_{rx}^{BB}(t) \cong A\sqrt{\sigma\, A_{eff}}\ \frac{\xi\left(\theta,\phi,f_0\right)}{r_0^2}\, e^{j\left(w_0\frac{2r_0}{c}-\frac{\mu}{2}\left(\frac{2r_0}{c}\right)^2+\frac{N-1}{2}\left(T_l-\frac{d\cos\theta_0}{c}\right)\left(w_0-\mu\frac{2r}{c}\right)\right)} \\ s\left(t-\frac{2r_0}{c}\right)\ e^{j\mu t\left(\frac{2r_0}{c}+\frac{N-1}{2}\left(T_l-\frac{d\cos\theta_0}{c}\right)\right)}\frac{\sin\left(N\Psi/2\right)}{\sin\left(\Psi/2\right)} \tag{2.23}$$

This spectral component can be found as in the Eq-2.24. This beat frequency represent only single tone signal. On the other hand, the downconverted signal has bandwidth rather than the single tone due to the nature of the LFMCW-FDA even for a point scatterer target assumption. The bandwidth of it is a vital characteristic for target detection and it will be considered in the next section with more details. For a stationary point scatterer f_{beat} can be written as in below equation roughly.

$$f_{beat} = \frac{\Delta f}{\tau}\left(\frac{2r_0}{c}+\frac{N-1}{2}\left(T_l-\frac{d\cos\theta_0}{c}\right)\right)\cong\frac{\Delta f}{\tau}\frac{2r_0}{c} \tag{2.24}$$

2.2 Direction finding with the proposed LFMCW-FDA Radar

Target localization is the main motivation for the radar applications. Therefore, a method for DF is presented in this part of the study. DF applications were proposed and done in [5], [32], and [33]. Authors of [32] and [33] used two linear LFMCW-FDA that composed of 4 antenna elements as receiver. Captured voltage were combined with 0^o and 180^o degree phase differences to create sum and difference pattern. The method described in [5] is the proposed DF method. However, in this study, we will investigate DF method with different target examples and including sliding window approach that provide 2D radar images different that the previous works.

There are two inevitable parameter decision-making process for DF with the linear array and they are range and elevation angle. Before continuing with DF method explanations, it is better to define critical points in range and angle detection by defining resolutions for them. Finally, simulation results with the proposed approach are presented in this subsection.

2.2.1 Range Resolution (ΔR)

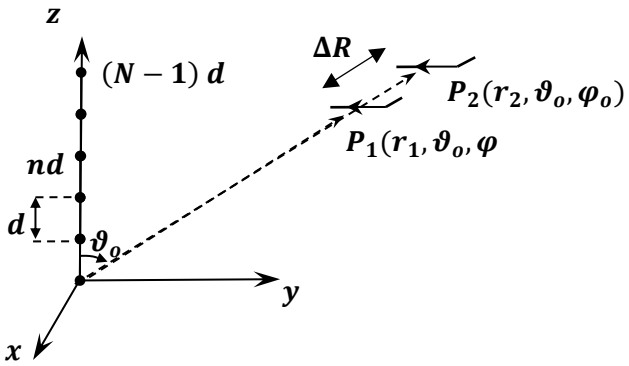

Figure 2.7. Two targets that located at points P_1 and P_2

Two targets, which are sketched as plane like shapes on the Figure 2.7, are assumed to be located on the points P_1 and P_2. Main lobe around maximum can be considered as a pulse that impinges on the target. Therefore, the duration of pulse becomes the null-to-null time period. That is found as $T_{nn} \cong \frac{2\,\tau}{\mathrm{N}\,\Delta f\left(T_l - \frac{d\cos\theta_0}{c}\right)}$. The time that is required for wave travelling the separation distance two times, must be less than T_{nn}, which is the so-called pulse duration for the proposed radar. Although, it is dependent on the parameters, this can be order of tens or hundreds of microseconds. As a result, it is not possible to resolve two targets that are separated by ΔR, which is much less than tens of kilometers, in time domain.

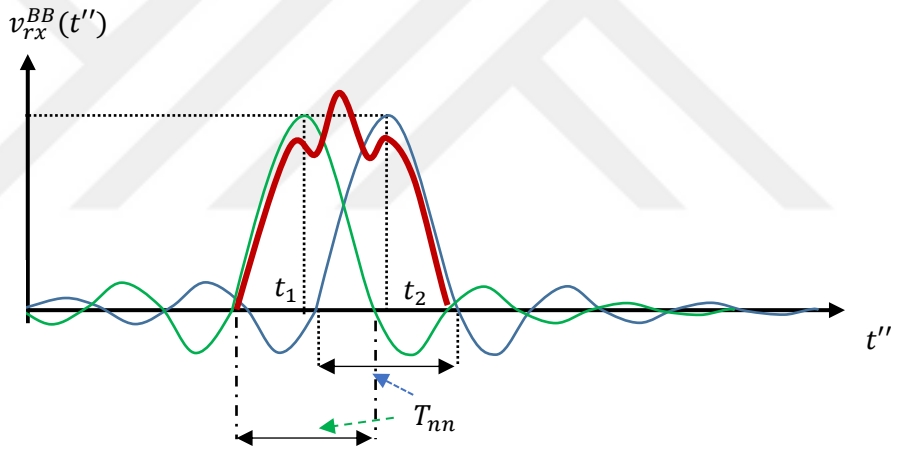

Figure 2.8. Envelope of the received waveforms

Green and blue signals on the Figure 2.8 are the received voltage, when the single point target is located at P_1 and P_2 respectively. If two identical point scatterers are located at P_1 and P_2 points, which are illustrated on the Figure 2.7, the red envelope is likely to be shown instead of the green and the blue voltage waveforms. Therefore, it would not be possible to decide the positions of the targets by using time domain envelope of the received voltage.

The range of the target can be determined by using frequency response of the voltage reflected to the receiver antenna. The beat frequency of the baseband signal at the output of the low-pass filter is calculated as in Eq-2.24. If there was no frequency diversity, that signal would have been composed of single tone sine. However, instantaneous frequency bandwidth, which is at the transmitter aperture, has been reflected back from the point scatterer. That has been shown as "$\frac{\Delta f}{\tau} T_{fill}$", where $T_{fill} = (N-1)T_l$. Figure 2.4 can provide useful illustration, in order to understand better the physical meaning of the instantaneous frequency bandwidth, which is also given on Eq-2.25.

$$\Delta f_{ins} = \frac{\Delta f}{\tau} T_{fill} = \frac{\Delta f}{\tau} (N-1) T_l \qquad 2.25$$

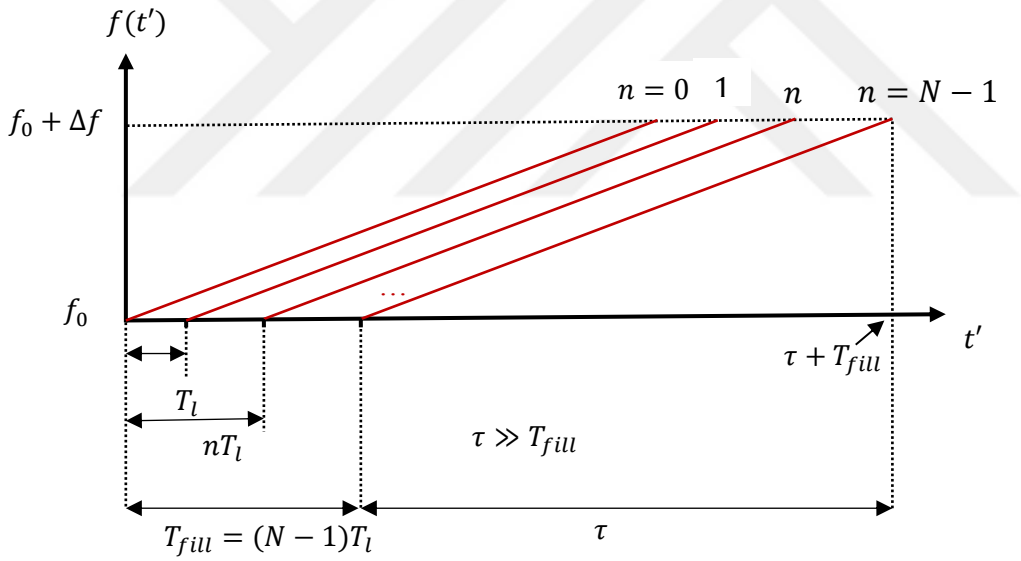

Figure 2.9. Instantaneous frequencies of the LFMCW transmitter antennas with respect to retarded time

The difference in the range brings the frequency difference along to the resulting baseband signal. Because the received signal from the first scatterer has bandwidth, the second scatterer should be separated by enough distance in order to cause

separable beat frequency. One can determine the lowest possible range between the separable targets as in Eq-2.26-2.28

$$f_{beat}(R_2) - f_{beat}(R_1) \; > \Delta f_{ins} = \frac{\Delta f}{\tau}(N-1)T_l \tag{2.26}$$

$$\frac{\Delta f}{\tau}\frac{2}{c}(R_2 - R_1) \; > \Delta f_{ins} = \frac{\Delta f}{\tau}(N-1)T_l \tag{2.27}$$

$$\Delta R \; > \frac{c}{2}(N-1)T_l \tag{2.28}$$

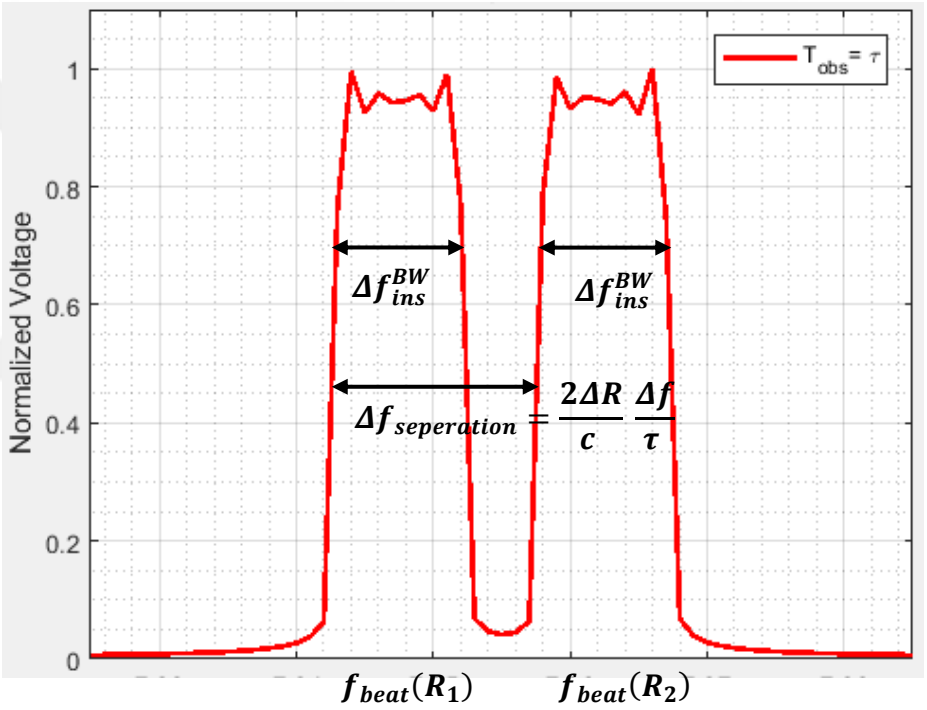

Figure 2.10. Frequency Spectrum of the baseband received signal

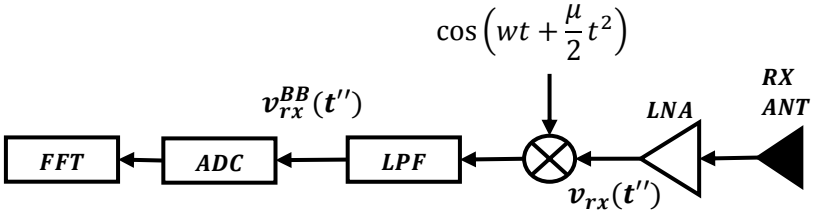

Figure 2.11. The Flow diagram of the receiver

An approach for resolving the targets is explained above. However, the range resolution is dependent on not only the instantaneous bandwidth but also the observation time for the targets located along same line. The output of FFT block on the Figure 2.11 has limited frequency resolution, due to the nature of FFT algorithm [42]. The smallest frequency step in the frequency domain, δf_{res}, can be defined by Eq-2.29. The observation time, T_{obs}, can be considered as the total pulse duration, τ. Then, the resolution in frequency domain would be $\frac{1}{\tau}$, which is usually in order of a few kHz. However, the direction of the main beam changes with time in the pulse duration. Therefore, energy on target is less than the case with the stationary radiation pattern. And, the observation time can be considered as the null-to-null time, T_{nn}. That makes the frequency resolution greater, but it gives better power levels in the frequency spectrum.

$$\delta f_{res} = \frac{1}{T_{obs}} \tag{2.29}$$

2.2.2 Angle Resolution ($\Delta\theta$)

Angle of a target with LFMCW-FDA has been decided in time domain. In another approach for estimating angle of the target is that one can deploy the phased array antenna as a receiver. Angle resolution would be dependent on the beam width of

the receiver phased array. Furthermore, estimation of AoA can be dependent on the radar properties. In this part, three different methods will be introduced without going into too many details for determining angle resolution. However, only one of them will be used in next sections. Frequency response of the signal captured by the single receiver antenna will be utilized in the proposed radar.

2.2.2.1 Phased Array Receiver

An electronically steered array (ESA) can be used to estimate the angle of arrival (AoA) of the reflected signal from the target. A phased array receiver would be able to increase the gain of the receiver and contribute advantages for the AoA process with higher SNR. Therefore, even though, there is self-scanning transmitter's radiation pattern with S-shapes, overall two-way beam pattern of the radar could be controlled by the PA receiver. Moreover, AoA estimation would be straight forward as in many examples in the literature. The angle resolution could be improved by using the PA receiver significantly depending on the chosen array, because, vital parameter would be beamwidth in total radiation pattern of the radar. The number of element in the RX array determines the radiation pattern of the PA, thus, half power beam widths of the two-way pattern. Without using any estimation algorithm such as MUSIC, LMS, maximum likelihood, etc., half power beam width could be considered as the angle resolution of the radar. This type of receiver is not in the scope of this work for the linear LFMCW-FDA. To have complete and low-cost example without using phased array, a single antenna receiver will be considered and evaluated for the linear array.

2.2.2.2 Single Antenna Receiver

Instead of the phased array receiver, low cost single receiver antenna can be used to exploit the advantages of the LFMCW-FDA. Then, the receiving signal is strongly

related to the fields on a target due to the LFMCW based FDA transmitter. The impinged signal on the observer at $P(r_0, \theta_0, \phi_0)$ is found as below equation.

$$\bar{E}_t(r,t) \cong \frac{\bar{\xi}(\theta_0, \phi_0, f_0)}{r_0} s\left(t - \frac{r_0}{c}\right) e^{j\left(w_0 t' + \frac{\mu}{2}(t')^2 - \frac{N-1}{2}\Psi\right)} \frac{\sin\left(N\Psi/2\right)}{\sin\left(\Psi/2\right)} \quad 2.30$$

$$\Psi = (w_0 + \mu t')\left(T_l - \frac{d\cos\theta_0}{c}\right) \quad 2.31$$

When isotropic antennas are used in transmitter array, magnitude of electric field multiplied with the distance can be written as below in order to find the beam width of radiation pattern.

$$|r_0 \bar{E}_t(r,t)| \cong \left| s\left(t - \frac{r_0}{c}\right) e^{j\left(w_0 t' + \frac{\mu}{2}(t')^2 - \frac{N-1}{2}\Psi\right)} \frac{\sin\left(N\Psi/2\right)}{\sin\left(\Psi/2\right)} \right| = \left| \frac{\sin\left(N\Psi/2\right)}{\sin\left(\Psi/2\right)} \right| \quad 2.32$$

$$\Psi|_{\theta=\theta_0} = (w_0 + \mu t_0)\left(T_l - \frac{d\cos\theta_0}{c}\right) = 2\pi p, \quad p \in \mathbb{Z} \quad 2.33$$

$$\Psi|_{\theta=\theta_0 \mp \frac{\theta_{Null-Null}}{2}} = (w_0 + \mu t_0)\left(T_l - \frac{d\cos\left(\theta_0 \mp \frac{\theta_{Null-Null}}{2}\right)}{c}\right) = 2\pi p \mp \frac{2\pi}{N}, \quad p \in \mathbb{Z} \quad 2.34$$

$\Delta\theta$, the 4dB beam width can be defined as half of $\Psi|_{\theta=\theta_0 + \frac{\theta_{Null-Null}}{2}}$

$$\Psi|_{\theta=\theta_0 \mp \frac{\Delta\theta}{2}} = (w_0 + \mu t_0)\left(T_l - \frac{d\cos\left(\theta_0 \mp \frac{\theta_{Null-Null}}{2}\right)}{c}\right) = 2\pi p \mp \frac{\pi}{N}, \quad p \in \mathbb{Z} \quad 2.35$$

$$(w_0 + \mu t_0)\left(\frac{d\cos(\theta_0)}{c} - \frac{d\cos\left(\theta_0 + \frac{\Delta\theta}{2}\right)}{c}\right) = \frac{\pi}{N} \quad 2.36$$

$$\cos(\theta_0) - \cos\left(\theta_0 + \frac{\Delta\theta}{2}\right) = \frac{c\pi}{Nd(w_0 + \mu t_0)} \quad 2.37$$

$$\cos(\theta_0) - \cos(\theta_0)\cos\left(\frac{\Delta\theta}{2}\right) + \sin(\theta_0)\sin\left(\frac{\Delta\theta}{2}\right) = \frac{c\pi}{Nd(w_0 + \mu t_0)} \quad 2.38$$

If narrow beam is assumed, one can write $\cos\left(\frac{\Delta\theta}{2}\right) \cong 1$ and $\sin\left(\frac{\Delta\theta}{2}\right) \cong \frac{\Delta\theta}{2}$, therefore $\Delta\theta$, the 4dB beam width, as in below equation.

$$\Delta\theta = \frac{2\pi\, c}{Nd(w_0 + \mu t_0)\sin(\theta_0)} \quad 2.39$$

2.2.2.3 Correlation Receiver

Angle resolution can be determined by radiation pattern beam width as in the previous section. Moreover, in the LFMCW based FDA may have another possibility to detect a target. In this type of radar, whereas different frequencies impinge on target, the band width of the received signal is limited by the array parameters. That can be called as frequency coding with respect to angle as well. Although, all frequency components radiated by the array to every point in space, strength of field changes with the array factor and time. In other words, some of the frequency components can be observed by an observer with significant strength, whereas the

rest can be sensed with lower power due to FDA pulse envelope. That is directly related to the radiation pattern of the transmitter array, which is changing with time. Therefore, reflected signal from a far-field target has information of the angular location which is embedded into the frequency as well.

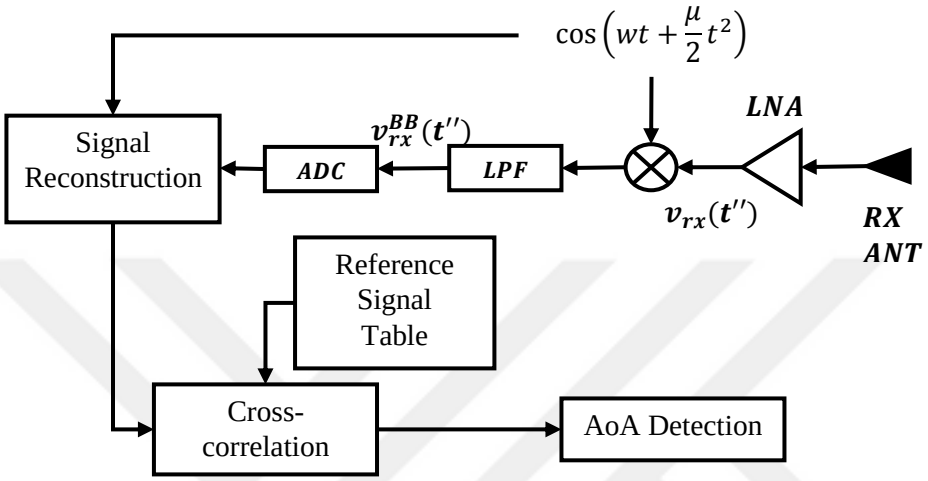

Figure 2.12. The Flow diagram of the receiver

A matched filtering is known to be the method that maximizes the output peak signal-to-mean-noise ratio, in the presence of the white noise on the input signal [43]. One can divide LFM pulse into different parts and use these piecewise portions for AoA determination by applying cross-correlation with the received signal. Rough illustrations of the envelope, frequency, signal itself and the resulting cross-correlation were given in the Figure 2.13 for LFM example from [44]. Whereas time offset, T_d, gives the radial distance $r_0 = \frac{cT_d}{2}$, comparison of the cross-correlation with the reference signals from the look-up table would give the AoA. Although, this approach is an implementable for the proposed radar, previous approach will be used in this work.

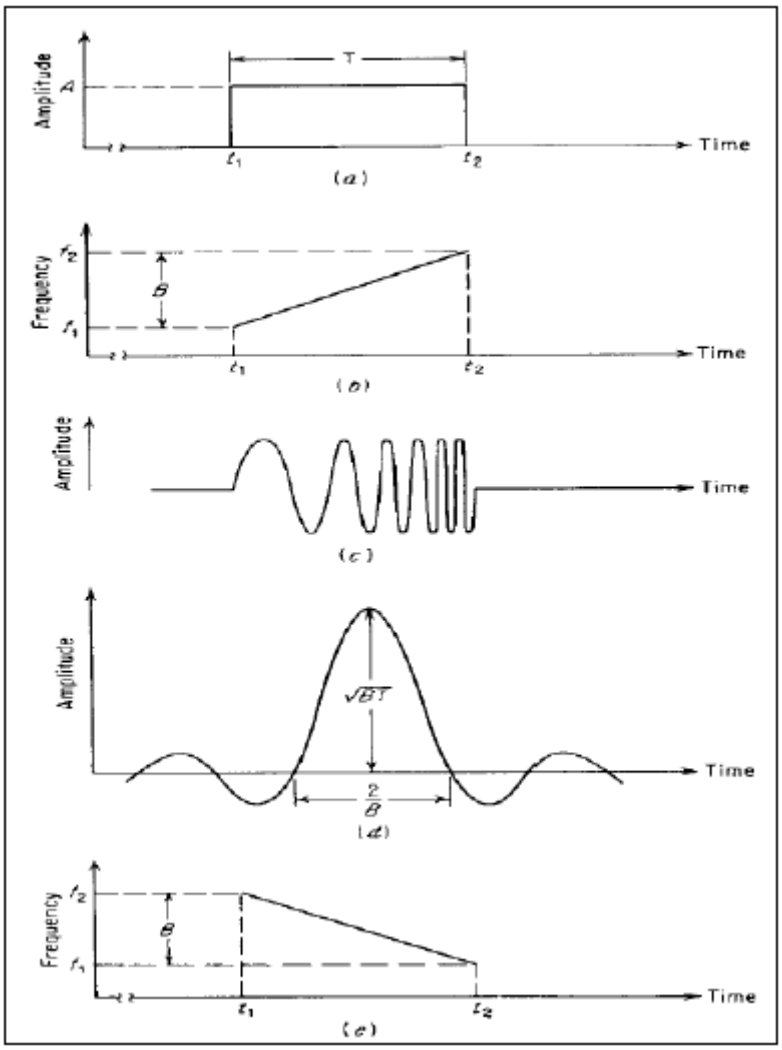

Figure 2.13. LFM Pulse Compression with Matched Filter Example from [44]

2.2.3 Proposed DF Method

This method relies on both frequency and time domain calculations. It is explained explicitly in the previous parts that range should be determined in the frequency domain, because time domain so-called pulse duration, T_{nn}, leads range resolution in km range. On the other hand, this $sinc-like$ envelope can still be useful for determining the angle-of-arrival (AoA).

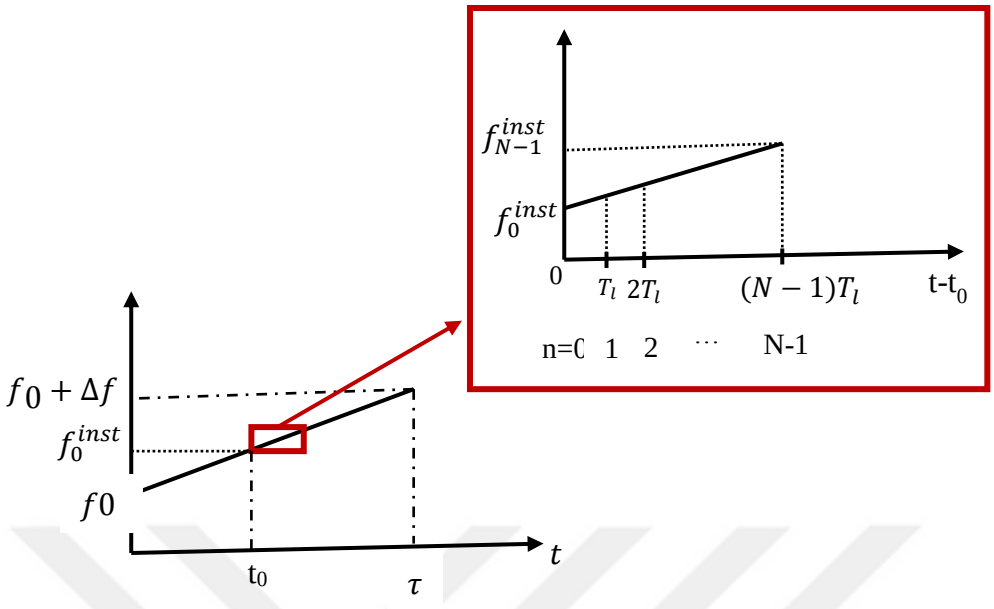

Figure 2.14. Frequency of LFMCW with respect to time

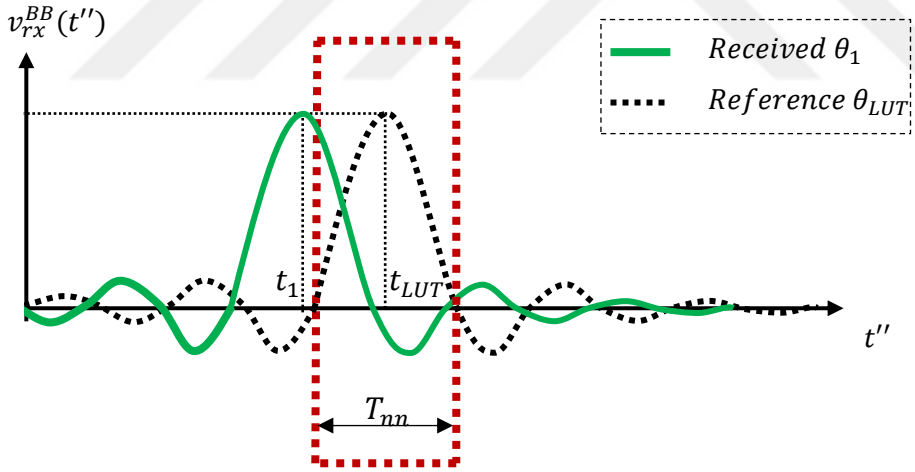

Figure 2.15. Received voltage envelope due to the target at $P_1 = (r_1, \phi = 90^o, \theta_1)$ whose peak is at $t'' = t_1$ does not coincide with the DF reference signal from LUT

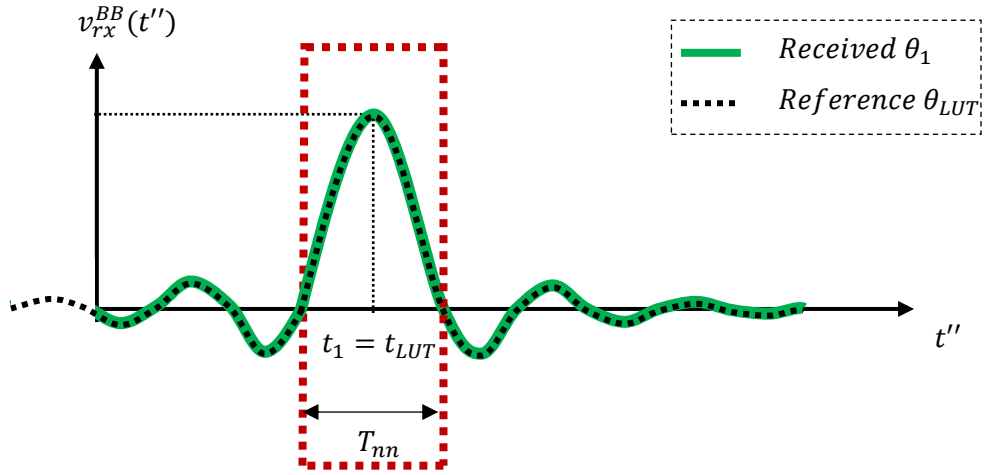

Figure 2.16. Received voltage envelope due to the target at $P_1 = (r_1, \phi = 90^o, \theta_1)$ whose peak is at $t'' = t_1$ coincides with the DF reference signal from LUT

Build-up time that is time of received waveform maximum can be determined for each angle separately in the presence of a single point scatterer. After acquiring the baseband signal, a sliding window whose length is T_{nn} , is taken into the FFT algorithm. Expected main lobe of the signal is illustrated on the Figure 2.15 and Figure 2.16 with the black dotted lines. Also, the green solid lines show the received waveform due to point scatterer on the far field point P_1, that lies on xy-plane. Weighting coefficients for FFT window are chosen as the envelope of the main lobe of the reference signal. In other words, the sliding window is equivalent to beam steering for two-way radiation pattern. Therefore, one can determine the presence of a target along corresponding angle by calculating the energy in the window. It can be interpreted that there would be side lobes as well. That will be illustrated in next sections with numerical examples. Another way of the AoA estimation can be possible in frequency domain together with the range. Range determination is nothing but the changing frequency axis with the distance by applying the below equation. This is simple beat frequency calculation for general LFMCW radars.

$$\mathrm{R_{det}} = \frac{c\tau}{2\Delta f} f_{beat} \qquad 2.40$$

2.2.3.1 Range-Angle Ambiguity

In the proposed LFMCW-FDA concept, the two-way radiation pattern is not linear along range. The two-way radiation pattern contains transmit pattern of the LFMCW-FDA and omnidirectional receiver. Spiral like pattern would seem as S shape, if the radiation pattern was plotted in rectangular coordinates with range and angle instead of the polar coordinates. Therefore, there is the range-angle ambiguity for the DF application in this concept. The

Figure 2.17 shows the possible range-angle ambiguity that shows the concept better. There are two far field point scatterers at different angles and ranges defined by P_1 and P_2. The estimation of the AoA is made by using the time of the maximum point. With the fact that s-shape radiation pattern, one could realize that different target positions may result in same build-up time, that makes impossible to determine the exact angle. However, the LFM signal brings advantage of the range determination independent from the angle. Procedure stays same until the step of range determination in the frequency domain with presumed angle. After finding the exact range, one could determine the angle with one more iteration. Even though, there are many target positions that may result in same maximum timing, unique pair can be found with the known range. That is one of the outstanding advantages of the LFMCW-FDA concept.

The steps of the procedure could be summarized as the following flow;

i. Assume target lays on $r = 0$ distance, for angle estimation process.
ii. Find the AoA that maximizes the received energy window with weightings found from $sinc$ function's main lobe envelope
iii. Find the frequency response of the given window by taking FFT
iv. Apply decision making algorithm if any target is detected
v. The radial distance can be found by the beat frequency with the Eq-2.40

Then one could find the exact location with corrected/compensated angle as in the Figure 2.17. Because the ambiguity curve lies along the two-way radiation pattern.

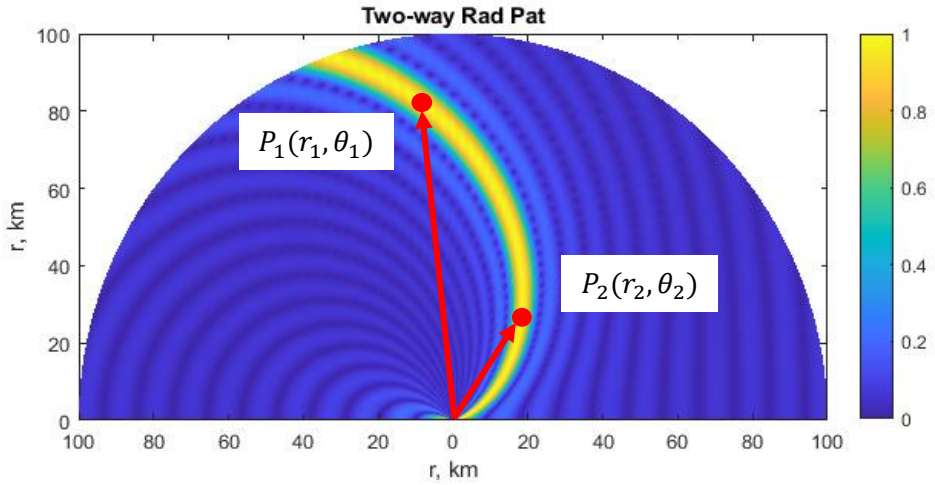

Figure 2.17. Example two-way pattern with LFMCW-FDA transmitter and the omnidirectional receiver that contains the angle-range ambiguity illustration

2.2.4 Example and Simulations Results

Two examples for the implementations of the proposed method is given in this section. Two different arrays with different number of antenna elements is considered by leaving rest of the parameters same. The example with 32 elements array will be used for the comparison with an example from literature, which is known as spatially modulated radar. In this section, received signal, which is obtained from simulations, will be processed in time domain and the frequency domain from different types of target combinations. Therefore, target-locating process with the proposed set-up will be detailed by the realistic examples. Used parameters in the simulations are given on the Table 2.2.

2.2.4.1 Linear TX Array with 16 antenna elements and omnidirectional RX antenna

In this section, simulation results obtained by using LFMCW-FDA transmitter composed of 16 elements and a single omnidirectional antenna receiver are given. Receiver unit illustrated in the Figure 2.11. As it can be seen in the figure, a direct

conversion receiver is utilized. The reflected RF signal is captured by the antenna and down converted by multiplying with the LFM signal, which is coherent local oscillator of the radar. Then, it passes through low-pass filter, in order to obtain only low frequency component of the mixer output. The base band IF signal is sampled by the analog-to-digital converter (ADC). Digital signal processes are applied in order to determine the locations of the targets, that is explained above.

Table 2.2 Linear Transmitter Array Parameters

Parameter	*Value*	Parameters	*Value*
N	16	Δf	15%
$Antenna$	$Isotropic$	r	$1000m$
fc	$7.84GHz$	d	$\frac{\lambda_c}{2}$
τ	$1ms$	θ	$\epsilon\,[0^0, 180^0]$
T_l	$0.51nsec$	ϕ	90^0

In first case, single point scatterer is assumed and located on the far field point $P_1: (R_1 = 1000m, \theta_1 = 90^o)$. The maximum of the received voltage is normalized for all the cases in this section. The time domain waveform of the baseband received voltage is given on the Figure 2.18. As expected, received waveform's low frequency envelope is $\sin\left(\frac{N\gamma}{2}\right)/N\sin\left(\frac{\gamma}{2}\right)$. Indeed, there is intermediate beat frequency due to the two-way propagation delay. Also, calculated range and the corresponding voltage level is given on the same figure. Range is determined by changing the frequency axis of the FFT domain defined in the Eq-2.40. This plot highlights very small range to illustrate the details of the received signal spectrum. Whole waveform with and without $sinc$ shape window weights limited with T_{nn} can be used for FFT operation. Results for both cases can be seen on the figure. Due to the frequency diversity over aperture, frequency spectrum is different from the classical LFMCW whose beat frequency is single tone for the point target.

In the second case, two targets that lie along same angular position are considered to show the range resolution performance. They are placed along boresight of the radar i.e. $\theta = 90^o$ and radial distances are $1000m$ and $1002m$. One of the limiting factor for the range resolution is the instantaneous bandwidth, as explained in the previous sections. The bandwidth occupied by the LFMCW based linear FDA is $9.2kHz$. When it is converted to range, that makes $1.17m$. Therefore, the range resolution must be greater than this value. On the other hand, range resolution is constrained by the resolution of the FFT i.e. the length of the time domain signal, types of weighting or length of weighting window. These may widen the bandwidth therefore degradation may be observed. The Figure 2.19 shows both time domain waveform and the range vs voltage plot reconstructed from the frequency response.

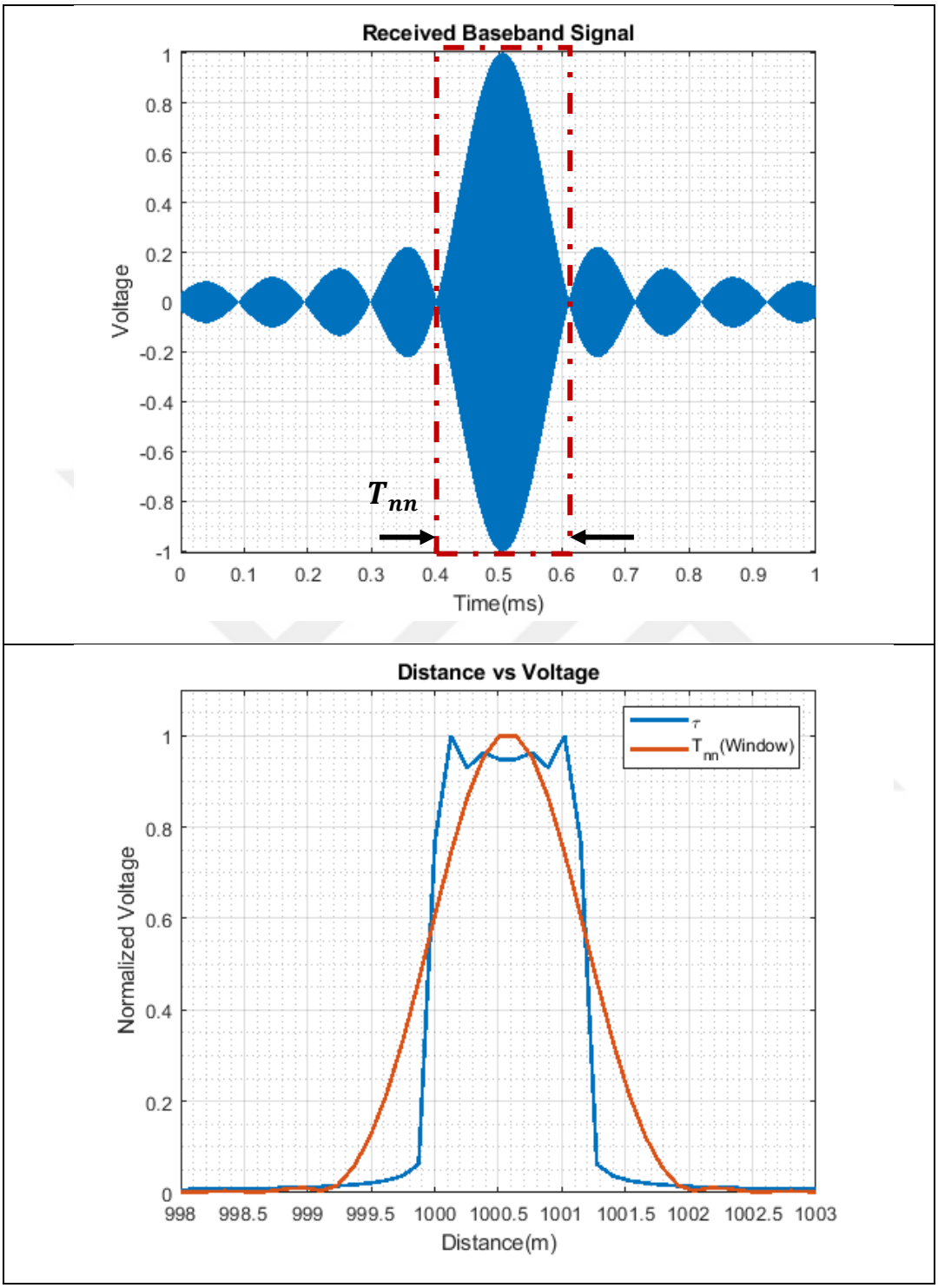

Figure 2.18. Time domain baseband received waveform and calculated range with single target located on the distance R_1=1000m with angle θ_1=90º

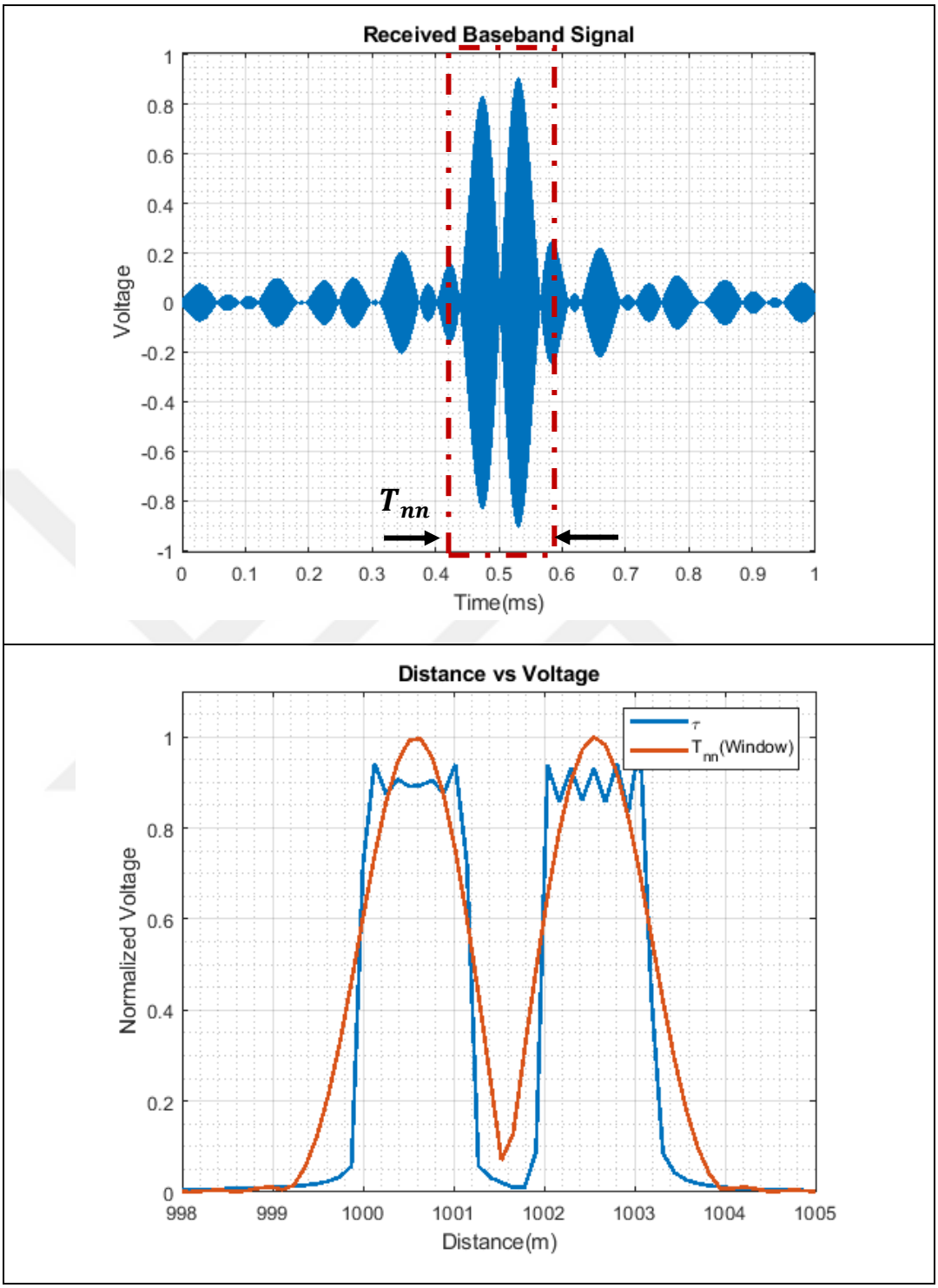

Figure 2.19. Time domain baseband received waveform and calculated range with two targets located on different distances $R_1 = 1000m$ and $R_2 = 1002m$ with same angle $\theta_{1,2}$=90º

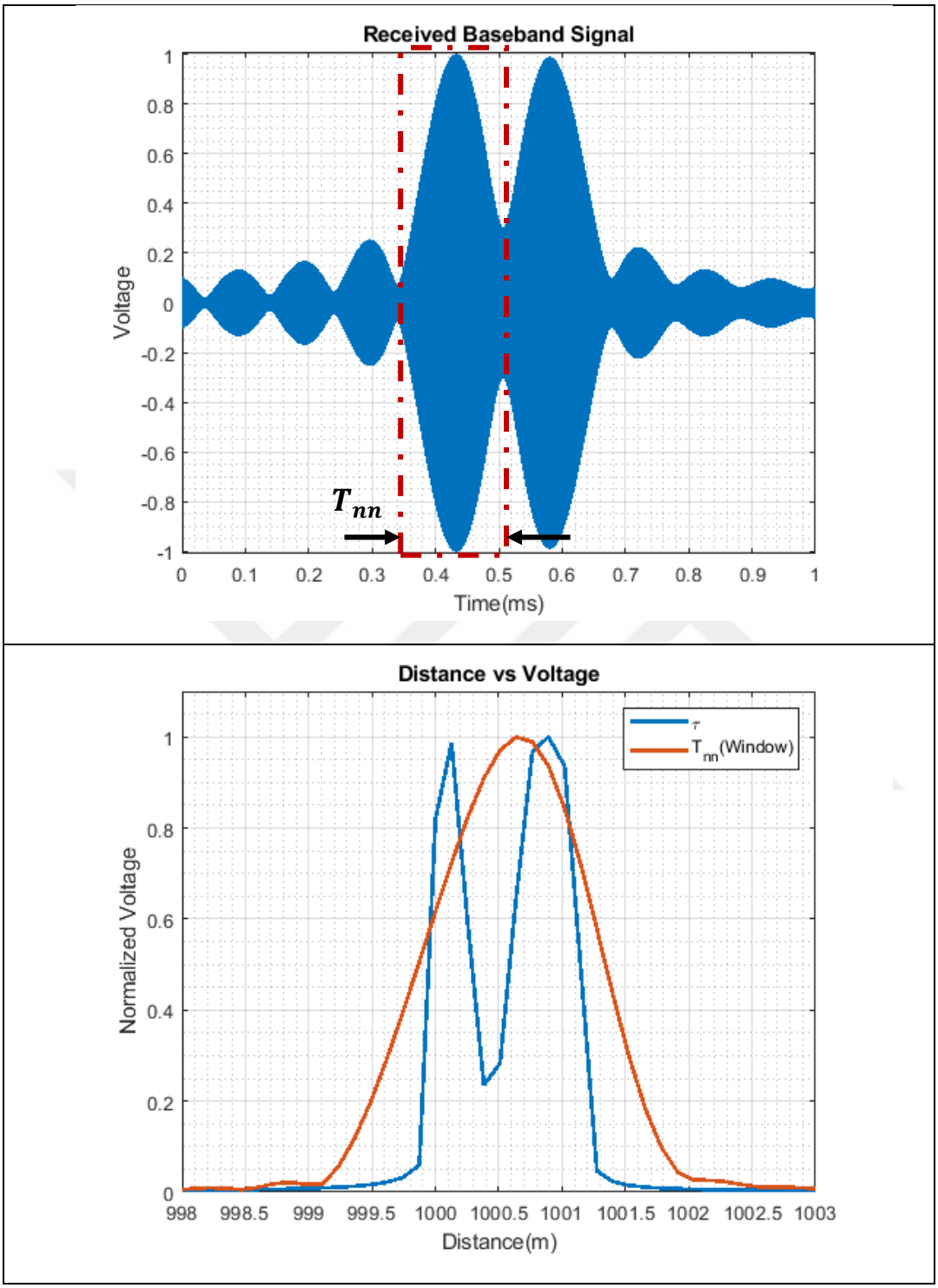

Figure 2.20. Time domain baseband received waveform and calculated range with two targets located on same distance $R_{1,2} = 1000m$ with angles θ_1=85º and θ_2=95º

The enlargement in the FD can be seen on the figure as well. Therefore, the displacement between the targets is selected as $2m$, even though smaller distance would be also possible with $3dB$ deep between targets. However, $20dB$ deep between target range estimation is accomplished in this example with $2m$ distance.

In the third case, two identical point targets are located on the same range but different angular positions. Two $sinc$ functions form the waveform as self-scanning radiation pattern takes place. The Figure 2.20 shows the reflected waveform and its range response, that was found from frequency response. Because the LFMCW-FDA scans all field of view (FOV) with a single LFM pulse, all targets are illuminated so received voltage is amplitude modulated. The effect of the amplitude modulation is also visible on the frequency response, that shows the necessity of the $sinc$ window weighted FFT. Otherwise, it is not possible to resolve these targets with the omnidirectional receiver. When the weighted frame is used, these targets can be distinguished. Below figure shows the frequency response of the part that is in red dashed lines. This frame coincides with the look angle 95^o in this example. In other words it only means that there is one target located on P_2 $(R = 1000m, \theta = 95^o)$. It does not show the possible targets along any other angles. In order to illustrate that, reconstructed radar image based on the aforementioned method will be explained with an example of multiple targets.

In the last case, five targets are located on the X shape on the ranges $995m$, $1005m$, $1000m$, $995m$, and $1005m$ with angles 80^o, 80^o, 90^o, 100^o, and 100^o respectively. The Figure 2.21 illustrates the time waveform and voltage distribution over range, that is calculated from indicated window. The framed portion of the waveform corresponds to the direction of $\theta = 100^o$. By sliding this window all over the time waveform, one can reconstruct the radar image as in the Figure 2.22. The radar image shows resolved targets by this method both in angular and spatial position.

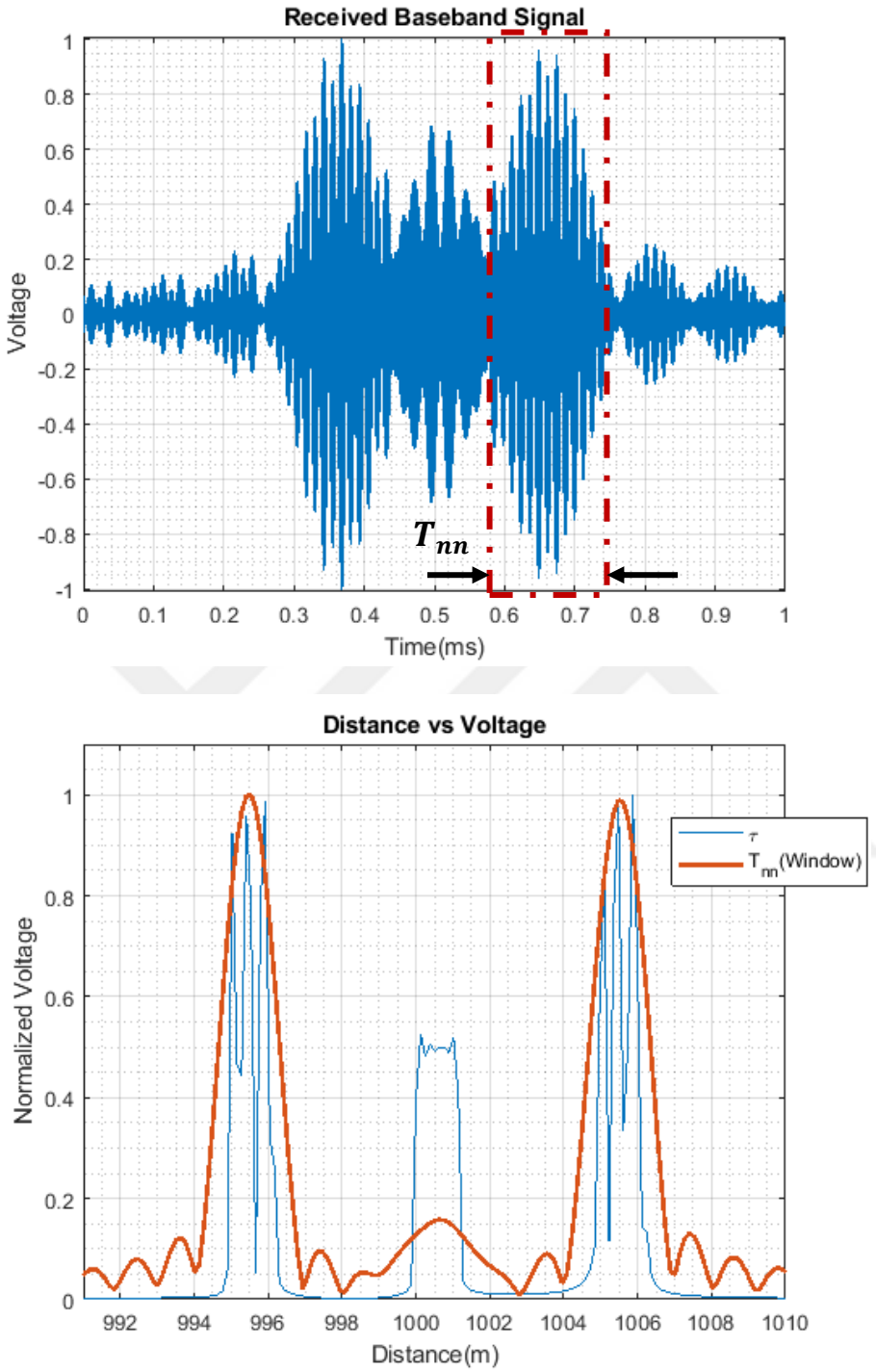

Figure 2.21. Time domain baseband received waveform and calculated range with five targets located on the ranges $995m, 1005m, 1000m, 995m, and\ 1005m$ with angles $80^o, 80^o, 90^o, 100^o, and\ 100^o$ respectively.

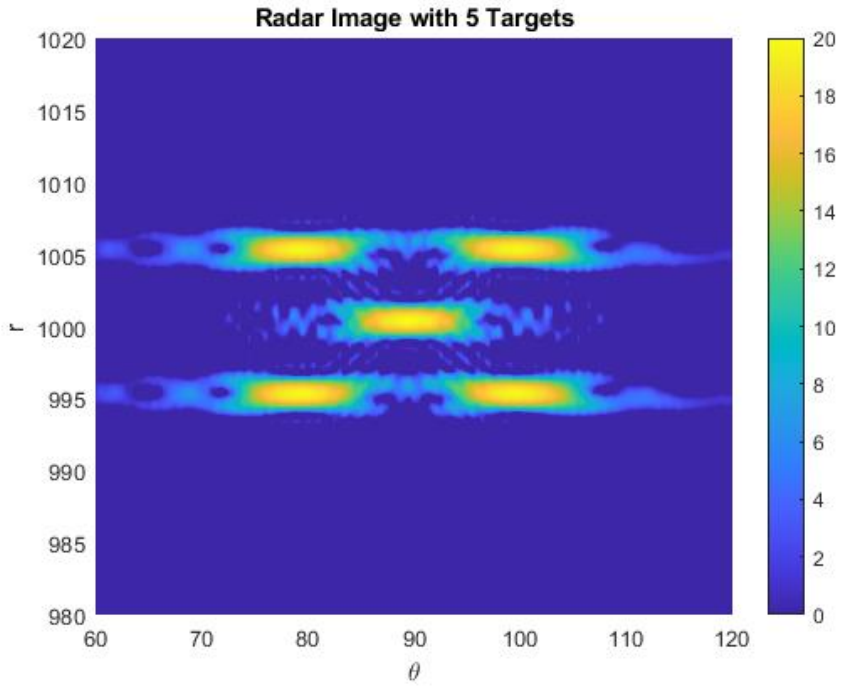

Figure 2.22. Radar image (dB) with five targets located on the ranges $995m, 1005m, 1000m, 995m, and\ 1005m$ with angles $80^o, 80^o, 90^o, 100^o, and\ 100^o$ respectively.

2.3 Conclusion

In this chapter, derivation of the transmitted fields was given starting from scratch. Transmitted field in time domain and radiation patterns have been illustrated with simulations. Spiral like shape in the radiation pattern has been observed, as it has been showed many times in the literature. Therefore, space time adaptive processing (STAP) has be considered for this type of radar. Before describing the DF method, the received voltage expression due to the reflection from the far-field target was found. The omnidirectional single receiver antenna is utilized. One could have used a PA as a receiver with digital beamforming, in order to increase gain of the receiver antenna. However, the goal of this study was to build and show the setup comprised of only LFMCW based FDA without phase shifters with single downconverter unit.

Range and angle resolutions have been found by considering the realistic signal processing steps. They are illustrated with the simulations as well. One of the accomplishments of this study is to show the DF performance of the linear array. The proposed system is able to successfully resolve different target combinations. Both definitions for angle and range resolutions have been validated by simulations in the presence of multiple targets. This method will also be used in the next chapter to compare it with the MIMO example.

CHAPTER 3

LFMCW-FDA AND SPATIALLY MODULATED RADAR COMPARISON

This chapter reviews the state of art MIMO radar example [41] from the literature by repeating some derivation steps in detail. The repetition of their work takes place in this study, because their study focuses on the benefits of the spatial modulation which is suggested as "*a biological counterpart of fixational eye movement*". The term spatial modulation stands for the creation of the radiation pattern that depends on both time and the spatial position of the observer. That types of radiation patterns are formed by the FDA as well, due to its nature. This example is not a randomly selected example. It is selected because of its similarities to the LFMCW-FDA. Obtaining intended fields costs lower with less complexity in implementation by deploying LFMCW-FDA instead of the competitor MIMO radar. Furthermore, simulation results for the DF process will be presented for the similar cases that was reported in [41]. The natural behavior of the LFMCW-FDA, that was implemented by MIMO radar by applying phase coded waveform diversity [41], has been seen as an advantage in DF applications. That complies also with the early findings of the LFMCW-FDA researches in [1], [2], [4], [11].

An attractive biological phenomenon about eye movements of human beings and animals has been researched by many scientists. In addition to gazing at an object or a point and rather slow movements to change direction, the eyes show rapid movements known as *microsaccades* [45], [46]. In Figure 3.1, the example of eye movements during fixation, *microsaccades* and *drifts* can be seen over photoreceptors.

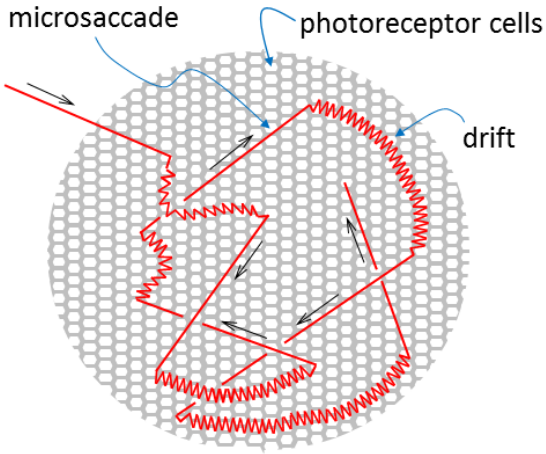

Figure 3.1. Example of eye movement during fixation [40], [41]

As a novel approach to usage of the radar waveforms, spatially modulated radar waveforms have been introduced and detailed in [40], [41] in 2014. The main inspiration of the research was declared as trying to bring the advantages of the *fixational eye movement* in visual acuity which have been presented in [47] into the radar field by applying on the approach in a Multiple Input Multiple Output (MIMO) radar. Therefore, a small perturbation in terms of the angle around the radar look angle was intended to obtain as the drafts movement of the eyes.

3.1 Spatially-Modulated Radar Waveforms Inspired by Fixational Eye Movement

This subsection is composed of the review of the work are done in [40], [41] in order to make it easy to understand the evaluation on LFMCW based FDA in terms of this approach. In the example work, a linear antenna array, which contains M antenna elements, is used. Every element is assumed to have own transmitter and receiver units in the research. That MIMO radar make it possible to radiate different waveforms from every unit at the same time, meanwhile, independent receiver units are able to effectively capture and process the received signals from the antennas.

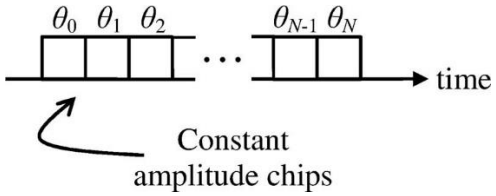

Figure 3.2. Constant Amplitude Chips of Polyphase-Coded Wave [48]

3.1.1 Polyphase-Coded FM Wave

Implementation of Polyphase-coded FM Waves was proposed with the detailed calculations and optimized in 2014 [48], [49]. A theoretical background of the implementation of the polyphase-coded FM waves will be reviewed and used for showing benefits of LFMCW based FDA.

Efficiency of the occupied frequency band in terms of bit rate has been focus of different researches. In order to have better bits per hertz (bits/Hz), the transition between two different phase states must be as smooth as possible. Therefore, continuous phase codes will be implemented. Phase states can be infinitely many on phase constellation diagram. Phase modulation can be implemented by using IQ modulation. In-phase and Quadrature components of baseband signal are realized with two different Digital-to-Analog converters on rather low-frequencies. However, instantaneous phase changes increase the spread of spectrum. Therefore, phase jumps between consecutive states within the phase codes array must be eliminated by using filter. Generic Continuous Phase Modulation block diagram for implementation can be seen in Figure 3.3.

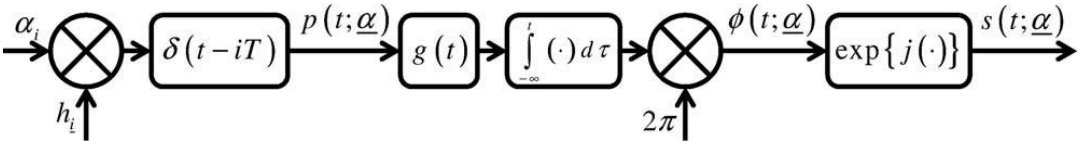

Figure 3.3. Generic CPM implementation for communication [48]

Data symbol stream, a_i is multiplied by modulation indexes, h_i. In order to obtain the stream of symbols, an impulse train whose repetition duration is T is used. Then, the sequence of weighted symbols are put into a pulse shaping filter, $g(t)$. After convolution, this time domain signal is integrated over time in order to obtain the continuous filtered pulse sequence. The shaping filter can be one of various filters such as, rectangular or raised cosine etc. The phase of the CPM signal, $s(t)$ is calculated by scaling the output of shaping filter with 2π.

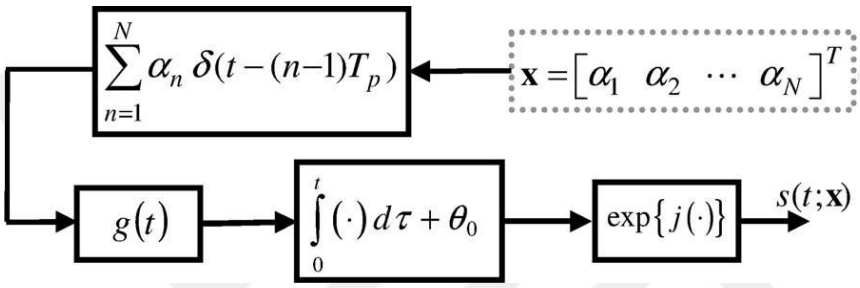

Figure 3.4. CPM Filter Proposed in [48]

The block diagram in Figure 3.4 is the block diagram of the proposed CPM implementation to generate polyphase-coded FM waveforms in [48] and the one used in [40], [41] to implement a spatially modulated radar. A linear M elements antenna array is proposed for this type of radar. Phase coded signal is composed of N phase codes. An impulse train $\sum_{n=1}^{N} \delta(\tau - (n-1)T_p)$ with phase codes a_n, which can be considered as weighting factors over total pulse duration of T, is used, that can be seen in Figure 3.5.

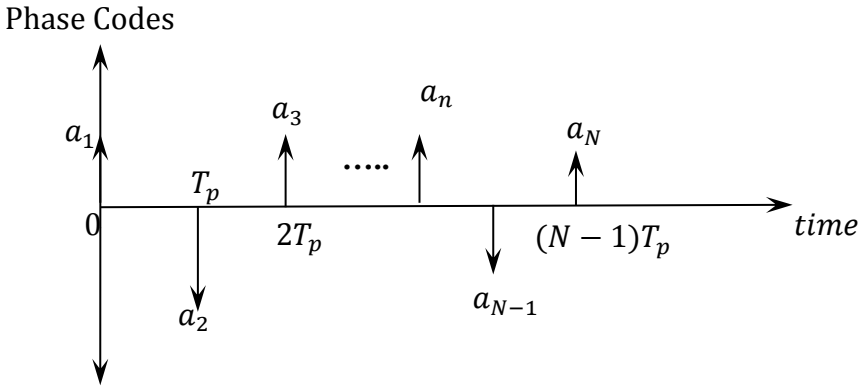

Figure 3.5. Impulse train weighted by phase codes

In order to avoid the phase jumps whose magnitudes are greater than π, the phase codes must be checked. If such phase difference between the consecutive codes occurred, the phase change must be made same on phase plot by subtracting or adding 2π as defined in Eqn-3.1.For example a phase code of $\tilde{a}_n = 8\pi/6$ must be converted to $a_n = -4\pi/6$ by subtracting 2π from itself. Another example can also be given with $\tilde{a}_n = -9\pi/6$, which must be converted to $a_n = 3\pi/6$ by adding 2π to itself.

$$a_n = \begin{cases} \tilde{a}_n & , \quad |\tilde{a}_n| \leq \pi \\ \tilde{a}_n - 2\pi\, sgn(\tilde{a}_n), & |\tilde{a}_n| > \pi \end{cases} \tag{3.1}$$

$$\tilde{a}_n = \phi_n - \phi_{n-1} \;\; for\; n = 1,2,\dots,N \tag{3.2}$$

Convolution of the shaping filter and an impulse with unity amplitude would give the shaping filter's itself. Therefore, the duration of the shaping filter must be within the single chip duration ,T_p, of the CPM signal in order to avoid interference of a phase code to neighbor chips' phase codes. There are two requirements about shaping filter that are declared in [48]. The shaping filter must integrate to unity over the real line and have time support on [0,T_p].

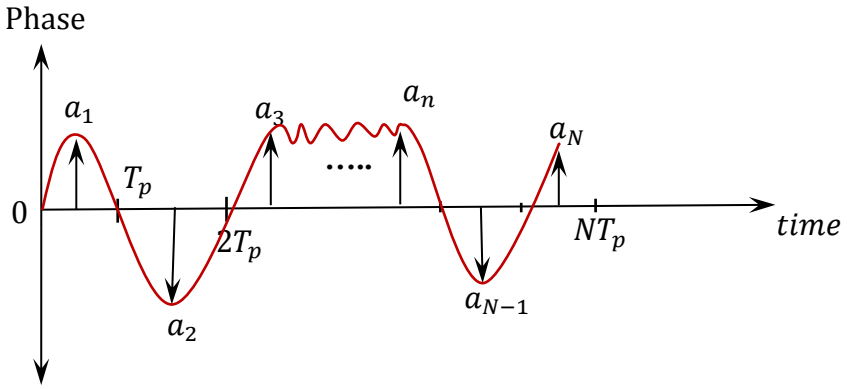

Figure 3.6. Filtered Phase Codes with Raised Cosine Filter Rough Example

A coarse sketch of the raised cosine filter output whose input is the weighted impulse train is illustrated in Figure 3.6. In order to notice peak values of filters that are equal to a_n, time axis of impulses is shifted by $T_p/2$.

$$s(t;x_w) = \exp\left\{ j\left(\int_0^t g(\tau) * \left[\sum_{n=1}^{N} \alpha_n \, \delta\left(\tau - (n-1)T_p\right) \right] d\tau \right) \right\} \qquad 3.3$$

Taking integrate the filter output over time will give the phase term of baseband signal. The integration gives the continuous function even if phase codes at the beginning are discrete values. Baseband signal, $s(t;x_w)$, for the up-converters located behind every antenna would be same, if there was no spatial modulation. That baseband phased coded signal is given in Eqn-3.3 and same at every transmitter unit's up-converter.

$$b^m\,(t;x_s) = \exp\left\{ -jm\left(\int_0^{t'} g(\tau) * \left[\sum_{n=1}^{N} \varepsilon_n \, \delta\left(\tau - (n-1)T_p\right) \right] d\tau - \Delta_0 \right) \right\} \qquad 3.4$$

In order to steer the beam to required angle, one must utilize the spatial modulation during the pulse transmission. That can be implemented to the phase codes by assigning different phases on signal radiated from each antenna element. Generally, beam steering can be done by giving linearly increasing phase to all transmitter

antenna elements on the linear antenna array. A spatial phase modulation is formulated in Eqn-3.4. According to the equation, same procedure is applied to the phase codes of the spatial modulation. "Δ_0" is the phase difference, that is required to direct the beam to the angle at the beginning of the pulse train. In other words, the baseband signal arising from spatial modulation $b^m\ (t = 0; x_s)$, which is given in Eqn-3.4 would be simplified to $e^{jm\Delta_0}$. Therefore, the maximum radiation direction can be found for the M element linear array by maximizing the function given in Eqn-3.5. Independent from the presence of the spatial modulation, initial radiation direction, $\theta_0^{initial}$, can be arranged with $\Delta_0 = kd\cos(\theta_0^{initial})$.

$$AF_{1D} = \frac{\sin(\frac{M}{2}\ (\Delta_0 - kd\cos(\theta_0))}{M\sin(\frac{1}{2}\ (\Delta_0 - kd\cos(\theta_0))} \qquad 3.5$$

Beside the initial condition on the radiation, it is possible to change the direction of the maximum radiation within overall pulse duration. Generally, the phase codes are same for every element, however inserting the progressive phases along the array elements so that the beam steering angle can be rearranged at the beginning of the chips. In Eqn-3.6, there is a term "ε_n" that is used for the beam steering during the pulse transmission. This term is calculated, regarding the required angle of the spatial modulation. Second half of the phase term in Eqn-3.6, which is coming from Eqn-3.4, is linearly increasing over the array, that can be seen the multiplication by m in this part.

$$s_m(t, \theta_c; x_w, x_s) = \frac{1}{\sqrt{T}}\sum_{m=0}^{M-1} a_m^{weighting}\ \exp\left\{j\left(\left(\int_0^{t'} g(\tau) * \left[\sum_{n=1}^{N} \alpha_n\ \delta\left(\tau - (n-1)T_p\right)\right]\ d\tau\right)\right.\right.$$
$$\left.\left. - m\left(\int_0^{t'} g(\tau) * \left[\sum_{n=1}^{N} \varepsilon_n\ \delta\left(\tau - (n-1)T_p\right)\right]\ d\tau\right) - m\,\Delta_0\right)\right\} \qquad 3.6$$

Above equation can be rewritten as in the Eqn-3.7 by reordering the phase terms and uniting the phase codes of data and the spatial modulation as $(\alpha_n - m\,\varepsilon_n)\delta$.

$$s_m(t,\theta_c;x_w,x_s) = \frac{1}{\sqrt{T}}\sum_{m=0}^{M-1} a_m^w \ \exp\left\{j\left(\left(\int_0^{t'} g(\tau) * \left[\sum\nolimits_{n=1}^{N}(\alpha_n - m\,\varepsilon_n)\delta\left(\tau-(n-1)T_p\right)\right]d\tau\right) - m\,\Delta_0\right)\right\} \quad 3.7$$

$$rE_{tx}^{MIMO-BB}(t) = \sum_{m=0}^{M-1} a_m^w\, s(t;x_w)\, b^m\,(t;x_s)\, e^{jm\frac{2\pi}{\lambda}d\cos\theta} \quad 3.8$$

The total electric field multiplied by the distance between transmitter and the target on a point scatterer target due to the proposed CPM MIMO array in [41] can be written as in Eqn-3.8 after the normalization and the scaling electric field.

Receiver of the proposed radar in [41] will be considered in this subsection. But the receiver of LFMCW FDA case is composed of the system explained in the previous chapter. Although, it is possible to implement match filtering for LFMCW FDA radar, frequency domain analysis will be considered.

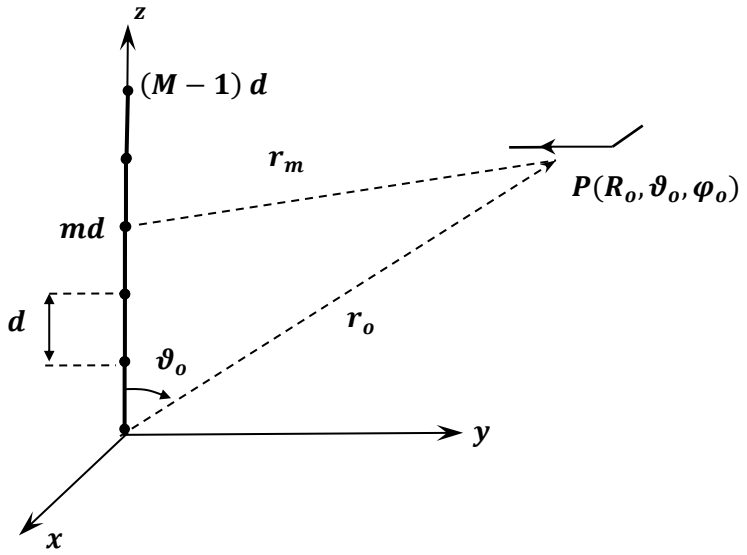

Figure 3.7. Proposed Linear LFMCW based FDA

3.2 Linear LFMCW based FDA implementation with Polyphase-Coded FM Wave

The linear array that uses LFMCW with linearly increasing true time delays between consecutive elements was proposed and evaluated in [5] and [4]. Its advantages are proven method both analytically and experimentally by [3] in terms of agility to multipath effects and the target radar cross section fluctuation characteristic. The implementation of the phase modulation is reviewed in the previous subsection, that is proposed in [40], [41], [48]–[50]. The proposed LFMCW-FDA implementation is assumed to be different from the MIMO studies, because it utilizes only delay lines instead of the separate transmitter units. However, it is still possible to modulate same baseband signal in front of each transmitter antenna at the same time with different frequencies. The LFM signal is used as the local oscillator signal for up-converter units. Because of true time delays between the local oscillators of the up converter units, the m^{th} up-converter would have delayed version of LFMCW signal, as that can be seen in Figure 3.8. Therefore, the related antenna would be radiating at the center frequency that is different from others. The frequency diversity among the elements of the array is brought into the calculations. The boxes signed with U/C are up-converter units that utilize the delayed version of the LFMCW signal as the local oscillator. These units also contain the power amplifiers to make the proposed setup more realistic. Details and design of the up converters are not in the scope of this study, indeed it is unnecessary for the implementation in the next steps. This variation of the implementation is given here only to show the similarities better.

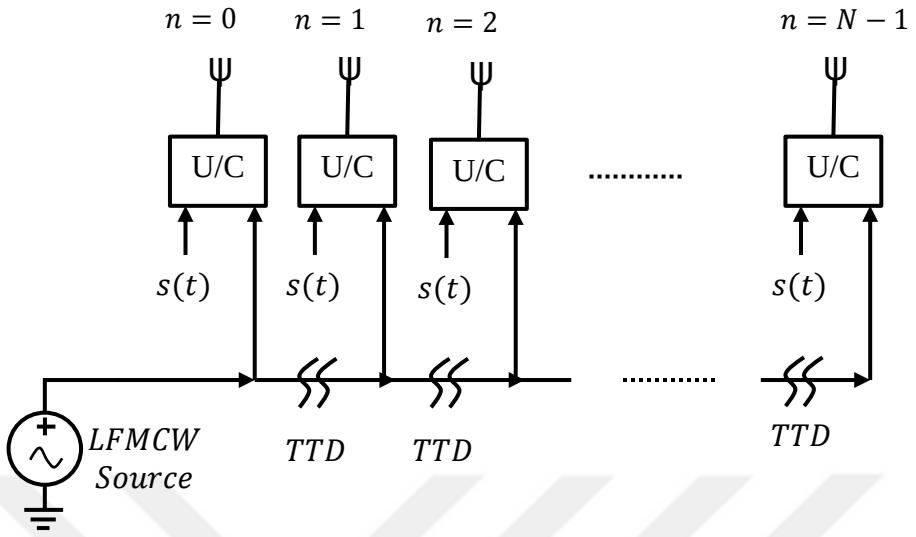

Figure 3.8. Proposed Feed Network of the CPM with Linear LFMCW-FDA

In the above figure, the CPM baseband signal is given as $s(t)$. All the up-converter units are fed by same baseband signal. Using the same signal reduce the cost of employing the M number of Digital-to-Analog Converter (DAC) to single DAC. Also that significantly decreases the burden on the processor and the complexity of the phase codes.

$$\bar{E}_t(r,t) = \sum_{m=0}^{M-1} \frac{a_m^w}{r_m}\; s_m(t, x_w)\; \bar{\xi}_m(\theta, \phi, f_m)\; e^{j\left[w_0\,(t-t_m)+\frac{\mu_0}{2}(t-t_m)^2\right]} \qquad 3.9$$

One may find the transmitted electric field by the proposed structure as in the Eq-3.9. Assuming that all elements are identical, element pattern can be taken out of the summation. Furthermore, the radial distance to far field observation point can be found different for amplitude and phase terms as in the Eq-2.4. Also, the TTD for m^{th} element is mt_d. Propagation delay from each antenna is $\frac{r}{c} - md\cos\theta$. Substituting these into the above equation, one may obtain the Eq-3.10. High

frequency term for the transmitted electric field is $e^{j\left[w_0\,(t-t_0)+\frac{\mu_0}{2}(t-t_0)^2\right]}$ which is the delayed LFM chirp by t_0.

$$\bar{E}_t(r,t)=\frac{1}{r}\bar{\xi}(\theta,\phi,f)\,e^{j\left[w_0\,(t-t_0)+\frac{\mu_0}{2}(t-t_0)^2\right]}\sum_{m=0}^{M-1}a_m^w\;s_m(t,x_w)\;e^{-jm\left(t_d-\frac{d\cos\theta}{c}\right)\left[w_0+\mu_0\left(t-\frac{r}{c}\right)\right]} \tag{3.10}$$

Omnidirectional antennas will be considered as array element. Therefore, one could omit the element pattern $\bar{\xi}(\theta,\phi,f)$ in the formulas. The baseband signal of transmitted signal with omnidirectional antenna array that is rescaled by the observer radial distance can be found as in the Eq-3.11.

$$rE_{t,Baseband}(t)=\sum_{m=0}^{M-1}a_m^w\;s_m(t',x_w)\;e^{-jm\left(t_d-\frac{d\cos\theta}{c}\right)\left[w_0+\mu_0\,t'\right]} \tag{3.11}$$

Let $w(t')\triangleq w_0+\mu_0\,t'$ and $s_m(t)=s(t)$ for all m in this topology.

$$rE_{tx}^{LFM-BB}(t)=\sum_{m=0}^{M-1}a_m^w\;s(t,x_w)\;e^{-jm\,t_d\,(w_0+\mu_0\,t')}\,e^{jm\frac{2\pi}{\lambda}d\cos\theta} \tag{3.12}$$

The total electric field multiplied by the distance on a point scatterer target or observer due to the proposed CPM LFMCW-FDA, can be written as in Eqn-3.12.

$$rE_{tx}^{MIMO-BB}(t)=\sum_{m=0}^{M-1}a_m^w\,s(t;x_w)\,b^m\,(t;x_s)\,e^{jm\frac{2\pi}{\lambda}d\cos\theta} \tag{3.13}$$

It is the main aim to compare the resulting transmitted fields, which are obtained from two different arrays. LFMCW-FDA and MIMO examples gives Eq-3.12 and Eq-3.13 respectively. One could even make equal them by having the following equality. Providing such condition makes the LFMCW-FDA a special case of the MIMO implementation.

$$b^m\,(t; x_s)\; = e^{-jm\,t_d\,(\,w_0\,+\,\mu_0\,t')} \qquad 3.14$$

It is obvious that $s(t, x_w)$ is contained by both equations. Phase differences due to the uniform phase and amplitude fed linear array are formulized by $e^{jm\frac{2\pi}{\lambda}d\cos\theta}$ depending of the electrical distance and the direction of the target. This part is also equal in both equations. "a_m^w" values are the weighting factors of the antenna array that can be used for suppress the side lobes on the radiation pattern. The MIMO solution, of course, provides more general solution to beam steering. However, the proposed LFMCW-FDA accomplishes the self-scanning property during the pulse transmission. The MIMO implementation can be simplified to the LFMCW-FDA implementation in order to show that the spatial modulation proposed in this work has different proven advantages shown by [41].

$$\int_0^{t'} g(\tau) * \left[\sum_{n=1}^{N} \varepsilon_n\,\delta\left(\tau - (n-1)T_p\right)\right] d\tau - \Delta_0 = t_d\,(\,w_0\,+\,\mu_0\,t') \qquad 3.15$$

Internal term in exponential function in Eqn-3.8 and $e^{-jm\,t_d\,(\,w_0\,+\,\mu_0\,t')}$ that is a part of Eqn-3.12 can be equalized to show the MIMO simplification to the LFMCW-FDA. That calculation is given in Eqn-3.15. On the right hand side of the equation, there is a continuous function over time. The main aim of implementation of the shaping filter, $g(t)$, on the left hand side is to obtain the continuous phase change. Therefore, this equation holds with the correct choices of the variables. Therefore, $\Delta_0 = -t_d w_0$ can be found by taking the retarded time as zero at the beginning of the first chip and pulse. Then $\varepsilon_n = t_d\,\mu_0$ can be found, which yields continuous and linear change in the resulting function. In other words, the constant rate of change of the term in the exponential function is required to validate the equation.

3.3 Example and Simulation Results

In this part simulation results from both MIMO and LFMCW-FDA will be illustrated and compared with each other. Array parameters of the LFMCW-FDA are selected

as similar as possible in the MIMO example given in [41]. The main difference between them is total frequency band occupied. Due to the nature of the LFMCW-FDA, it is more than the MIMO. Whereas spatial modulation by the phase shift in the MIMO is supplied, spatial modulation is created and increased by the frequency bandwidth of the LFM pulse in the proposed array. These parameters are almost same as the example in the previous chapter as well. Number of antenna element and frequency bandwidth are different than $M = 16$ and $\Delta f = 15\%$, in order to have higher similarity between the MIMO and the LFMCW-FDA.

Table 3.1 Array Parameters of LFMCW based linear FDA Transmitter

Parameter	*Value*	Parameters	*Value*
M	30	Δf	$0\%, 1.5\%, 3\%, 5\%$
$Antenna$	$Isotropic$	r	$200m$
f_c	$7.84GHz$	d	$\frac{\lambda_c}{2}$
τ	$1ms$	θ	$\epsilon\ [0^0, 180^0]$
t_d	$0.51nsec$	ϕ	90^0

Both radar utilizes the LFM pulse as the continuous phase modulation (CPM), which is easy to implement than some other CPM types [48]. Because it does not require a deployment of an arbitrary waveform generator (AWG), which may cost too much especially for several number of transmitters [40]. Furthermore, the LFMCW implementation costs even less than the MIMO with LFM.

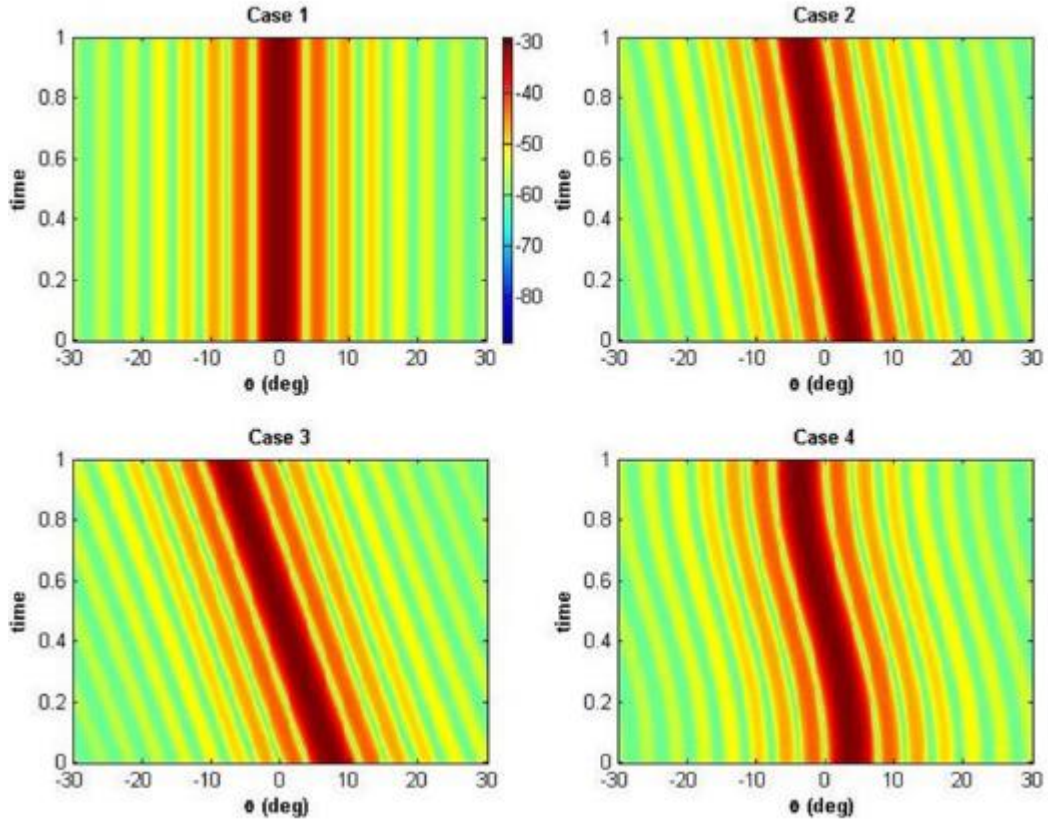

Figure 3.9. Beam Pattern vs Time in [41]

In the MIMO example, four different spatial modulations within a pulse are considered. Three of these cases can be provided by the LFMCW-FDA as well. First case is no spatial modulation and it can be implemented by using only constant frequency single tone signal in the proposed array. The radiation pattern is constant in this case. The first null beam width is used as the amount of the spatial modulation in the second case. Therefore, case 1 scans $\theta \in [-3.8^o, +3.8^o]$. The beam width of second nulls on both sides is used as the amount of the spatial modulation in the third case. These two cases utilize the linear spatial modulation, that is also available with the LFMCW-FDA. The fourth case uses the spatial modulation between the first nulls as in the first case but it changes with $sine\ function$ instead of linear $ramp\ function$. This is yet not possible to implement with the proposed method. As discussed before, this implementation is a special case for the spatially modulated MIMO example. Instead of nonlinear spatial modulation, wider beam steering will

be considered as fourth case with the LFMCW that uses 5% bandwidth. Variations of the beam pattern with respect to time are illustrated in the Figure 3.9 and Figure 3.10 for the MIMO and the LFMCW-FDA respectively. As explained above, the first 3 cases are same for both implementations. Furthermore, beam patterns are different because of the different spatial modulations in the fourth case.

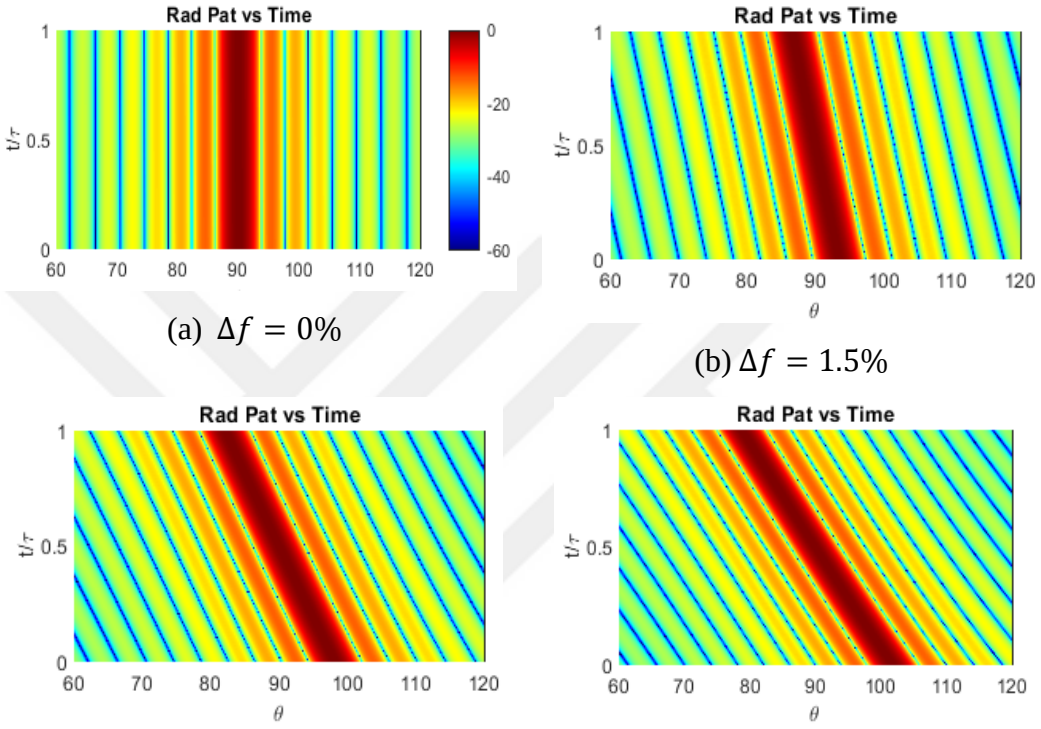

(a) $\Delta f = 0\%$ (b) $\Delta f = 1.5\%$

(c) $\Delta f = 3.5\%$ (d) $\Delta f = 5.0\%$

Figure 3.10. Beam Pattern vs Time with LFMCW-FDA

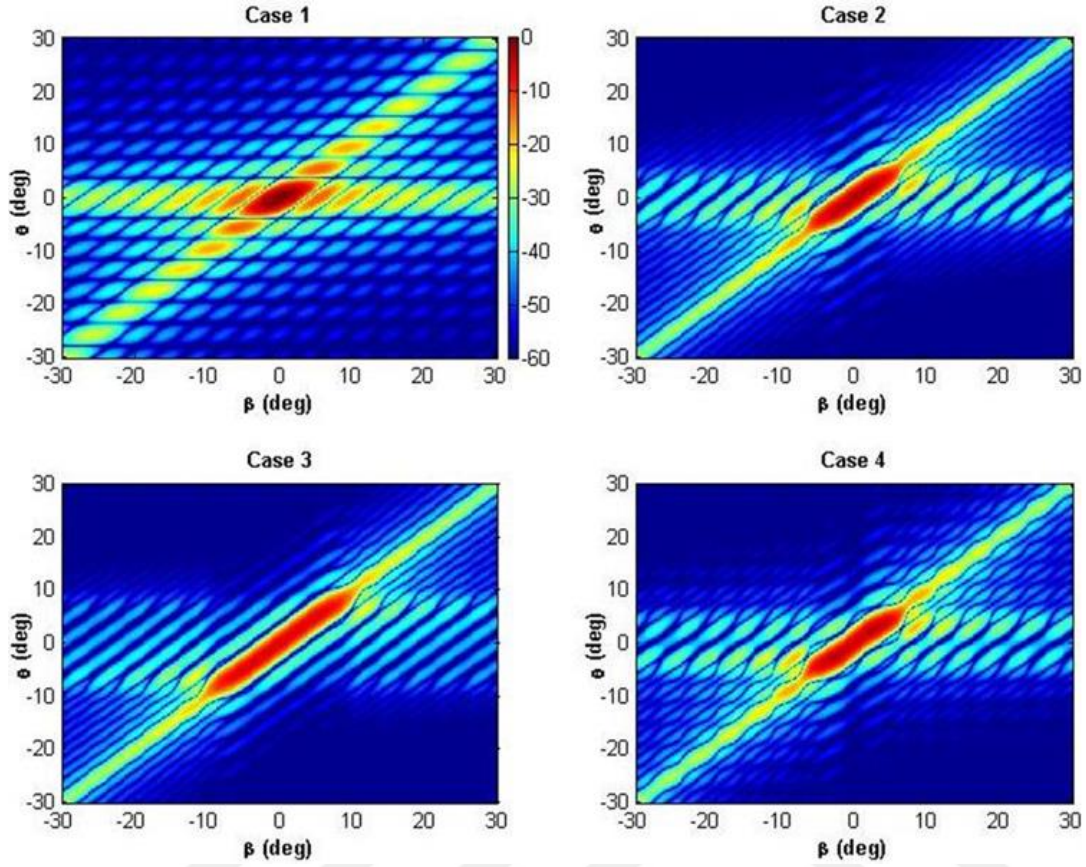

Figure 3.11. Ambiguity Function Plots in [41]

For the sake of the fair comparison, both receivers were assumed to be same as the one explained in [40]. It relies on the matched filters, that maximize the SNR in case of the system contains stochastic noise [51]. Therefore, the received waveform due to a target's presence contains the information of both angular position and the radial distance. Both can be resolved by the cross-correlating the signal with the predetermined waveform that corresponds specific target location. There is an *angle delay ambiguity function* defined in [40]. These functions are given in Figure 3.11 and Figure 3.12 for the MIMO and the LFMCW-FDA respectively. In these plots, θ describes the real angular position, whereas β represents the estimated AoA by assuming that the time delay of arrival is estimated exactly. Consequently, similarities exist also in these plots that shows the ability of the LFMCW-FDA one more time.

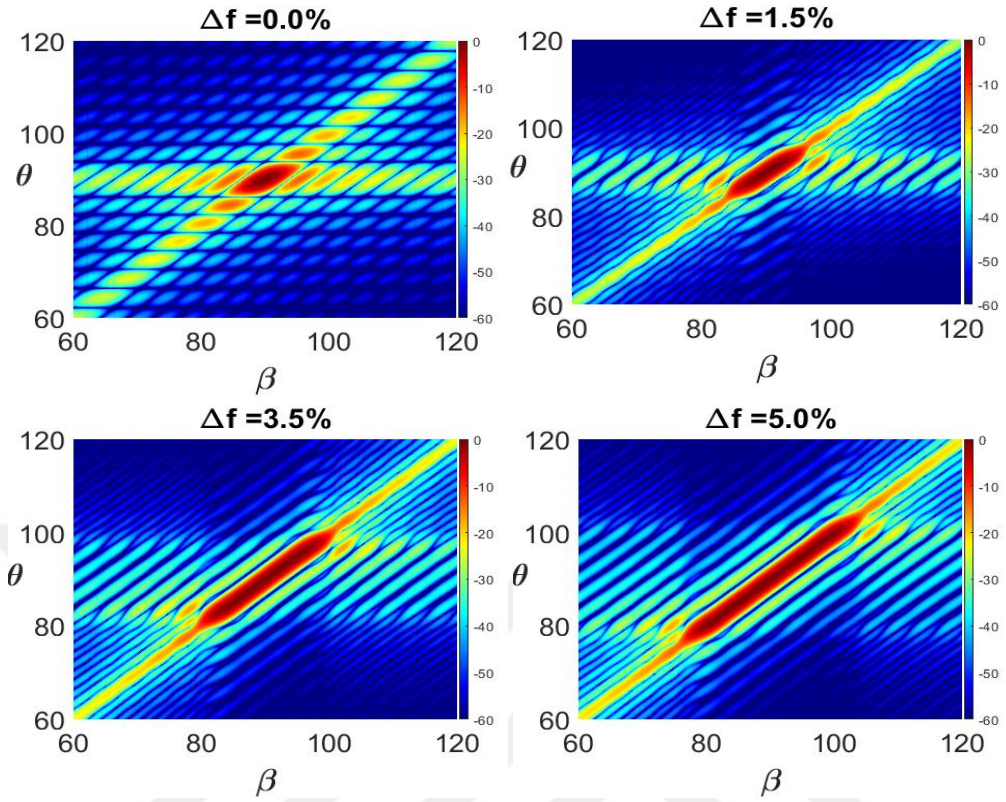

Figure 3.12. Calculated Ambiguity Function with different fractional bandwidth of the LFMCW pulses

Cut of the peak normalized ambiguity functions is illustrated in the Figure 3.13 and Figure 3.14 for the MIMO and the LFMCW-FDA respectively. These plots show the estimations of the AoA when θ is directed to boresight such that $\theta = 0^o$ for the MIMO example or $\theta = 90^o$ for the LFMCW-FDA. Furthermore, the estimations of the delay are assumed to be exactly correct. Therefore, one can see the effects of the spatial modulation explicitly on the ambiguity function. These plots also confirm that the first three cases result in same ambiguity function under aforementioned conditions. Because of the different implementations in the fourth case ambiguity functions are slightly different. The first side lobes around boresight are lower in the MIMO, it may be an advantage. However, use of 5% fractional bandwidth in LFMCW-FDA lowers the rest of the side lobes significantly. That may be counted as a benefit of the proposed system.

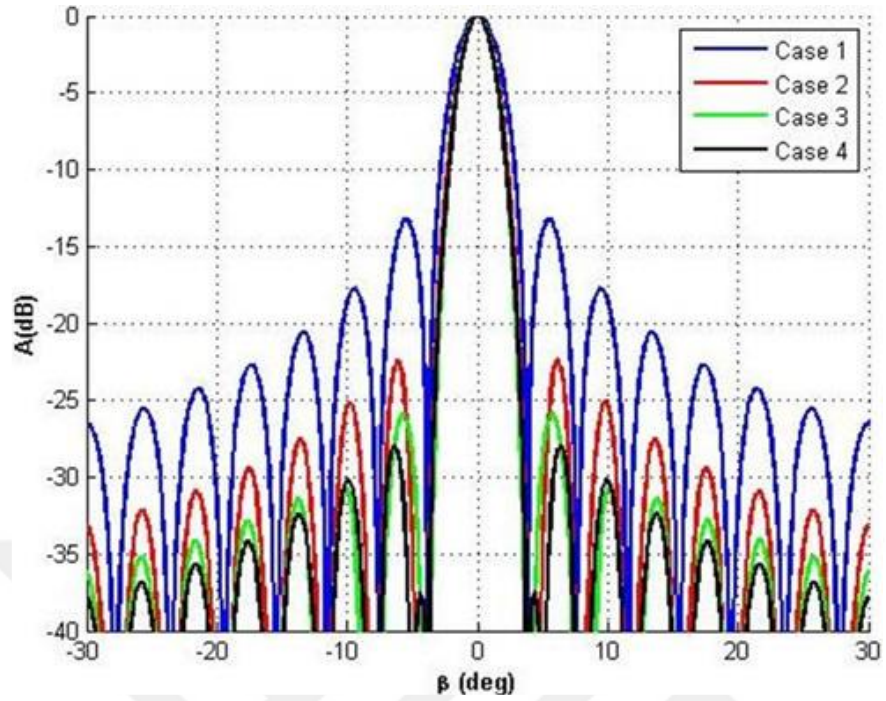

Figure 3.13. Peak-normalized t = 0, θ = 0° cut of angle-delay ambiguity function for all cases of the spatial modulations in [41]

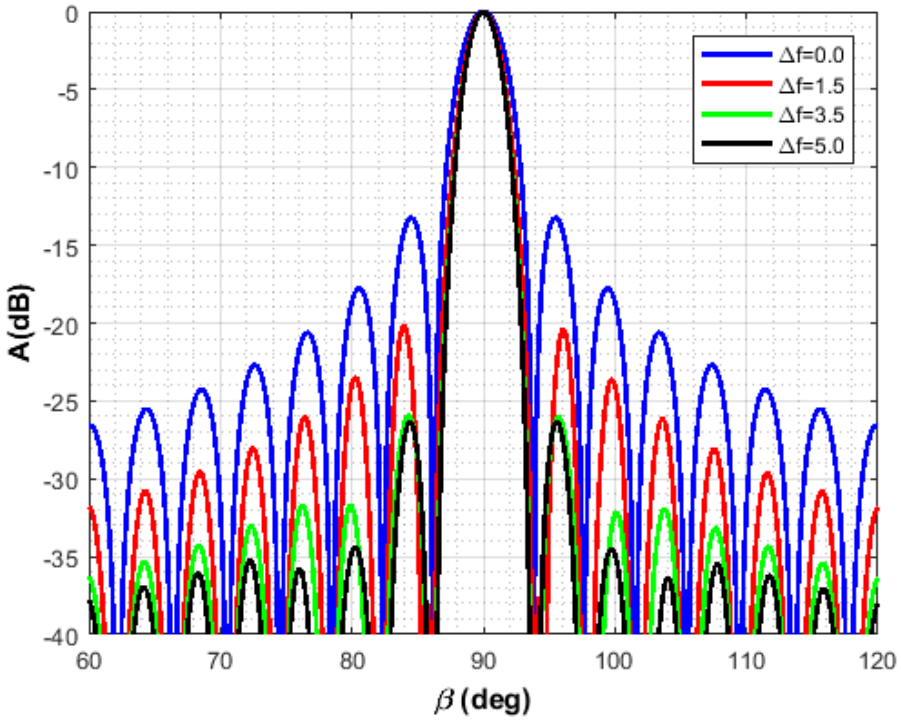

Figure 3.14. Peak-normalized t = 0, θ = 0° cut of angle-delay ambiguity function for the LFMCW-FDA with different bandwidths

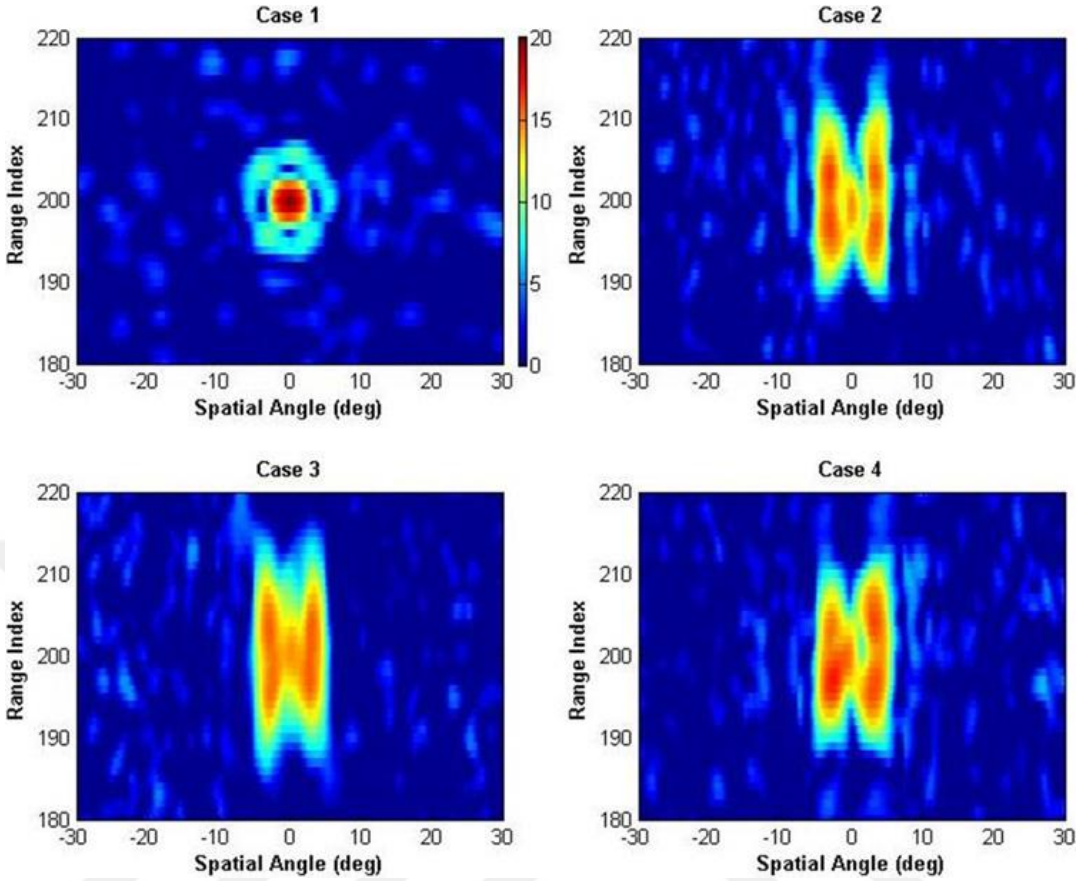

Figure 3.15. X shaped 5 target detection in [41]

Reconstructed radar images are given for both implementations in the Figure 3.15 and Figure 3.16. Radar image reconstruction method which the proposed LFMCW-FDA uses, is explained in the previous section in detail. The image is comprising of the frequency spectrum of the sliding windowed parts of the time domain received signal. It is also possible to use cross-correlation method, which is equivalent to the match filtering. However, frequency domain analysis obtained by FFT is chosen here, because it puts less burden on the computations. Furthermore, this approach is adequate for such operation that has been shown in the previous section. DF performance with the MIMO changes with the type or amount of the spatial modulation as in the above figure. The target at the boresight can be seen with no spatial modulation case. However, it is not possible to distinguish the 4 other targets around the main beam. In the Case 2, beam is steered $\pm 3.8^{o}$ around the boresight,

therefore, it gives better radar image that shows better the other 4 targets. Although, resolution in range is not still enough to distinguish the separate targets, one could realize that there are at least three different angular positions for possible targets. When the spatial modulation is raised to cover second null positions of the static radiation pattern case, range resolution is getting worse. The MIMO example utilizes the constant frequency bandwidth. Range resolution of the LFMCW radars is directly related to their frequency bandwidth [52]. On the other hand, the frequency bandwidth of the field impinged on a single far field point decreases, when the beam steers within larger angular space. Because, the radiation patterns are not constant, the bandwidth of the signal reached to the point scatterers becomes more effective on range resolution. Therefore, as the amount spatial modulation increases, the range resolution gets worse. That can be observed in the results of the MIMO Case 2 and Case 3 example as well.

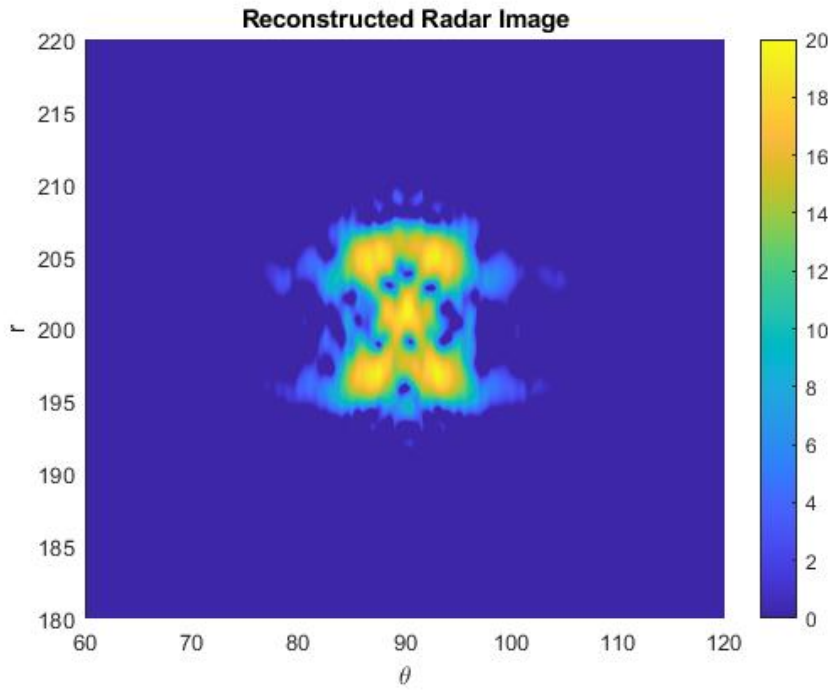

Figure 3.16. Five targets located on ranges R_1=200m, R_2=196m, R_3=196m, R_4=204m, R_5=204m with angles θ_1=90º, θ_2=87º, θ_3=93º, θ_4=87º, θ_5=93º

Reconstructed radar image by FFTs is illustrated in the Figure 3.16. Some details of this DF process are given in the following subsection. Heat map of the target locations obtained by the LFMCW-FDA shows the five targets that can be distinguished both in angular and radial locations. That is given only for one fractional frequency bandwidth. Because of the structure of the LFMCW-FDA method, frequency bandwidth that impinged on the target does not change, even if the overall frequency bandwidth of the LFM pulse increases. The increase in the occupied BW makes the scanned angular space larger. Therefore, the result does not change significantly with the higher BW pulse. However, it can be controlled by the physical structure, which is not easy to change. The useful comparison can be done by deploying the LFMCW-FDA which is able to scan whole FOV with only single LFM pulse. The proposed array with the parameters on the Table 3.1 can scan large angular space by using 15% fractional BW. This value may cause misunderstandings that it can improve the range resolution proportionally. However, the BW that is transmitted to the custom angle does not change with BW of the LFM pulse. It uses wider BW, whereas it can be implemented by only using single transmitter unit on the PCBs easily.

3.3.1 DF with Linear TX Array with 30 antenna elements and omnidirectional RX antenna

For the sake of the clarity, DF with the proposed array will be detailed in this part. All the transmitted fields are calculated on each target location. Assuming the all targets are identical with the same radar cross section (σ), the overall scattered field is calculated as described in the second chapter. The received voltage is calculated by using the same receiver as in the Figure 2.6. Then the waveform of the baseband signal is found as in the Figure 3.17. The $sinc$ function weighted window, whose duration is the half of the expected null-to-null time width, is sliding over the time in order to check the presence of any target by taking FFT of the weighted samples. Those FFT results reconstruct the radar image, that can show possible target

locations. The Figure 3.18 and Figure 3.19 illustrate the FFT results which obtained from different windows that can be seen on the Figure 3.17 with red and yellow dashed lines. Red frame shows the window location for $\theta = 90^o$ and yellow frame coincides with the reflections from $\theta = 93^o$. The resulting waveform in frequency domain is give in the next figures, by interchanging the frequency axis with the corresponding ranges. FFT of the all received baseband signal would give the frequency domain waveform with pale blue line in the both figures. As discussed in the previous chapter, it is not possible to resolve the angular location with omnidirectional receiver antenna without applying the FFT windows.

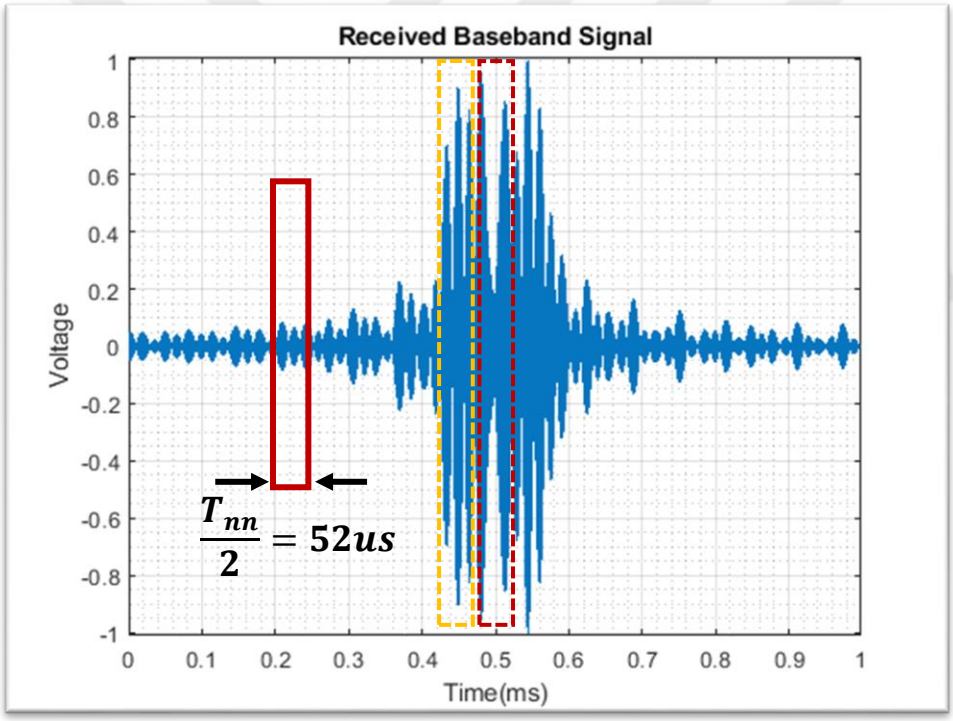

Figure 3.17. Baseband Received Signal when five targets located on ranges R_1=200m, R_2=196m, R_3=196m, R_4=204m, R_5=204m with angles θ_1=90º, θ_2=87º, θ_3=93º, θ_4=87º, θ_5=93º

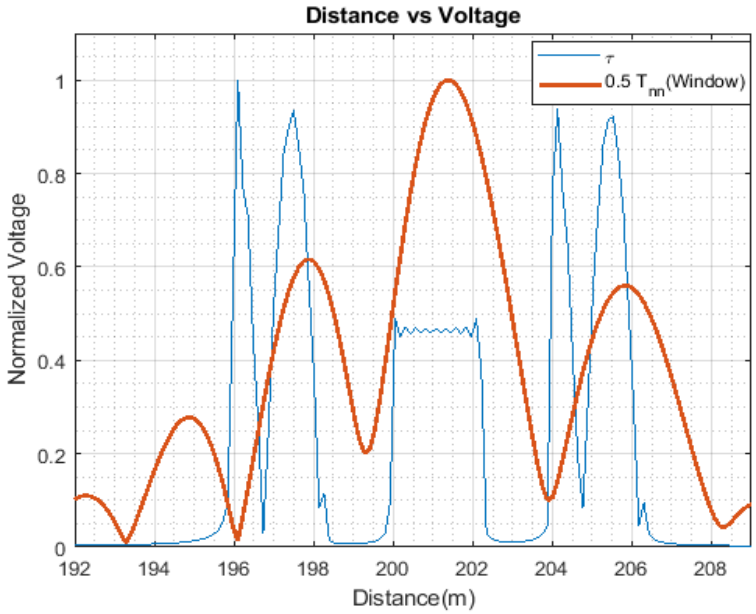

Figure 3.18. Frequency (equivalent to the range) domain for the estimated AoA ($\beta = 90^o$) in case of five targets located on X shape

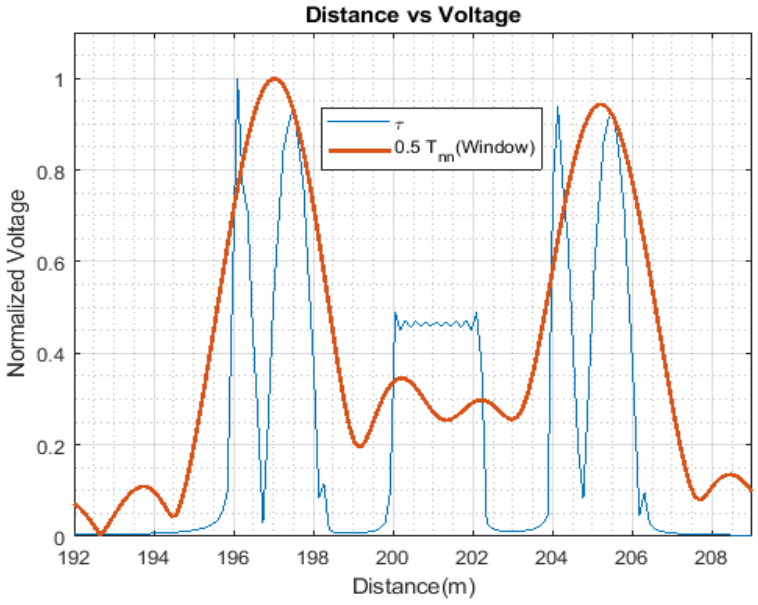

Figure 3.19. Frequency (equivalent to the range) domain for the estimated AoA ($\beta = 93^o$) in case of five targets located on X shape

3.4 Conclusion and Discussion

In the Chapter 3, the background of the spatially modulated radar approach given by [40], [41] was repeated for the sake of clarity. Therefore, similarities between this MIMO implementation and the LFMCW-FDA could be revealed. In that study, researchers have utilized 3 different types of the spatial modulation and one without spatial modulation as a reference. Three of them could be implementable with LFMCW-FDA as well. No spatial modulation is applied in the first case, that is nothing but using continuous wave without LFM as feed signal for our proposal. In the second case, spatial modulation was applied in order to steer the maximum radiation direction from one first null to the first null on the other side. The scanned space was doubled in the third case. Both spatial modulations were made of linear sweep of the spatial modulation. Due to nature of the LFMCW-FDA, deploying the chirp as radar signal brings forth same effect of the linear spatial modulation. The amount of the beam steering can also be controlled by the occupied band width of the LFM pulse. Therefore, first null-to-null linear spatial modulation was realized by using 1.5% fractional bandwidth with the given 30 elements LFMCW based linear FDA. The second null-to-null spatial modulation was accomplished by using 1.5% fractional bandwidth. Nevertheless, the complex MIMO arrays present much more flexibility than other types. Therefore, researchers made the use of the MIMO, while implementing the fourth spatial modulation that was the null-to-null half-cycle sinusoidal. It might not be possible to implement such modulation without changing some parts of the hardware of the proposed setup. Even though it could be seen as a drawback, the outstanding results obtained with the LFMCW based linear FDA has been already shown by simulations.

CHAPTER 4

LFMCW BASED PLANAR FDA RADAR

Advantages of the FDA radar are utilized by the LFMCW based FDA radars with the linear arrays in [4], [11]. These works show the beneficial usages of the linear LFMCW-FDA. Moreover, some superiorities are claimed and shown. By taking into consideration the findings in the previous chapter, its performance in DF application is comparable with the performance of the state of art radars. However, the target localization with the linear array is accomplished within only two of the three possible axis. In other words, it is able to decide the distance to the target and only one of the angles in the spherical coordinates. The decidable angle depends on the axis that the array located on. Consequently, it is just related to definition of the axes around the array and the ability of the predecessors are limited due to the nature of its structure.

The main motivation of this study is to contribute the LFMCW based FDA literature in order to reveal its abilities and potential as much as possible. 3D scanning is possible by using many conventional methods. This has been a gap in the LFMCW based FDA until this study. In order to determine exact location of the target with the LFMCW based FDA by utilizing 3D beam scanning, we have proposed a novel method in [12] that utilizes a planar array. That method will be shown to scan whole region of interest within only single LFM pulse duration, that can be properly determined with other radar parameters. This fast self-scanning feature is standing out because it makes possible to track targets with high SNR. Moreover, the feature of being low cost gets more important as number of the antenna elements increases in planar array implementation.

In this chapter, design steps and the critical points are explained starting from the LFMCW based planar FDA transmitter. The derivation for the transmitted signal by

the proposed array is given. The transmitted field that is observed at a far field point have single peak points in time domain, that is important design parameter for this study. Therefore, effects on the build-up timings are presented. Another useful derivation is for the null-to-null time widths due to x and z axis related radar parameters. These time widths can also be considered as the dwell time for the radar application that will be given in the next subsections. Then, beam steering capability of the transmitter will take place with a numerical example in order to show the possible coverage diagrams. In case of the target presence in region of interest, observed field at the origin that is reflected will be investigated with the aforementioned steps for the transmitted signal. The reflected signal is evaluated with simulation results. Finally, the proposed transmitter and the PA receiver will form the radar. This realistic radar will be evaluated by the simulations whose coverage diagram is roughly $\theta \sim 38^o \rightarrow 143^o$ and $\phi \sim 30^o \rightarrow 134^o$. The outperforming results of a canonical example are given that show the promising performance in tracking the targets with high RCS.

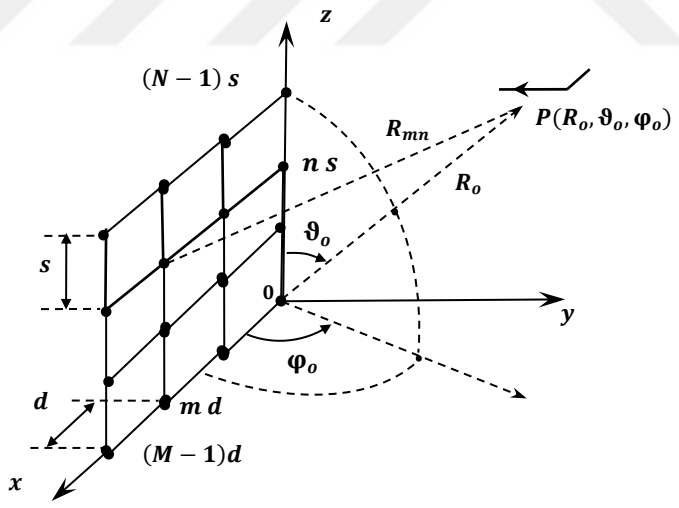

Figure 4.1. Proposed planar array with the far field target located at P

The rough sketch of the planar array can be shown on Figure 4.1 that illustrates the planar LFMCW-FDA, which consists of *M* by *N* identical antenna elements along *x*

and *z axis*. The inter-element spacing along *x-axis* is uniform and *d*, and it is also uniform and defined by *s* along *z-axis*. A single RF source feeds all the antennas with different time delays. The time delays can be realized by transmission lines or using different the oscillators whose phases are locked. It is assumed that each antenna is fed by same LFM chirp with different time delays. The time delay of the RF signal at the mn^{th} antenna element is defined as t_{mn}. That helps to derive electric fields at a far field point. However, the realization of the proposed array will be discussed in the further sections.

4.1 Transmitter signal of the planar LFMCW-FDA

Each transmitting elements of the classical FDA generally radiates single tone continuous wave signals whose frequencies are constant and different from each other. In other words, transmitting antennas have frequency diversity and their frequencies do not change. The LFMCW-FDA has been proposed by [5]. The frequency difference between consecutive elements stayed constant, whereas the frequencies of all elements are increasing linearly with time. It may also be a decreasing for a negative slope of frequency change.

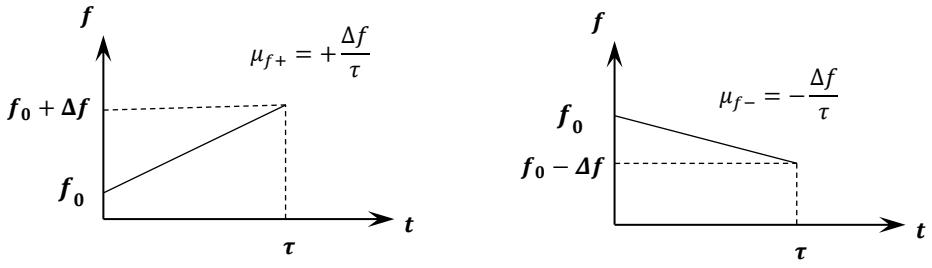

Figure 4.2. Frequency vs time graphs of the proposed waveforms with positive and negative slope

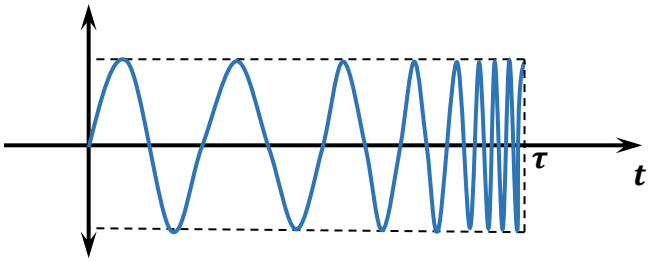

(a)

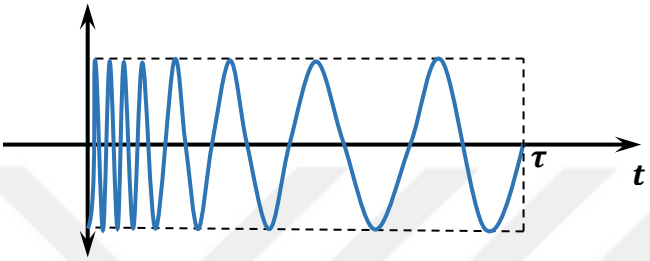

(b)

Figure 4.3. Time domain signals during the pulses that have a positive (a) and a negative (b) slope

Rough sketches of the time domain signals for both positive and negative slope pulses can be seen on the Figure 4.3. One can define a unit rectangular pulse, in order to express the LFMCW pulse mathematically. Let $P(t)$ be the unit rectangular pulse, which equals to 1 when time is between 0 and τ. And it gives zero otherwise.

$$P(t) = \begin{cases} 1, & 0 \le t \le \tau \\ 0, & t < 0 \quad or \quad \tau < t \end{cases} \tag{4.1}$$

The instantaneous frequency of the LFWCW signal can be written as in Eqn-4.2, where μ is radian slope of the LFMCW pulse. It is equal to $2\pi\mu_f, where\ \mu_f = \Delta f/\tau$ Then the phase of it can be written as in Eqn-4.3.

$$\mathrm{w}_{LFM}(t) = w_0 + \mu\, t \tag{4.2}$$

$$\Phi_{LFM}(t) = e^{j\left[w_0\, t + \frac{\mu}{2} t^2\right]} \tag{4.3}$$

4.2 Derivation of Transmitted Field by the Planar LFMCW-FDA

Derivation of the total field that is transmitted by the planar array gives transmitter radiation pattern of the proposed radar. The voltage applied on any TX antenna can be written as in the following equation, where $t_{d,mn}$ is the total true time delay. This delay is defined as the latency of the signal shown in Eqn-4.3 to the mn^{th} antenna element.

$$V_{mn}(t') = a_{mn}\ P(t'_{mn}, \tau)\ e^{\mathrm{j}(\omega_o(t-t_{d,mn}-t_p)+\frac{\mu}{2}(t-t_{d,mn}-t_p)^2)} \qquad 4.4$$

Transmitted electric field by a single element can be written as in Eqn-4.5. The distance between the transmitter antenna element and the observation point, $\mathbf{P}(\boldsymbol{R_o}, \boldsymbol{\vartheta_o}, \boldsymbol{\varphi_o})$, eventuates in the propagation delay, which can be shown by $t_p = R_{mn}/c$. The distance from the mn^{th} antenna element to the point P is R_{mn} and c is the velocity of light in free space. The vector radiation pattern is shown by $\bar{\xi}_{mn}(\theta_0, \phi_0, f_{mn})$. The pattern is dependent on the elements and the instantaneous frequency, f_{mn}, at which the corresponding element radiates.

$$\boldsymbol{E_{mn}}(r,t) = \frac{1}{R_{mn}}\ P(t'_{mn}, \tau)\ \bar{\xi}_{mn}(\theta_0, \phi_0, f_{mn})\ e^{\mathrm{j}(\omega_o(t-t_d-t_p)+\frac{\mu}{2}(t-t_d-t_p)^2)} \qquad 4.5$$

The dependence of the single antenna radiation pattern on the frequency will be omitted for further derivation. Also, it is assumed that each antenna element has same radiation pattern. These two assumption yield the simplification of the vector radiation pattern as in the following equation.

$$\bar{\xi}_{mn}(\theta_0, \phi_0, f_{mn}) \cong \bar{\xi}(\theta_0, \phi_0) \qquad 4.6$$

The distance between the mn^{th} antenna to $\mathbf{P}(\boldsymbol{R_o}, \boldsymbol{\vartheta_o}, \boldsymbol{\varphi_o})$ can be written as in the Eqn-4.7. The location of the antenna is expressed by $\boldsymbol{r'_{mn}}$, whereas $\boldsymbol{R_o}$ is the position of the observer.

$$\boldsymbol{R_{mn}} = \boldsymbol{R_o} - \boldsymbol{r'_{mn}} \tag{4.7}$$

The inter-element spacing between consecutive elements are *d* and *s* along *x-axis* and *z-axis* respectively and they are assumed to be constant. Then, one can rewrite the terms in the Eqn-4.7 in terms of the unit vectors of $\hat{\boldsymbol{a}}_{\boldsymbol{x}}, \hat{\boldsymbol{a}}_{\boldsymbol{y}}, and\ \hat{\boldsymbol{a}}_{\boldsymbol{R}}$.

$$\boldsymbol{r'_{mn}} = md\ \hat{\boldsymbol{a}}_{\boldsymbol{x}} + ns\ \hat{\boldsymbol{a}}_{\boldsymbol{y}} \tag{4.8}$$

$$\boldsymbol{R_o} = R_0\ \hat{\boldsymbol{a}}_{\boldsymbol{R}} \tag{4.9}$$

$$\begin{aligned} \hat{\boldsymbol{a}}_{\boldsymbol{x}} &= \sin\theta_0 \cos\phi_0\ \hat{\boldsymbol{a}}_{\boldsymbol{R}} + \cos\theta_0 \cos\phi_0\ \hat{\boldsymbol{a}}_{\boldsymbol{\theta}} - \sin\phi_0\ \hat{\boldsymbol{a}}_{\boldsymbol{\phi}} \\ \hat{\boldsymbol{a}}_{\boldsymbol{y}} &= \sin\theta_0 \sin\phi_0\ \hat{\boldsymbol{a}}_{\boldsymbol{R}} + \cos\theta_0 \sin\phi_0\ \hat{\boldsymbol{a}}_{\boldsymbol{\theta}} + \cos\phi_0\ \hat{\boldsymbol{a}}_{\boldsymbol{\phi}} \\ \hat{\boldsymbol{a}}_{\boldsymbol{z}} &= \cos\theta_0\ \hat{\boldsymbol{a}}_{\boldsymbol{R}} - \sin\theta_0\ \hat{\boldsymbol{a}}_{\boldsymbol{\theta}} \end{aligned} \tag{4.10}$$

The propagation delay of a signal, t_p is dependent on the position of transmitter antenna and was defined as $t_p = R_{mn}/c$. Then, R_{mn} can be written for delay terms as in the Eqn-4.11, when the classical far-field approximations are employed. The dependence on the m and n terms must be considered in the calculations for delay terms. On the other hand, one can ignore these terms for a far-field observation point for amplitude terms, the Eq-4.12 holds.

$$\begin{aligned} R_{mn} = |R_0\ \hat{\boldsymbol{a}}_{\boldsymbol{R}} - md\ \hat{\boldsymbol{a}}_{\boldsymbol{x}} + ns\ \hat{\boldsymbol{a}}_{\boldsymbol{z}}| \cong \\ R_0 - md\sin\theta_0\cos\phi_0 - ns\cos\theta_0 \end{aligned} \tag{4.11}$$

$$R_{mn} \cong R_0 \tag{4.12}$$

$$\begin{aligned} u_x &\triangleq \sin\theta_0\cos\phi_0 \\ u_z &\triangleq \cos\theta_0 \end{aligned} \tag{4.13}$$

In order to determine the total delay of the signal that is transmitted by the mn^{th} element, a feed network must also be defined. For more general solution, linearly increasing true time delays along each axis were assumed and proposed in this work. In other words, the time delay in the path that lays between the LFMCW source and

the mn^{th} transmitter is increasing linearly with both m and n values. The constant rate of change in the TTDs are T_{lx} and T_{lz} along x-axis and z axis respectively.

$$t_{d,mn} = mT_{lx} + nT_{lz} \tag{4.14}$$

Then, the total time delay can be found as in the Eqn-4.15. By substituting that value into the Eqn-4.5, one may get the following equation for the total delay of the electric field at the far field point due to the single TX antenna.

$$t_{td,mn} = mT_{lx} + nT_{lz} + \frac{(R_0 - m\,d\,u_x - n\,s\,u_z)}{c} \tag{4.15}$$

By rearranging the equation with respect to m and n values, the following equation would be useful for the further derivations. Also, the term of R_0/c is equal for every antenna within the array. Therefore, one can define a retarded time at the observation point as $t' = t - R_0/c$. Then total time delay in terms of the retarded time would be as the following formula.

$$t'_{td,mn} = m(T_{lx} - \frac{d\,u_x}{c}) + n(T_{lz} - \frac{s\,u_z}{c}) \tag{4.16}$$

$$\boldsymbol{E_t}(r,t) = \frac{\xi(\theta_0,\phi_0)}{R_0} \sum_{m=0}^{M-1} \sum_{n=0}^{N-1} \left\{ P\left(t' - t'_{td,mn}, \tau\right) e^{j\left\{\omega_o\left(t' - m(T_{lx} - \frac{d\,u_x}{c}) + n(T_{lz} - \frac{s\,u_z}{c})\right) + \frac{\mu}{2}\left(t' - m(T_{lx} - \frac{d\,u_x}{c}) - n(T_{lz} - \frac{s\,u_z}{c})\right)^2\right\}} \right\} \tag{4.17}$$

The total electric field transmitted from the planar array can be written as in the Eqn-4.17. However, it is not easy to have an interpretation of the resulting electric field expression intuitively, due to the complexity of it. One could make use of it by simplifying it with approximations, in order to exploit it as easily as possible. Firstly, duration of the pulse function could be selected as 1 msec. When the longest aperture delay ,which could also be called as aperture filling time, $T_{fill} = T_{lx}(M-1) + T_{lz}(N-1)$, and is around a few tens of nanoseconds, is compared with the duration of the pulse, it can be neglected for the argument of the pulse function.

$$P\left(t' - t'_{td,mn}, \tau\right) \cong P(t', \tau) \tag{4.18}$$

The second part of the phase term in the Eqn-4.17 still has complex terms that hinder the simplified solution. To manipulate the phasor term, it is useful to define new variable which make representations easier.

$$\begin{aligned} \nu_{ox} &= f_0\left(T_{lx} - \frac{d\,u_x}{c}\right) = f_0 T_{lx} - \frac{d}{\lambda_0}u_x \\ \nu_{oz} &= f_0(T_{lz} - \frac{s\,u_z}{c}\ ) = f_0 T_{lz} - \frac{s}{\lambda_0}u_z \end{aligned} \tag{4.19}$$

$$\left(t' - m\frac{\nu_{ox}}{f_0} - n\frac{\nu_{oz}}{f_0}\right)^2 = t'^2 - mt'\frac{2\nu_{ox}}{f_0} - nt'\frac{2\nu_{oz}}{f_0} + m^2\frac{\nu_{ox}^2}{f_0^2} + 2mn\frac{\nu_{ox}\nu_{oz}}{f_0^2} + n^2\frac{\nu_{oz}^2}{f_0^2} \tag{4.20}$$

By making use of the Eqn-4.19 and 4.20, one can manipulate the Eqn-4.17, in order to obtain exponential function separated into different parts with respect to their dependencies on *m* and *n* terms. This dependency can be classified into three groups. First group has relation with neither m nor n. The second group is linearly dependent on either m or n. Components of the third and the last group are function of one of the following terms, m^2, n^2 or mn. The phase terms in the third group, which are not linear function of m and n, may be ignored in the calculations, since they are bounded by the value of $\pi\ x\ 10^{-3}$.

$$\begin{aligned} \frac{\mu}{2}m^2\frac{\nu_{ox}^2}{f_0^2} = \frac{2\pi\Delta f}{2\tau}m^2\frac{\nu_{ox}^2}{f_0^2} &\le \pi(M-1)^2\frac{\Delta f}{\tau}\left(T_{lx} + \frac{d}{c}\right)^2 < \pi\ x\ 10^{-3} \\ \mu\, mn\frac{\nu_{ox}\nu_{oz}}{f_0^2} &\le 2\pi\ \frac{\Delta f}{\tau}\ (M-1)(N-1)\left(T_{lx} + \frac{d}{c}\right)\left(T_{lz} + \frac{s}{c}\right) < \pi\ x\ 10^{-3} \\ \frac{\mu}{2}n^2\frac{\nu_{oz}^2}{f_0^2} &\le \pi(N-1)^2\frac{\Delta f}{\tau}\left(T_{lz} + \frac{s}{c}\right)^2 < \pi\ x\ 10^{-3} \end{aligned} \tag{4.21}$$

Therefore, their contribution to the phase of the inside of the summation will be negligible. Exponential components could be taken as one, for further simplified demonstrations as in the Eq-4.22.

$$\exp\left\{j\frac{\mu}{2}m^2\frac{v_{ox}^2}{f_0^2}\right\} = \exp\left\{j\pi M^2\frac{\Delta f}{\tau}\left(T_{lx}+\frac{d}{c}\right)^2\right\} \cong 1$$
$$\exp\left\{j\mu\, mn\frac{v_{ox}v_{oz}}{f_0^2}\right\} = \exp\left\{j2\pi\,\frac{\Delta f}{\tau}\,(M-1)(N-1)\left(T_{lx}+\frac{d}{c}\right)\left(T_{lz}+\frac{s}{c}\right)\right\} \cong 1 \qquad 4.22$$
$$\exp\left\{j\frac{\mu}{2}n^2\frac{v_{oz}^2}{f_0^2}\right\} = \exp\left\{j\pi(N-1)^2\frac{\Delta f}{\tau}\left(T_{lz}+\frac{s}{c}\right)^2\right\} \cong 1$$

$$\boldsymbol{E_t}(r,t) = \boldsymbol{A}'(t')\sum_{m=0}^{M-1} a_m\, e^{-\mathrm{jm}\,(\omega_o+\mu t')(T_{lx}-\frac{d\,u_x}{c})}\sum_{n=0}^{N-1} b_n\, e^{-\mathrm{jn}\,(\omega_o+\mu t')(T_{lz}-\frac{s\,u_z}{c})} \qquad 4.23$$

where

$$\boldsymbol{A}'(t') = \frac{\boldsymbol{\xi}(\theta_0,\phi_0)}{R_0}P(t')e^{\mathrm{j}\left\{\omega_o t'+\frac{\mu}{2}\,t'^2\right\}} \qquad 4.24$$

After having the simplified form, the summations can be written independently and, uniform excitation over array is assumed. Therefore, they can be illustrated as the known $digital\ sinc$ functions.

$$\boldsymbol{E_t}(r,t') = \boldsymbol{A}'(t')\,e^{\mathrm{j(M-1)}\frac{\gamma_x}{2}}\,\frac{\sin\left(\frac{M\gamma_x}{2}\right)}{\sin\left(\frac{\gamma_x}{2}\right)}\,e^{\mathrm{j(N-1)}\frac{\gamma_z}{2}}\,\frac{\sin\left(\frac{N\gamma_z}{2}\right)}{\sin\left(\frac{\gamma_z}{2}\right)} \qquad 4.25$$

where

$$\gamma_{\mathrm{x}}(t') = -2\pi\,\nu_{ox}\left(\frac{t'}{T_f}+1\right);\quad \gamma_z(t') = -2\pi\,\nu_{oz}\left(\frac{t'}{T_f}+1\right) \qquad 4.26$$

ν_{ox} and ν_{oz} were given in the Eqn-4.19. $T_f = f_0/\mu_f$. Exponential phasor terms can also be taken into $\boldsymbol{A}(t') = \boldsymbol{A}'(t')\,e^{\mathrm{j(M-1)}\frac{\gamma_x}{2}}\,e^{\mathrm{j(N-1)}\frac{\gamma_z}{2}}$. During the investigation of the overall transmitted field, a meaningful focus must be on the magnitude of the fields

which is a function of the retarded time. The magnitude of the field is dependent on both parameters along x and z axis, i.e. $T_{lx}, T_{lz}, d, s, \theta_0 \; and \; \phi_0$. It eases the handling with the expressions, that dividing the equation into two parts. These two functions give their maximum values, when $\gamma_x(t_{0x}) = 2\pi p$ and $\gamma_z(t_{0z}) = 2\pi q$ and $p, q \in \mathbb{Z}$.

$$\mathrm{F_M} = \frac{\sin\left(\frac{M\gamma_x}{2}\right)}{\sin\left(\frac{\gamma_x}{2}\right)} \; ; \qquad \mathrm{F_N} = \frac{\sin\left(\frac{N\gamma_z}{2}\right)}{\sin\left(\frac{\gamma_z}{2}\right)} \tag{4.27}$$

4.3 Time of maximum field occurred at a point $(\boldsymbol{R_0}, \boldsymbol{\theta_0}, \boldsymbol{\phi_0})$

Occurrence of a peak field strength is an essential term for beam scanning in radars. In other words, the beam steering is that the change in direction of the maximum radiation in phased arrays. One of the biggest differences in FDA fields is that the location of the maximum field strength is also dependent on the time and the distance in addition the direction. In order to determine the time of it, the built-up time (BUT) is defined for both parts, which were given by Eqn-4.27. The built-up times of the signals, which are t_{0x} and t_{0z}, can be calculated separately for $\mathrm{F_M}$ and $\mathrm{F_N}$ by applying $\gamma_x(t_{0x}) = 2\pi p$ and $\gamma_z(t_{0z}) = 2\pi q$ where $p, q \in \mathbb{Z}$.

$$t_{0x}^{+} = T_f \left(\frac{-p}{\nu_{ox}} - 1\right) > 0 \quad ; \quad t_{0z}^{+} = T_f \left(\frac{-q}{\nu_{oz}} - 1\right) > 0 \tag{4.28}$$

The BUTs must be greater than zero, because a physical system must be casual. Furthermore, it must be smaller than the summation of the T_{fill} and τ, because the step pulse is non-zero only within this duration. Therefore, p and q can take values from the limited set of numbers. That sets are defined by the limitations on the Eq-4.29 , where $p_{min} = CE\{-\nu_{ox}\,(1+\eta)\}$ and $p_{max} = CE\{-\nu_{ox}\}$.Similar set of q values is bounded by $q_{min} = CE\{-\nu_{oz}\,(1+\eta)\}$ and $q_{max} = CE\{-\nu_{oz}\}$.

$$-\nu_{ox} > p > -\nu_{ox}\,(1+\eta)\,; \quad -\nu_{oz} > q > -\nu_{oz}\,(1+\eta) \tag{4.29}$$

4.4 Null-to-Null Time Widths, T_{nnx} and T_{nnz}

Null-to-Null duration of the transmitted field in another radar parameter, which can also be considered as a pulse duration. In this part distance between the first nulls around the maxima is considered. Because the radar signal impinged of the target outside of this time duration is significantly low. A general formula to be used in the further investigations is given in this section. Time domain signal contains multiplication of the terms F_M and F_N. Since both *sinc* functions have own null to null time widths, minimum of them will be the overall T_{nn} value of the planar LFMCW-FDA because of the multiplication. With the aforementioned fact that one of the TTD must be much larger than the other one, in order to have raster scan in the transmitter's radiation pattern, one of the T_{nn} values is much less than the other ones. The envelope of the high frequency waveform has maxima, when $\gamma_x(t_{0x}) = 2\pi p$ and $\gamma_z(t_{0z}) = 2\pi q$ and $p, q \in \mathbb{Z}$. The functions in the Eq-4.27 have first nulls around t_{0x} and t_{0z}, the following equations can be solved for the smallest T_{nn} values.

$$\frac{\mathrm{M}\gamma_x}{2}\Big|_{t'=t_{0x}\mp\frac{T_{nnx}}{2}} = -2\pi\, M\nu_{ox}\left(\frac{t_{0x}\mp\frac{T_{nnx}}{2}}{T_f}+1\right) = 2\pi p \pm \pi, \quad p \in \mathbb{Z} \tag{4.30}$$

$$\frac{\mathrm{N}\gamma_z}{2}\Big|_{t'=t_{0z}\mp\frac{T_{nnz}}{2}} = -2\pi\, N\nu_{oz}\left(\frac{t_{0z}\mp\frac{T_{nnz}}{2}}{T_f}+1\right) = 2\pi q \pm \pi, \quad q \in \mathbb{Z} \tag{4.31}$$

Then, one can find the T_{nnx} and T_{nnz} as in the following form, where $T_f = f_o/\mu_f$, $\nu_{ox} = f_0\left(T_{lx} - \frac{d\,u_x}{c}\right)$, and $\nu_{oz} = f_0\left(T_{lz} - \frac{s\,u_z}{c}\right)$

$$T_{nnx} \cong \frac{2\,T_f}{\mathrm{M}\,\nu_{\mathrm{ox}}} \quad and \quad T_{nnz} \cong \frac{2\,T_f}{\mathrm{N}\,\nu_{\mathrm{oz}}} \tag{4.32}$$

4.5 Beam steering capability of the proposed transmitter

Radiation pattern of the LFMCW-FDA transmitter changes automatically with the time within the pulse duration of τ, which differs it from the phased arrays. Although, there are more conditions on the radiation pattern for a radar transmitter, the direction of the maximum radiation is an essential term to be considered in this part of this work. The proposed transmitter has the radiation pattern whose peak direction is able to scan the space partially with the properly selected parameters.

The built-up-times (BUT) for x and z related parts of the equation should be investigated for finding the θ_0 and ϕ_0 values with respect to the time. The BUTs must be same for x and z, in order to have overall maximum value on the radiation pattern. Therefore, equalizing them would end up with discovering the relation between θ_0 and ϕ_0 angles. Indeed, one can obtain how other radar parameters contribute this relation, by making t_{0x}^{+} equal to t_{0z}^{+} as in the following equation, where $\nu_{ox}$and ν_{oz}were given as in Eq-4.19. ν_{oz} is independent from ϕ_0, whereas $\nu_{ox}$is function of both θ_0 and ϕ_0 angles.

$$T_f\left(\frac{-p}{\nu_{ox}}-1\right)=T_f\left(\frac{-q}{\nu_{oz}}-1\right) \tag{4.33}$$

In order to exploit the relation between angles to decide the exact direction of the maximum radiation angle, one can solve the following equations for every θ_0 value.

$$\nu_{ox}=f_0\left(T_{lx}-\frac{d\ \sin\theta_0\cos\phi_0}{c}\right)=\frac{p}{q}\nu_{oz} \tag{4.34}$$

Using all possible p and q values which are bounded by the Eq-4.29, one can solve the Eq-4.35, in order to get real valued ϕ_0 with respect to θ_0 values. With the proper choice of the parameters, one can have effective coverage for beam scanning of this type of the transmitter.

Table 4.1 Array Parameters of an Example Planar Transmitter

Parameter	*Value*	Parameters	*Value*
M	4	Δf	20%
N	8	r	200m
f_c	10GHz	d	$\frac{\lambda_c}{2}$
τ	1ms	s	$\frac{\lambda_c}{2}$
T_{lx}	4.0 $nsec$	θ	$\epsilon\ [0^0, 180^0]$
T_{lz}	0.4 $nsec$	ϕ	$\epsilon\ [0^0, 180^0]$

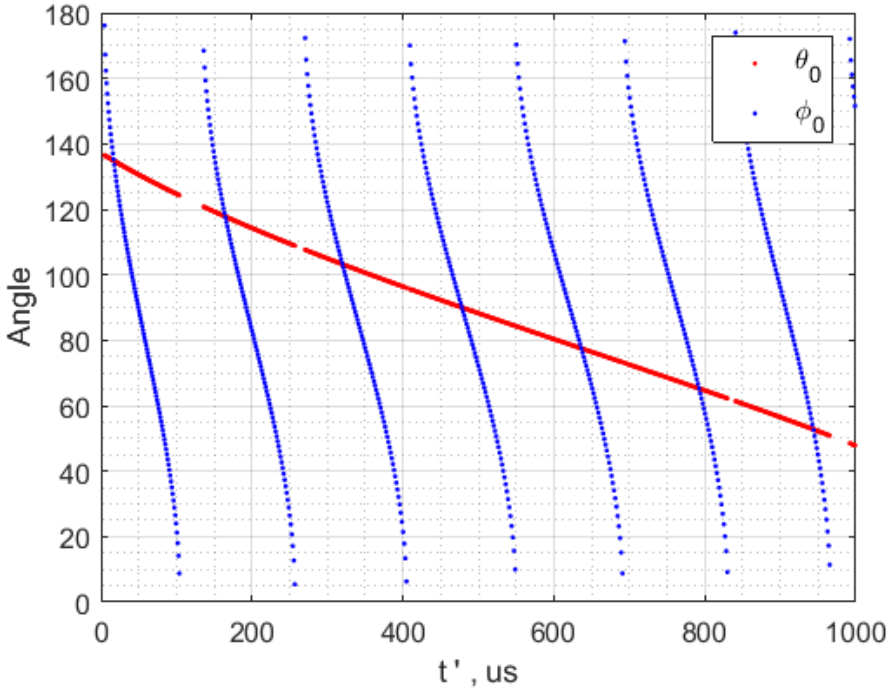

Figure 4.4. $\theta_0$and ϕ_0 variation of the maximum direction of the array factor over τ

$$\cos\phi_0 = \frac{f_0 T_{lx} - \frac{p}{q}\nu_{oz}}{\frac{d}{\lambda_0}\sin\theta_0} \qquad 4.35$$

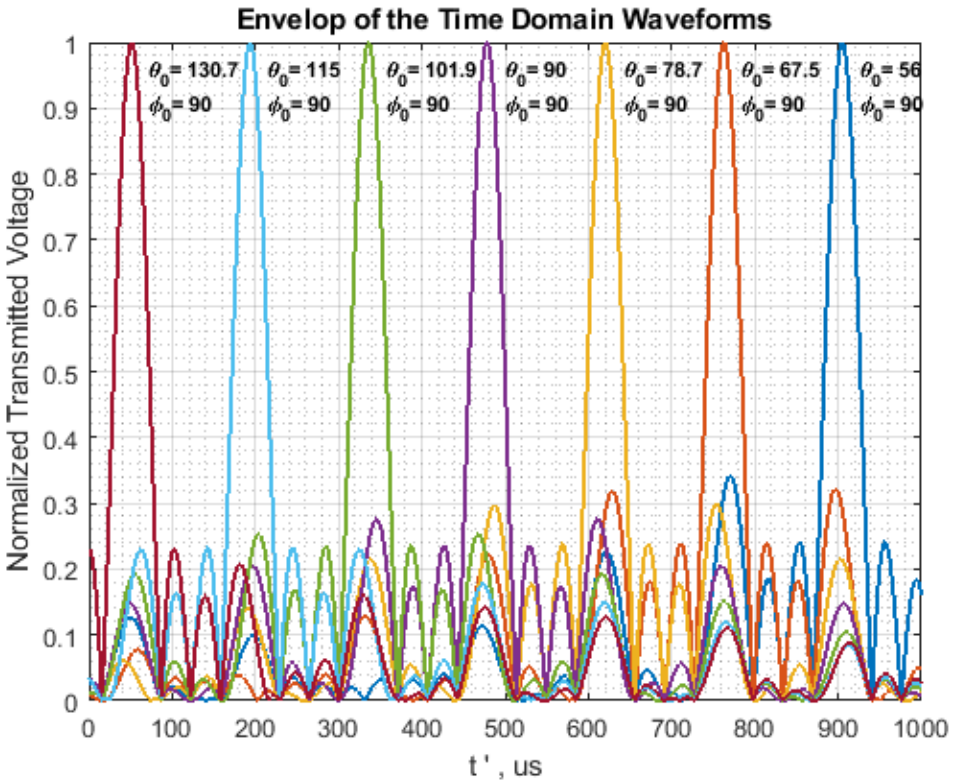

Figure 4.5. The envelopes of the time domain signals at different observation angle θ_0, when $\phi_0 = 90^o$

4.6 Transmitted Fields in Frequency Domain

Radiation pattern of the LFMCW-FDA transmitter changes automatically with the time within the pulse duration of τ. At the same time, the frequencies of the transmitter elements are changing, as in the frequency scanning arrays (FSA). However, main difference between the FSAs and the LFMCW-FDA is that, each

element is excited by the signal whose instantaneous frequencies are distant, unlike the FSAs. Therefore, the bandwidth of the transmitted signal comprised of the summation of these diverse frequencies due to the TTDs.

4.7 Observed Field at the Origin that is reflected back from a point target

Radars try to detect signals reflected from the target that is needed to be observed for different types of applications. The reflected signal from a point target is vital for a radar investigation. In this subsection, the received signal will be formulized for the point target as a general solution.

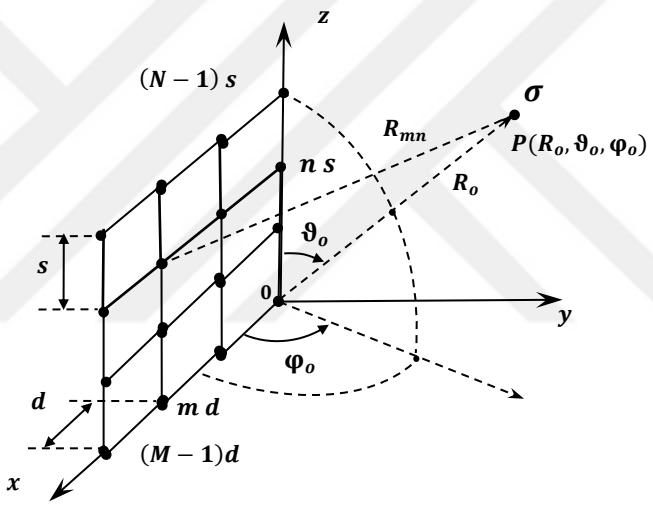

Figure 4.6. Proposed planar array with the far field point target, σ, located at P

4.7.1 In Time Domain

Transmitted electric field must be shown firstly. Then one can continue to derivation of an incident electric field on the point target due to the transmitter. The incident electric field which is transmitted by the mn^{th} antenna element can be written as Eq-4.36. The time delays can be shown as t_d and t_p, for feeding delay of the

corresponding element and propagation delay of the field which can be observed as R_{mn}/c in free space, where c is the velocity of light in free space.

$$\boldsymbol{E^t_{mn}}(r,t) = \frac{1}{R_{mn}}\, P(t'_{mn},\tau)\, \bar{\xi}_{mn}(\theta_0,\phi_0,f_{mn})\, e^{\mathrm{j}(\omega_o(t-t_d-t_p)+\frac{\mu}{2}\,(t-t_d-t_p)^2)} \qquad 4.36$$

Each incident electric fields components would be scattered with scaling of the complex value of $\sqrt{\sigma/(4\pi R^2)}$ back to the origin, where the radar is positioned. On the way back, all components propagate along same way from the point target to receiver antenna, therefore it would be resulted in constant propagation time delay. One can write the received electric field at the origin, which is transmitted from mn^{th} element and scattered from the point target as following equation.

$$\boldsymbol{E^r_{mn}}(R_0,t) = \sqrt{\frac{\sigma}{4\pi R_0^2}}\,\frac{1}{R_{mn}}\, P(t'_{mn},\tau) \qquad 4.37$$
$$\bar{\xi}_{mn}(\theta_0,\phi_0,f_{mn})\, e^{\mathrm{j}(\omega_o(t-t_{dmn}-t_{pmn}-t_{p0})+\frac{\mu}{2}\,(t-t_{dmn}-t_{pmn}-t_{p0})^2)}$$

Summation of the received field results in the total reflected field at the origin. It has already been shown that R_{mn} equals to R_0 in amplitude related terms for the target located in far-field. In order to find the received voltage by the receiver antenna, one can scale the total electric field because of the effective area of the antenna. Furthermore, vector electric field pattern can be written as single variable by assuming the patterns be same for each antenna element. Due to the aperture delays are much less than the duration of the unit pulse, τ, we can assume that $P(t'_{mn},\tau)$ is same every element. The received voltage can be obtained as in the Eq-4.38, by adding all common terms into the value, A, that also includes the all proportional values related with the conversion of the total electric field to the received voltage such as antenna efficiency, etc.

$$v^r_{mn}(\boldsymbol{R_0},t) = A\sqrt{\frac{A_{eff}\sigma}{4\pi}}\,\frac{1}{R_{mn}\,R_o}\, P(t,\tau)\,\bar{\xi}(\theta_0,\phi_0) \qquad 4.38$$
$$e^{\mathrm{j}(\omega_o(t-t_{dmn}-t_{pmn}-t_{p0})+\frac{\mu}{2}\,(t-t_{dmn}-t_{pmn}-t_{p0})^2)}$$

For the sake of the simplicity in illustration of the equation, let the constant time delays be subtracted from time in order to be demonstrated as the retarded time, t'.

$$v^{rx}(\boldsymbol{R_0}, t) = A\sqrt{\frac{A_{eff}\sigma}{4\pi}}\,\frac{1}{R_0^2}\,P(t,\tau)\,\bar{\xi}(\theta_0,\phi_0) \sum_{m=0}^{M-1}\sum_{n=0}^{N-1} e^{\mathrm{j}(\omega_o(t-t_{dmn}-t_{pmn}-t_{p0})+\frac{\mu}{2}\,(t-t_{dmn}-t_{pmn}-t_{p0})^2)} \tag{4.39}$$

$$t - t_{dmn} - t_{pmn} - t_{p0} = t' - t_{dmn} - t_{pmn}$$
$$where\ t_{dmn} = mT_{lx} + nT_{lz}\ and\ t_{pmn} = m\frac{d}{c}\sin\theta_o\cos\phi_o + n\frac{s}{c}\cos\theta_o \tag{4.40}$$

One can repeat the same steps as given in the equations from 4.7 to 4.27, in order to obtain the simplified voltage formula that is reflected back to an isotropic antenna. Then the simplified form of the formula could be written as in the Eq-4.41, after imposing the phasor terms $e^{\mathrm{j}(\mathrm{M}-1)\frac{\gamma_x}{2}}$ and $e^{\mathrm{j}(\mathrm{N}-1)\frac{\gamma_z}{2}}$ into the complex scaler value of $A(t')$.

$$v^{rx}(\boldsymbol{R_0}, t) = A(t')\sqrt{\frac{A_{eff}\sigma}{4\pi}}\,\frac{1}{R_0^2}\,\frac{sin\left(\frac{M\gamma_x}{2}\right)}{sin\left(\frac{\gamma_x}{2}\right)}\,\frac{sin\left(\frac{N\gamma_z}{2}\right)}{sin\left(\frac{\gamma_z}{2}\right)} \tag{4.41}$$

where

$$\gamma_{\mathrm{x}}(t') = -2\pi\,\nu_{ox}\left(\frac{t'}{T_f}+1\right)$$
$$\gamma_z(t') = -2\pi\,\nu_{oz}\left(\frac{t'}{T_f}+1\right) \tag{4.42}$$
$$A'(t') = |\boldsymbol{\xi}(\theta_0,\phi_0)|\,P(t')e^{\mathrm{j}\left\{\omega_o t' + \frac{\mu}{2}\,t'^2\right\}}\,e^{\mathrm{j}(\mathrm{M}-1)\frac{\gamma_x}{2}}\,e^{\mathrm{j}(\mathrm{N}-1)\frac{\gamma_z}{2}}$$

ν_{ox} and ν_{oz} were given in the Eqn-4.19. $T_f = f_0/\mu_f$. During the investigation of the total received voltage, a meaningful focus must be on the magnitude of the fields which is a function of the retarded time. The magnitude of the field is dependent on both parameters along x and z axis, i.e. $T_{lx}, T_{lz}, d, s, \theta_0\ and\ \phi_0$. It eases the handling with the expressions, that dividing the equation into two parts. These two functions

give their maximum values, when $\gamma_x(t_{0x}) = 2\pi p$ and $\gamma_z(t_{0z}) = 2\pi q$ and $p, q \in \mathbb{Z}$, as that was shown for the total transmitted electric field. Then, one can distinguish the difference in the effects of the radar parameters on the received field. Both F_M and F_N have maximum values on t_{ox} and t_{oz} times respectively, that can be called as build up time (BUT). The time of the maximum signal can be found by applying same steps as done in Section-4.3 in the Eq-4.44.

$$F_M = \frac{\sin\left(\frac{M\gamma_x}{2}\right)}{\sin\left(\frac{\gamma_x}{2}\right)} \; ; \qquad F_N = \frac{\sin\left(\frac{N\gamma_z}{2}\right)}{\sin\left(\frac{\gamma_z}{2}\right)} \tag{4.43}$$

$$t_{0x}^{+} = T_f \left(\frac{-p}{\nu_{ox}} - 1\right) > 0 \;\; ; \quad t_{0z}^{+} = T_f \left(\frac{-q}{\nu_{oz}} - 1\right) > 0 \tag{4.44}$$

By making BUTs equal, one can find maximum of the reflected signal in time domain. The location of the maxima is also dependent on the radial distance of the point scatterer.

4.7.2 In Frequency Domain

Frequency of the received field is essential and has the information about the properties of the target such as its location, its radial speed, etc. However, how to approach the signal in frequency domain would be related to how one processes the incoming signal. In this part, the approach that will be utilized is discussed. An omnidirectional antenna is considered as a receiver. The received echo is mixed with the local oscillator (LO) which is LFM signal. This process can also be called as dechirping. Then, the base band part of the resulting signal is same as the classical FMCW signal, that can be obtained by using low-pass filter. Moreover, the base band signal has an FDA envelope. There would be shift in frequency, which is Doppler effect, if the target is not stationary along radial axis in the echo signal. T_{do} is the

time offset for the Doppler frequency $\omega_{do} = 2\,\pi f_{do} = \mu\, T_{do}$. This effect is also considered in the received voltage equation as the Eq-4.57. In this equation, weightings for transmitter antenna elements along x and z axes are taken into consideration.

$$v_{mn}^{r}(\boldsymbol{R_0}, t) = A\sqrt{\frac{A_{eff}\sigma}{4\pi}}\,\frac{1}{R_{mn}\,R_o}\,P(t,\tau)\,\bar{\xi}(\theta_0,\phi_0) \qquad 4.45$$
$$a_m\;\; b_n\; e^{\mathrm{j}(\omega_o(t-t_{dmn}-t_{pmn}-t_{p0}+T_{do})+\frac{\mu}{2}\,(t-t_{dmn}-t_{pmn}-t_{p0}+T_{do})^2)}$$

The overall received voltage can be presented as in the Eq-4.46. After same manipulations as in the previous section and assuming that only the base band part can pass through the low-pass filter (LPF), one can get the baseband signal shown in the Eq-4.47.

$$V^{+}(\boldsymbol{R_0}, t) = A\sqrt{\frac{A_{eff}\sigma}{4\pi}}\,\frac{1}{R_o^2}\,P(t,\tau)\,\bar{\xi}(\theta_0,\phi_0) \qquad 4.46$$
$$\sum_{m=0}^{M-1}\sum_{n=0}^{N-1} a_m\;\; b_n\; e^{\mathrm{j}(\omega_o(t-t_{dmn}-t_{pmn}-t_{p0}+T_{do})+\frac{\mu}{2}\,(t-t_{dmn}-t_{pmn}-t_{p0}+T_{do})^2)}$$

$$V^{+}(t') \cong \mathbb{V}_o(t')\sum_{m=0}^{M-1} a_m\; e^{jm\gamma_x^{+}(t')}\;\sum_{n=0}^{N-1} b_n\; e^{jn\gamma_z^{+}(t')} \qquad 4.47$$

Resulting voltage can be written as above form. $\mathbb{V}_o(t) = V_o\, e^{j\psi(\mathrm{t}')}P(t',\tau)$, where V_o is the complex amplitude that also contains the amplitude and the phase of the radar transmit and receive functions and propagation paths along both direction. The retarded time , $t' = t - T_{po} = t - 2\,R_0/c$, is defined by subtracting the total propagation delay from the time, where $T_{po} = 2t_{po}$. The delay of the received echo also defines the effective beat frequency with the Doppler frequency. Beat frequency

due to the radial location of the target can be represented as $\omega_{bo} = \mu\, T_{po} = \mu\, 2R_0/c$. Furthermore, overall effective beat frequency $\omega_b = \omega_{bo} + \omega_{do}$ and $\omega_{do} = 2\,\pi f_{do} = 2w_0 v_{tg}/c$ is the Doppler frequency for the target whose velocity is $v_{tg} > 0$ along radial axis. Positive velocity means that the target is going away for this case. The beat frequency would be $\omega_b = -\omega_{bo} + \omega_{do}$ for the same target with the LFM pulse whose slope is negative. Fourier transform of the $V^+(t')$ is on the following equations. For negative slope chirp, one must interchange Ψ_{mn} with $(1+\eta)\Psi_{mn}$.

$$\tilde{V}^+(\omega) = \overline{\mathbb{V}}_o \sum_{m=0}^{M-1} \sum_{n=0}^{N-1} a_m\, b_n\, e^{-j2\pi\left(\Psi_{mn} + \frac{\bar{\omega}\,\tau}{4\pi}\right)}\, \frac{\sin(\bar{\omega}\,\tau/2)}{\bar{\omega}\,\tau/2} \qquad 4.48$$

where;

$$\overline{\mathbb{V}}_o = V_o\,\tau\, e^{-j\omega T_{po}} \qquad 4.49$$

$$\bar{\omega} = \omega - \omega_b + \omega_{mnf} \qquad 4.50$$

$$\Psi_{mn} = m\,\nu_{ox} + n\,\nu_{oz} \qquad 4.51$$

The spectral components (SC's) are $\omega_{fx} = 2\,\pi\nu_{ox}/T_f$ and $\omega_{fz} = 2\,\pi\nu_{oz}/T_f$. It has been presented in previous sections, that one of the TTD's T_{lx} or T_{lz} must be much larger than other one, in order to have raster scan. Consequently, the one with longer delay lines has much larger spectral components. The amount of the frequency step between consecutive elements along that axis is coherently much larger than the one with shorter delay line. Therefore, $\max(\omega_{fx}, \omega_{fz}) \gg \min(\omega_{fx}, \omega_{fz})$ is valid for a proper implementation of the planar LFMCW-FDA. The center frequency of the SC, due to the mn^{th} element, is $\bar{\omega}_{mnc} = \pm\omega_{bo} + \omega_{do} - \omega_{mnf}$. All the SC's are shifted by the beat frequency, $\omega_b = \pm\omega_{bo} + \omega_{do}$. the independent spectral contribution of the FDA is ω_{mnf}. The orthogonal SC's can be obtained, when $\mathcal{K}_x = \Delta f T_{lx}$ or $\mathcal{K}_z = \Delta f T_{lz}$ are integers. The center frequency of the SC's would occur at the $\mathcal{K}_{x,z}^{th}$ null of

the adjacent SC, if and only if, the corresponding $\mathcal{K}$ value is integer. The frequency bandwidth (FBW), $\omega_{BW} = 2\pi f_{BW}$, can be written as in the following equation.

$$\begin{aligned} \omega_{BW} &= (M-1)\omega_{fx} + (N-1)\omega_{fz} + \frac{2\pi}{\tau} \\ &\cong \frac{max((M-1)\mathcal{K}_x, (N-1)\mathcal{K}_z) + 2}{\tau/(2\pi)} \end{aligned} \tag{4.52}$$

Some parameters and specifications of the reflected wave in frequency domain were given in this part of the work. These parameters will be used in next sections to exploit the advantages of the planar LFMCW-FDA.

4.7.3 Transmitted Pulse Waveforms

Until this section, a single chirped with positive slope has been considered as transmitter waveform. In order to form a radar, more than one LFM pulse must be used. In the Figure 4.7, periodic coherent pulses can be seen. This sketch illustrates the time dependent frequency of the LFM signal. Frequency sweeps can be accomplished with the use of the linearly increasing or decreasing over single LFM pulse period, which is τ in this figure. Time axis for these multiple chirps is called as slow time, whereas time within a single chirp is called as fast time. After each sweep either with positive or negative slope, a silent time gap with the time duration, T_g, in which transmitter is off, is assumed. With the presence of these gaps between the pulses, the radar application can distinguish whether the reflection from a target is coming due to the previous pulse. If these gaps were not used, the ambiguity would arise during the beginning of every change in the frequency sweep slope. Therefore, the duration of the positive and negative pulse pair is T_p, which can be found as $2(\tau + T_g)$.

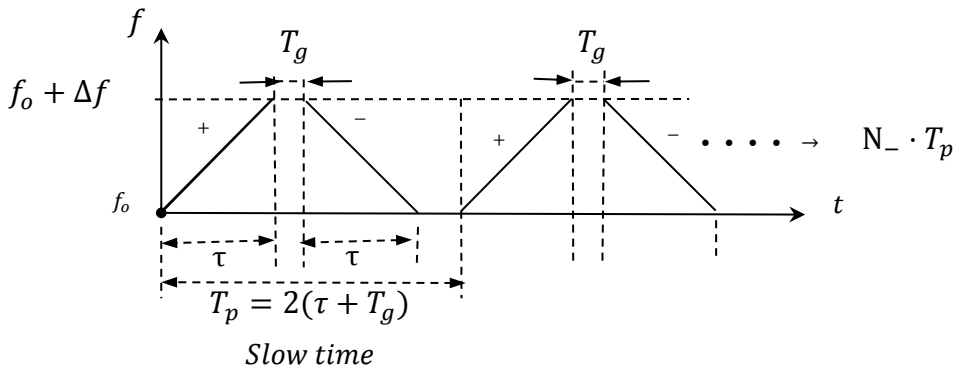

Figure 4.7. Periodic Coherent ± slope N_ radar pulses

4.7.4 Properties of the reflected signal for multiple Chirps

The accuracy of the measurement depends on the signal-to-noise ratio (SNR), which is defined by dividing the energy of the FDA signal by noise energy (E_o/η_o). By using noise temperature, T_s, and the Boltzmann's coefficient, k, the noise spectrum density can be defined, $\eta_o = kT_s$. When uniform weights are used in the FDA LFMCW transmitter, energy of the waveform is approximately $E_o \cong M^2N^2V_o^2\tau/\mathcal{K}$, where $\mathcal{K}$ is the max of $\mathcal{K}_x$ and $\mathcal{K}_z$ depending on the selection of the TTDs. In order to recover E_o, averaging the results from coherent pulses would be an effective way. With the assumption of the Swerling I (SW I) targets, chirps can be considered as coherent. The second Fourier transform gives the phase variation that is related to the velocity of the target. This procedure is nothing but the $2D\ \mathcal{FT}$ for FM/CW radar signal proposed and used by Khan and Power in [53]. The number of N_- coherent pulses are used to be averaged for recovering E_o. The second $\mathcal{FT}$ is taken along the N_- coherent pulses. The Doppler filters are formed in this Fourier domain, to utilize the '*velocity matched filters'* defined in [53]. Frequency of the reflected signal is given in previous subsection. However, the phase of the dechirped waveform is not constant for a non-stationary target. The general form of the phase of the n_-^{th} pulse is given in the Eq-4.53.

$$\psi_{n\_}\left[t' + (n\_ - 1)T\right] = \omega_{bn\_}\, t' + \alpha_{n\_} + \Phi_d \quad , \; where \quad 0 \le t' \le \tau \qquad 4.53$$

The beat frequency of the $n\_^{th}$ pulse, $\omega_{bn\_}$, is given in below formula. When the target is not stationary, the beat frequency changes from pulse to pulse, due to changing radial location of the target. $\Delta\varpi_{bn} = \mu(n\_ - 1)\; v_{tg}\; T/c.$

$$\omega_{bn} = \omega_{bo} + \omega_{do} + \Delta\varpi_{bn} \qquad 4.54$$

$$\alpha_{n\_} = -\Delta\varpi_{bn}\left[2\; R_o\; /c + (n-1)\; v_{tg} T/\; c\;\right] \qquad 4.55$$

$$\Phi_d = (n\_ - 1)\omega_{do} \qquad 4.56$$

At this point, one can also test above formula by substituting v_{tg} and ω_{do} with zero, in order to check if the stationary target has phase variation, when multiple chirps are utilized. Finally, $\omega_{bn} = \omega_{bo}$ for all pulses when the target is not moving.

4.7.5 Example and Simulation Results

In this subsection, a numerical example which is illustrating the aforementioned parameters and specifications of the reflected signal is given. To give the numerical example, the LFMCW-FDA parameters on the Table 4.1 are considered. The envelope of the normalized time domain waveforms for different point scatterers are given in the Figure 4.9. The locations of the scatterers can also be seen on the Figure 4.8.

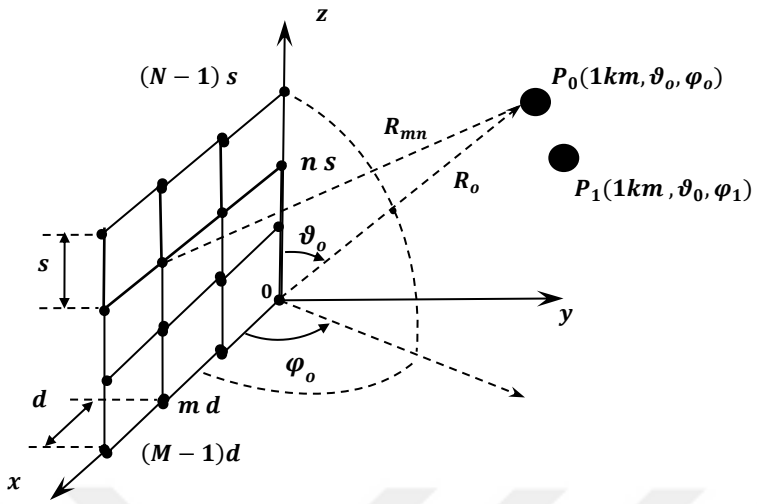

Figure 4.8. Two point scatterers with different azimuth locations

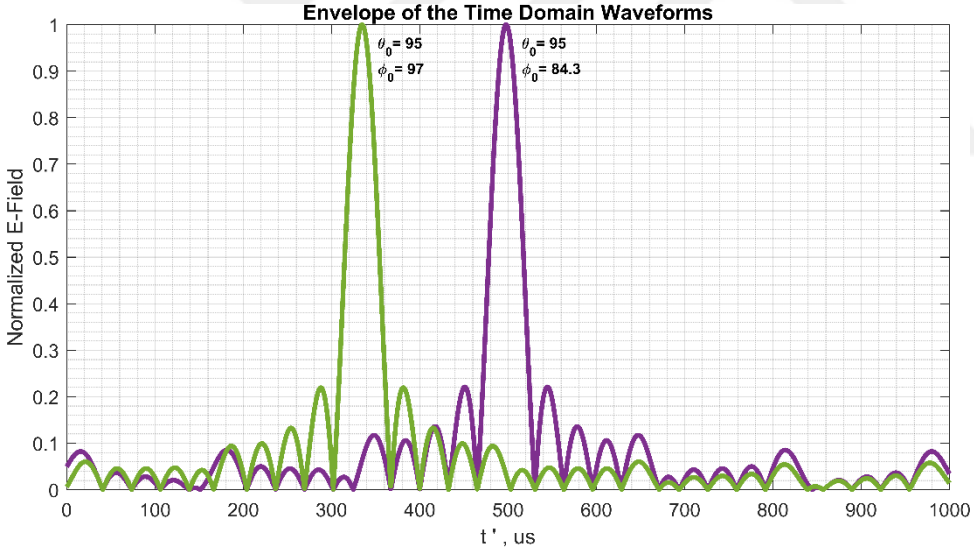

Figure 4.9. The envelope of reflected signal in time domain from two point scatterers with different azimuth locations

4.8 A Radar Example with Phased Array Receiver

Radars try to locate the target by determining angle and the distance of it with respect to its own local coordinates. In this chapter, the LFMCW based FDA transmitter was explained until here. The beam of it steers in the space with the aforementioned coverage of the space. Building a radar by utilizing such transmitter will be discussed with realistic scenarios. This example was proposed in [12], it will be explained with more details.

4.8.1 Transmitter LFMCW-FDA and its Radiation Pattern

Employing an LFMCW pulse is a well-known method to determine the distance of the target. It has many benefits and advantages. The most outstanding advantage of LFM utilizing radar is that, it can inherently determine the distance of the target, that is not even moving, more easily than others. Moreover, one can sequentially use this type of pulse with an increasing and a decreasing frequency over time. With the help of two different slope usage, velocity of the target can also be found by the LFM radar. Furthermore, it can also be determined, whether the target is receding or approaching the radar. Details of the implementation of the LFM radar will not be focused within this study. However, the proposed radar has also same abilities inherently, as it exploits the LFMCW pulse in order to effectuate the frequency diversity in different antenna elements. Therefore, these decision making processes can also be applied with the LFMCW-FDA radar.

The angle of the target is another unknown, which a radar must resolve. Because of the self-scanning behavior of the LFMCW-FDA transmitter and that the maximum radiation direction changes with time and distance, handling with this type of radar requires Space-Time Adaptive Processing (STAP). In order to build a radar, a phased array receiver can be used. Therefore, angle of arrival estimation can be done by changing the direction of the receiver's beam. In other words, the angle can be resolved by the classical phased array receiver.

Table 4.2 Array Parameters of an Example Planar Radar with phased array receiver

Parameter	*Value*	Parameter	*Value*
M	8	Δf	2999.7
N	5	r	1km
f_o	15.15GHz	d	$\frac{\lambda_o}{2}$
τ	1ms	s	$\frac{\lambda_o}{2}$
T_{lx}	0.2436nsec	θ	$\epsilon\ [0^0, 180^0]$
T_{lz}	2.04 $nsec$	ϕ	$\epsilon\ [0^0, 180^0]$

Coverage of the transmitter was shown before. However, this will be shown with a canonical example here. The parameters of the LFMCW FDA are tabulated on the Table 4.2. The scan of the transmitter is like raster scan. Therefore, numbers of elements along x and z axis are chosen as 8 and 5 respectively. That is required in order not to have large side lobes in time domain signal due to the scan of adjacent scan paths. In other words, the beam widths of the main lobe must be appropriate when it is considered with main radiation direction, in order not to redundantly transmit signal into one direction twice. The change of the main beam direction within the LFM pulse duration can be seen on the Figure 4.10. The points on the figure show the main beam directions, that was considered as reference direction to show the full coverage of the transmitter. One must consider those points as couples, that define the direction with known θ_0 and ϕ_0 values.

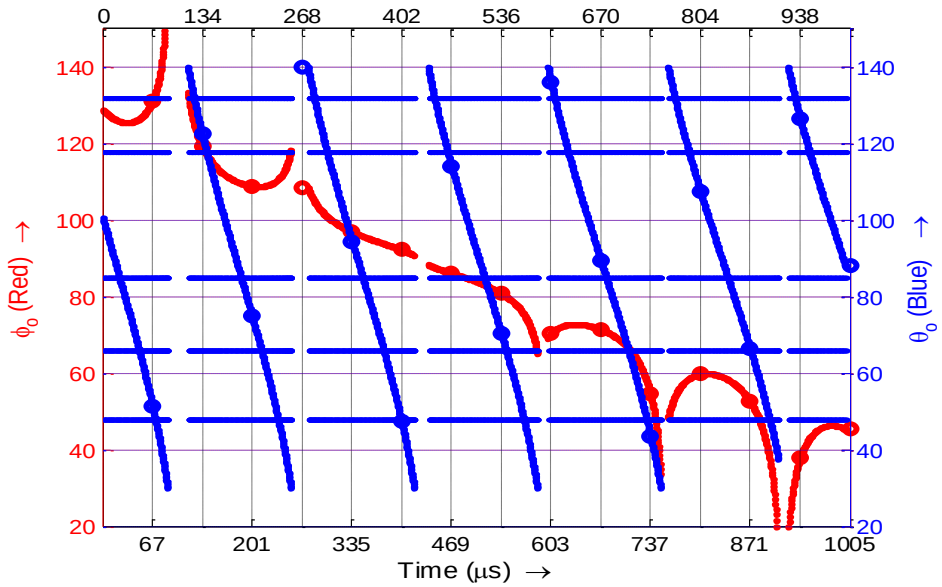

Figure 4.10. The general coverage diagram of the transmitter of the planar radar example

The selected θ_0 values are in $\{48^o, 66^o, 82^o, 98^o, 114^o, 132^o\}$. These values are selected not to have a gap in the region of interest. The build-up time for F_N, which was given in the Eq-4.43, should be found first for these selected θ_0 values. At this point, the procedure that is explained in the section 4.3 Time of maximum field occurred at a point $(\boldsymbol{R_0}, \boldsymbol{\theta_0}, \boldsymbol{\phi_0})$ is applied to determine the maximum timings. The valid p and q values are in sets of $\{-4\}$ and $\{-31, -32, -33, -34, -35, -36\}$ respectively. The corresponding BUTs, t_{oz}^{+}, found by the Eq-4.28, are 26.8us, 190.6us, 354.4us, 518.1us, 681.9us, and 845.7us only for single theta angle $\theta_0 = 82^o$. Time domain waveforms can be seen on the Figure 4.11, when elevation angle is constant but the azimuth angles are different for each waveform. With the selected $\theta_0 = 82^o$ value, ϕ_0 are in $\{57.7^o, 70.4^o, 82.7^o, 95.5^o, 109.3^o, 125.6^o\}$. The following six waveforms are observed at different six locations defined by θ_0 and ϕ_0 values. Time axis of the waveform shows the retarded time, which is defined by subtracting the propagation duration from the time of the LFM pulse.

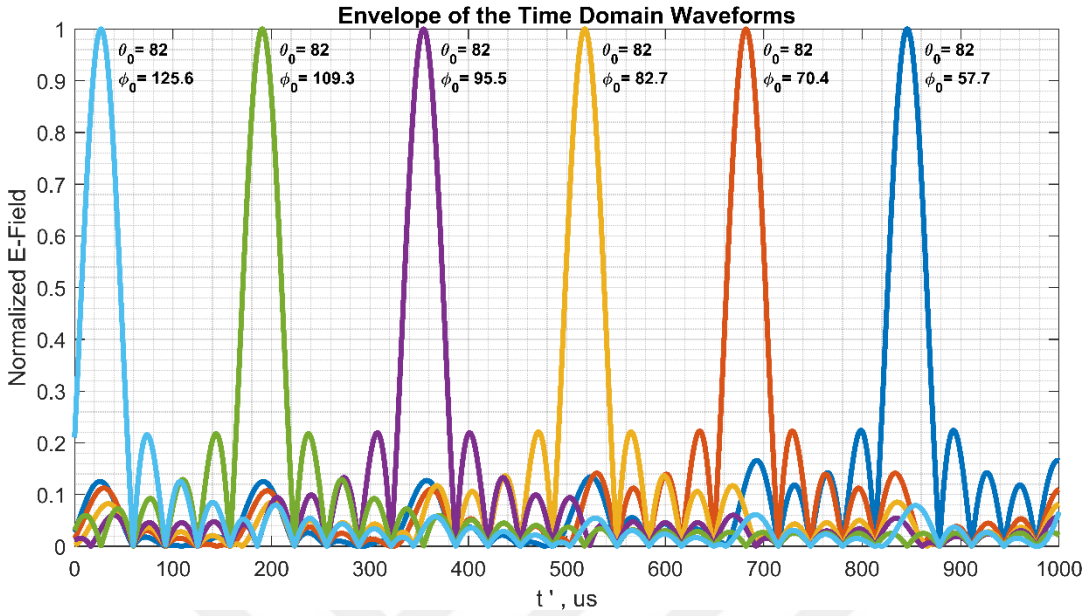

Figure 4.11. The normalized time waveforms of the fields transmitted by the LFMCW-FDA Radar

Related waveforms and corresponding peak time and azimuth angles were given for single angle. Moreover, one can generalize these waveforms for each elevation angle in given set. Then, envelope of the impinged signal on the 36 pre-determined observation points are shown as in the Figure 4.12. On the figure, one can also find the location of the observation point with elevation and azimuth angles. Times of the maximum location can be found as 25.8us, 45.9us, 65.8us, 127.8us, 147.7us, 168.1us, 189.5us, 210.3us, 230.8us, 289.6us, 310.1us, 331.2us, 353.3us, 374.7us, 395.8us, 451.4us, 472.5us, 494.2us, 517us, 539.1us, 560.9us, 613.2us, 635us, 657.3us, 680.8us, 703.5us, 725.9us, 775.1us, 797.4us, 820.4us, 844.5us, 867.9us, 891us, 936.9us, 959.9us and, 983.5us in time order within the single positive LFM sweep.

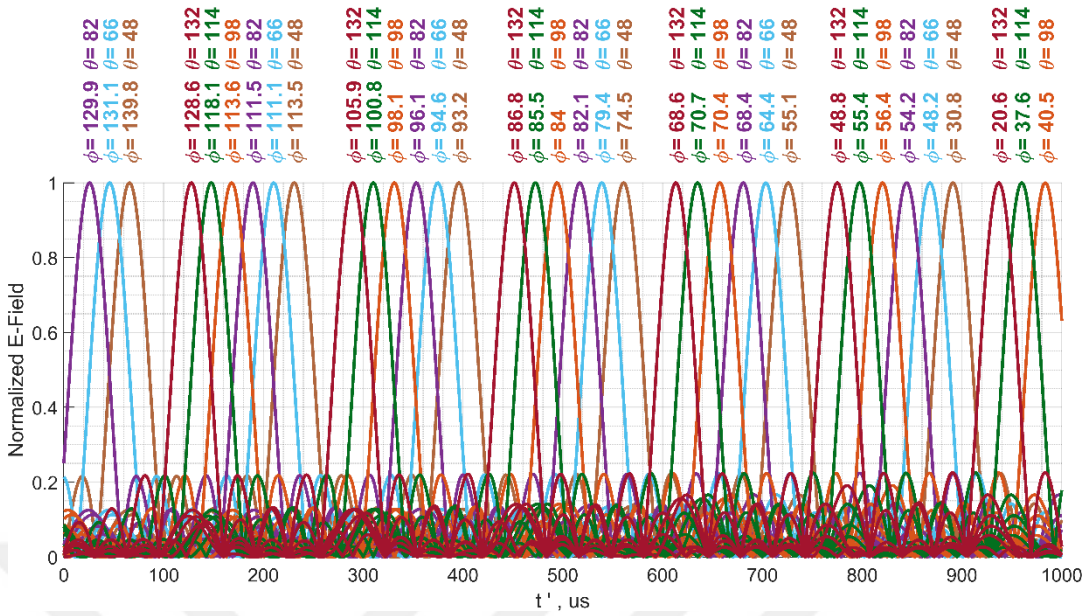

Figure 4.12. The normalized time waveforms of the fields, which are transmitted by the planar LFMCW-FDA Radar, observed at 36 selected points

Revisit of the main beam to one pre-determined elevation angle takes place at different ϕ_0 value. For the sake of gapless scanning, the half power beam widths must intersect each other's HPBW on azimuth plane at least. For example, one can investigate the locations of half power beam widths of the main lobe when it is directed to angle pairs of $\theta_0 = 82^o$, $\phi_0 = 109.3^o$ and $\theta_0 = 82^o$, $\phi_0 = 95.5^o$. HPBWs are given in the Eq-4.57 for both moments. One can simply calculate the locations of -3dB points, by assuming the main lobe is symmetrical around the peak location. Then, the following Eq-4.57 holds for this example. Therefore, gapless scan is accomplished in this region.

$$\text{HPBW}_{\text{azimuth}} \Big|_{\substack{\phi_0 = 109.3^o \\ \theta_0 = 82^o}} = 16.5^o, \qquad \text{HPBW}_{\text{azimuth}} \Big|_{\substack{\phi_0 = 95.5^o \\ \theta_0 = 82^o}} = 14.5^o \tag{4.57}$$

$$109.3^o - \frac{16.5^o}{2} = 101.25^o \leq 102.75^o = 95.5^o + \frac{14.5^o}{2} \qquad 4.58$$

All of the instantaneous one plane radiation patterns for all 36 pre-determined directions are shown in from Figure 4.13 to Figure 4.18 with different θ_0 values. Each pattern line shows the instantaneous pattern at the corresponding time that can be shown on the figure as the name of the legend. As the maximum radiation direction is moving away from broadside direction, half power beam widths are getting larger. Especially, when both the azimuth and the elevation angles are not close to broadside, shapes of patterns are getting poorer. That unwanted behavior can notably be seen in the Figure 4.13 and Figure 4.18. However, that would rapidly diminish, if the array was composed of the directional antenna elements instead of omnidirectional elements. Because of the assumption of that omnidirectional elements are deployed in the LFMCW-FDA, these radiation patterns are also equivalent to array factors. When we consider the $\theta_0 = 48^o$, the peaks occur at the angles $\phi_0 \in \{30.8^o, 55.1^o, 74.5^o, 93.2^o, 113.5^o, 139.8^o\}$. Moreover, for $\theta_0 = 66^o$, the peaks take place at $\phi_0 \in \{48.2^o, 64.4^o, 79.4^o, 94.6^o, 111.1^o, 131.1^o\}$. Therefore, -3dB coverage from 37^o to 145^oon azimuth plane is accomplished for aforementioned θ_0. Whereas ϕ_0 is between $45^o \; and \; 142^o$ for $\theta_0 = 82^o$, for $\theta_0 = 98^o$, ϕ_0 is between $30^o \; and \; 122^o$. These total radiation patterns for single θ_0, which can be considered as overall summation of the all radiation patterns in the single figure, are not symmetrical around broadside.

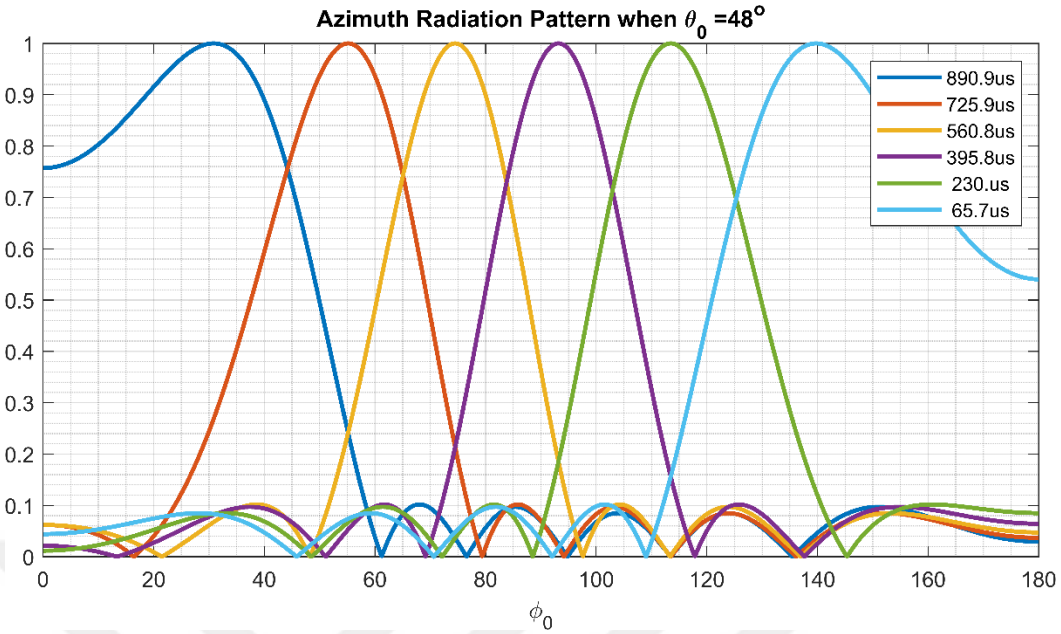

Figure 4.13. The normalized instantaneous azimuth radiation patterns at given time when $\theta_0 = 48^o$

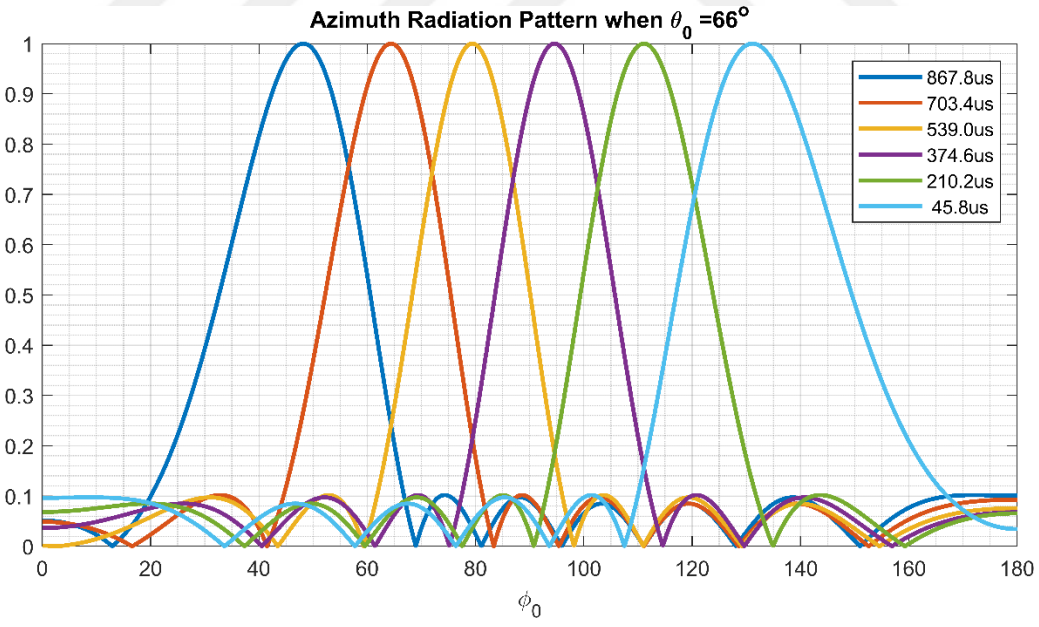

Figure 4.14. The normalized instantaneous azimuth radiation patterns at given time when $\theta_0 = 66^o$

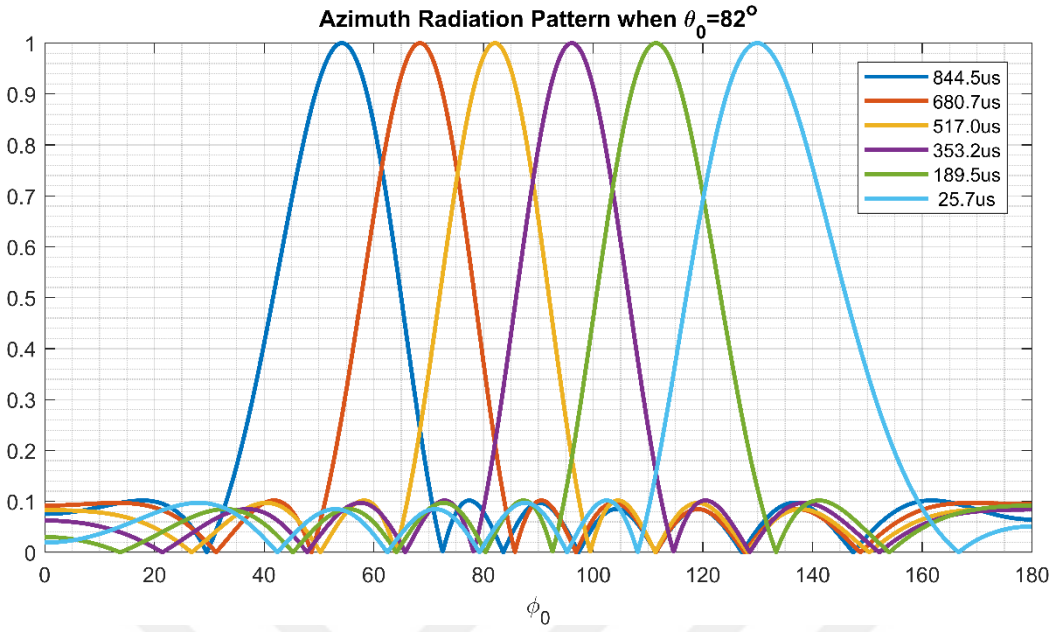

Figure 4.15. The normalized instantaneous azimuth radiation patterns at given time when $\theta_0 = 82^o$

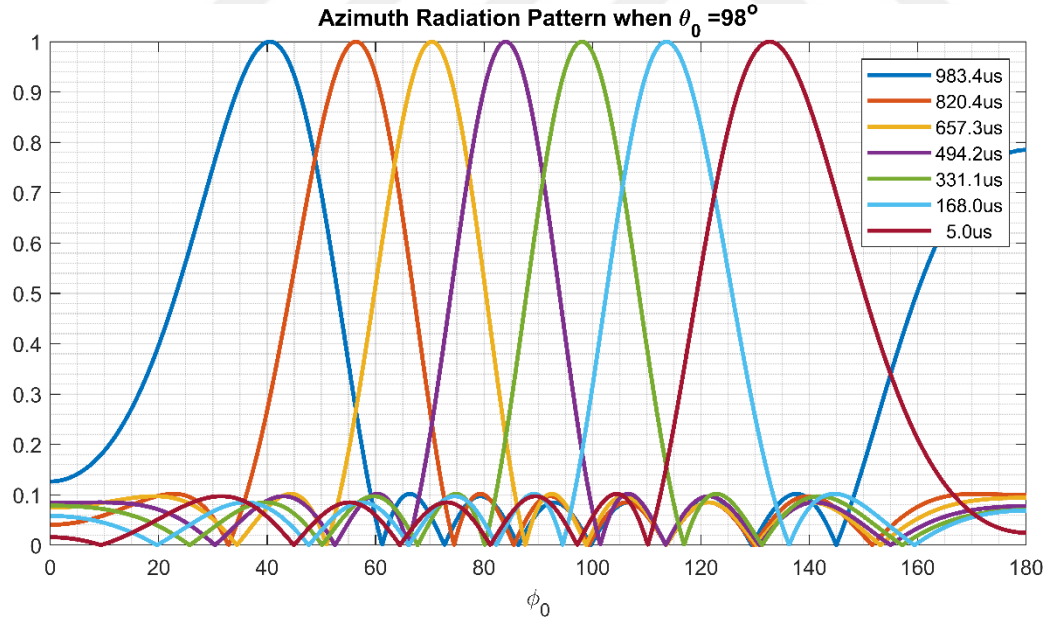

Figure 4.16. The normalized instantaneous azimuth radiation patterns at given time when $\theta_0 = 98^o$

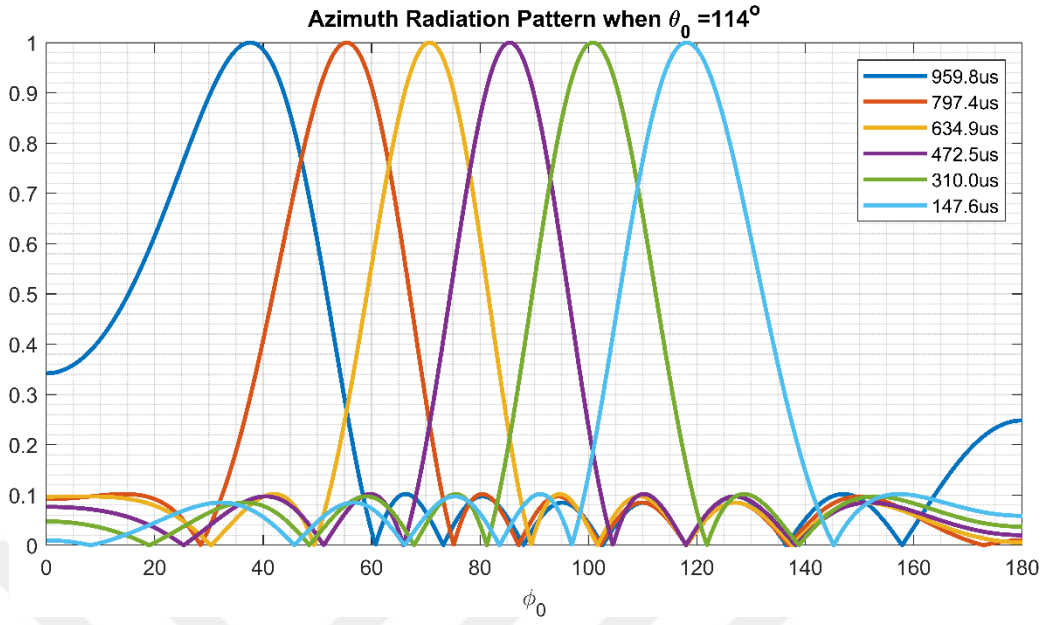

Figure 4.17. The normalized instantaneous azimuth radiation patterns at given time when $\theta_0 = 114^o$

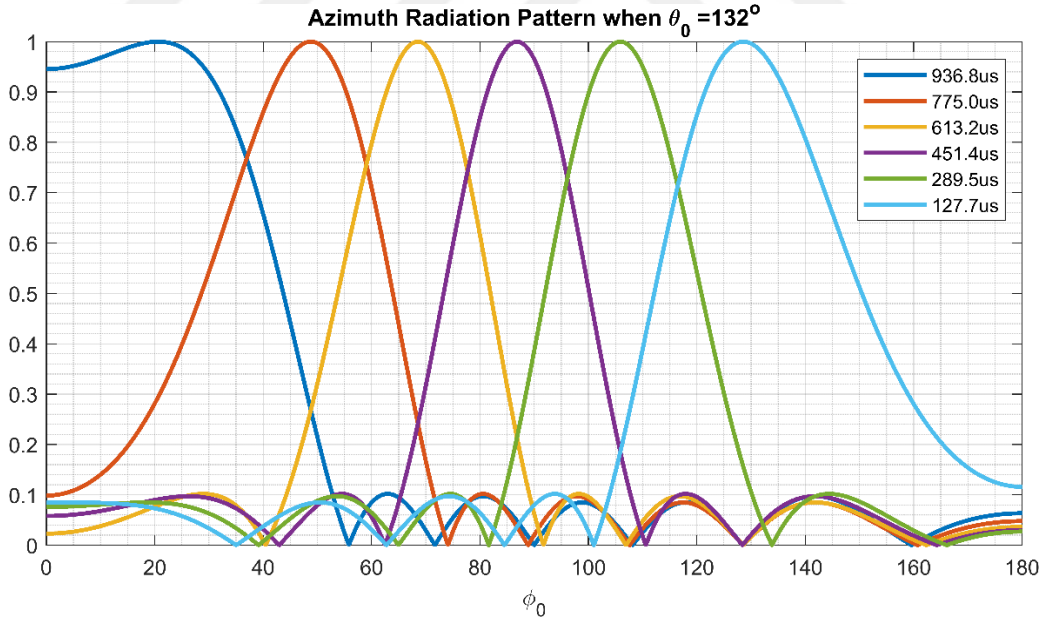

Figure 4.18. The normalized instantaneous azimuth radiation patterns at given time when $\theta_0 = 132^o$

One is tilted to higher ϕ, in the meanwhile other is tilted more to lower values. However, this is not a big problem for a realistic radar example, because overall

radiation patterns would have lower beam widths in the presence of the directive antennas.

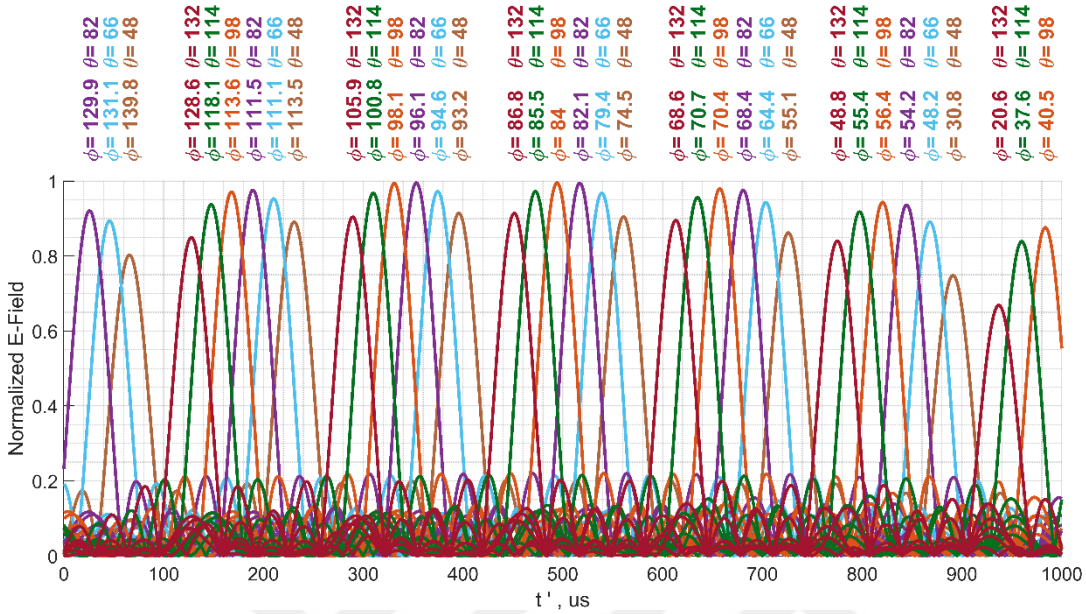

Figure 4.19. The normalized time waveforms of the fields, which are transmitted by the planar LFMCW-FDA Radar, observed at 36 selected points with the directional elements

Side lobe level has also vital role on the performance of the radar application. Excitation weights of the antenna elements in the array are directly related to the far-field radiation pattern, eventually to the side lobe level. Therefore, Taylor tapering weights a_m in M along x-axis was chosen, in order to have $SLL_m \leq -20dB,$ and $\tilde{n}_m = 3$. Along z-axis, any tapering was not applied, so that $b_n = 1$ for all n values. The reason for not using tapering along z-axis, unlike along x-axis, is that beam steering on elevation plane is continuous with almost constant ϕ angle. So, handling with side lobe interference gets easier. On the other hand, the complexity in dealing with the side lobe on the azimuth plane is much harder. One can also apply the aperture tapering along both axes to get lower side lobes, however, tapering only along one axis is used in this study. In order to calculate tapering coefficients, $taylorwin(M, \tilde{n}_m, SLL_m)$ function in MATLAB® was utilized. The calculated weighting coefficients are 0.7145, 0.8774, 1.1165, 1.2916, 1.2916, 1.1165, 0.8774

and 0.7145, for this radar example with $M = 8$. The resulting transmitted electric field pattern would be different than the uniformly excited array's field pattern. In the Figure 4.12Figure 4.12. The normalized time waveforms of the fields, which are transmitted by the planar LFMCW-FDA Radar, observed at 36 selected points would change with tapering. Peak field strengths are getting smaller, when the tapering is applied, because of the decrease in the effective antenna aperture. With the aforementioned weighting coefficients, 2.22 dB peak power level reduction with respect to uniformly excited array can be estimated. Moreover, half power beam width increases, whereas side lobe levels are getting smaller.

4.8.2 Phased Array Receiver

A planar phased array is deployed to capture the reflected signal from a target in this numerical example. For a radar application, detecting the angle of the target with respect to local coordinates and the distance to the reference point are main steps. Using the phased array as the receiver makes easily possible to resolve the angle-of-arrival of the reflected signal. Building the planar LFMCW-FDA is a novel and complicated process. Therefore, in order to perceive the possible advantages of the LFMCW-FDA, the phased array receiver will be utilized at the first step. Design of this receiver is not on the scope of this work. However, same number of antenna elements are used for the receiver PA. In the RX modules, incoming signal is mixed with the LO for the down-conversion. Down converted pulses are processed by using the digital beam forming (DBF) algorithms with the signal processing based on $2\mathcal{D}\ \mathcal{FT}$. As in the case of the transmitter, same 36 RX beams are needed to cover the aforementioned 2D angular space in the previous sub-section. That can be achieved with DBF algorithms. By resolving the angular location of the target using this type of PA receiver, the radial position and the velocity of the target can be decided by using the information in the frequency domain, because the base band signal is nothing but the one in the classical FMCW with an FDA envelope.

4.8.3 Range Resolution

The Fourier Transform of the reflected signal is given in the Eq-4.48 as a general formula. The spectral components (SC's) are $\omega_{fx} = 2\pi\,\nu_{ox} / T_f$ *and* $\omega_{fz} = 2\pi\,\nu_{oz} / T_f$. In this example, $\omega_{fz} \gg \omega_{fz}$, due to $T_{lz} \gg T_{lx}$ is chosen. There is an approximate spectral orthogonality, in contrary the fact that $\mathcal{K}$ values are not integer such that $\mathcal{K}_x = 0.731$ and $\mathcal{K}_z = 6.119$. Frequency bandwidth $\omega_{BW} = 2\pi f_{BW}$ is given in the following equation. The frequency bandwidth is a limiting parameter for the range resolution. Because, frequency spectrums of two targets on the same angular location must be resolved. Therefore, frequency bands must be adjacent to each other at least, that defines the range resolution of the radar which is ΔR_o. Step difference in the beat frequency is equal to f_{BW}.

$$\omega_{BW} = (M-1)\omega_{fx} + (N-1)\omega_{fz} + \frac{2\pi}{\tau} \cong \frac{(N-1)\mathcal{K}_z + 2}{\tau/(2\pi)} \qquad 4.59$$

$$f_{bo}(R) = \frac{\Delta f}{\tau}\frac{2R}{c} \quad and \quad f_{bo}(R+\Delta R_o) = \frac{\Delta f}{\tau}\frac{2(R+\Delta R_o)}{c} \qquad 4.60$$

$$\Delta R_o = \frac{\mathrm{f_{BW}}\,\tau\,c}{2\,\Delta f} \cong \frac{(N-1)cT_{lz}}{2} + \frac{c}{\Delta f} \qquad 4.61$$

In this case, $\mathrm{f_{BW}} = 31.2kHz$ therefore, $\Delta R_o = 1.573\,m$. The range resolution obtained in time domain is much larger than this one. Without processing signal in FD, the range resolution can be found by using the null to null pulse duration of the signal that impinged on the target. Therefore, that would be about ten kilometers for this example. Consequently, there is no benefit to use only time domain signal in order to detect location of two or more targets whose angular positions are within the main beam. The time for the signal propagates to target and reflected back to receiver is $2R/c$. For two targets are located on the points $R_o + R_{o1}$ and $R_o + R_{o2}$ where $R_o = 2km$, $R_{o1} = 0$ and $R_{o2} = 1.56m$. The beat frequency is around $f_b = \mu_f\,T_{po} = \frac{2999.7(MHz)}{1\,(msec)}\,\frac{2\,x\,2000\,(m)}{3x10^8(m/s)} \cong 40MHz$. To ease the illustration of

the IF spectrum, T_{LO}, true time delay, which is the same duration due to double way propagation of the signal, is applied on the LO for the receiver. Therefore, the beat frequencies can be seen around DC in the Figure 4.20.

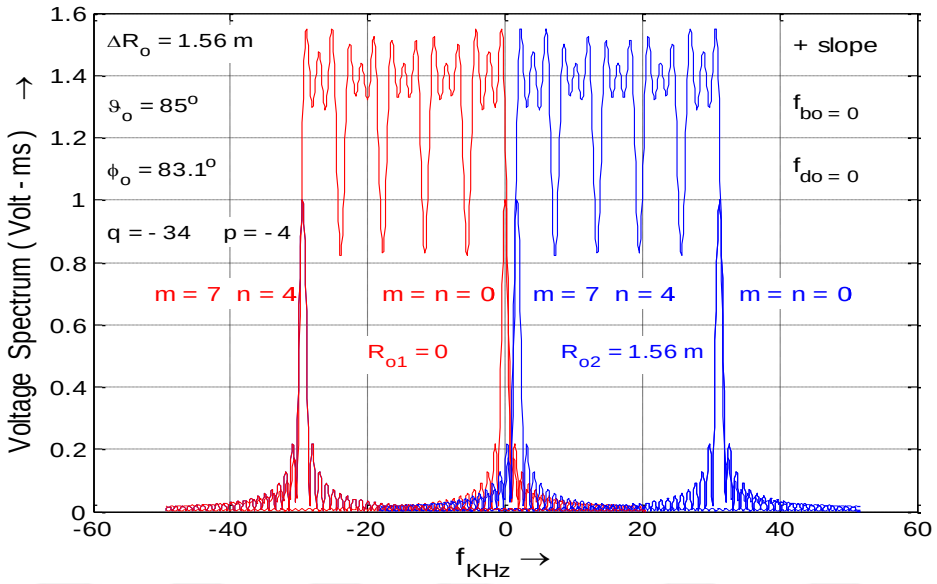

Figure 4.20. Fourier Transform spectrum for + slope and $\theta_0 = 85^o$; $\phi_0 = 83.1^o$ with two stationary point scatterers

When the target is not a stationary one, the Doppler effect would shift the beat frequency proportional to radial component of its velocity. For this part, the target which is coming toward the radar with the velocity of $v_{tg} = -25.73\, m/s$, so $f_{do} = 2.6\, kHz$. In order to distinguish its velocity and location precisely, we must utilize at least a pair of chirps with a positive and a negative slope frequency change. $R_o = 2km$ and $T_{LO} = 13.3\, \mu s$ are assumed. The resulting $f_{bo}^{+} = 37.7\, kHz$ and $f_{bo}^{-} = -37.7\, kHz$ for the positive and the negative slope respectively. The overall spectrum is given in the Figure 4.21.

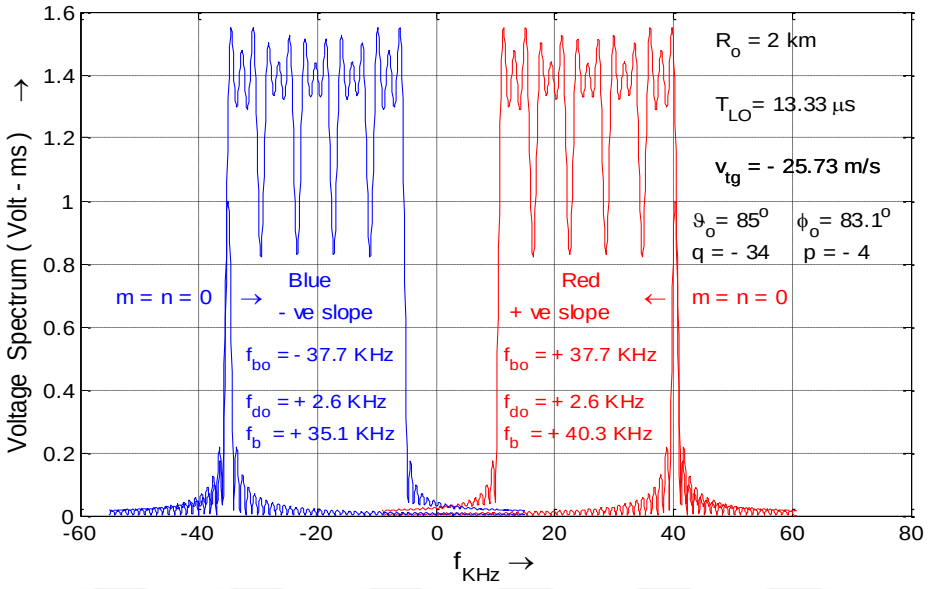

Figure 4.21. Fourier Transform spectrum for both $\mp$ slope and $\theta_0 = 85^o$ $\phi_0 = 83.1^o$with a point scatterer with $v_{tg} = -25.73\ m/s$

4.8.4 Realization of the Radar

This radar example can be realized by using wideband patch antennas. One example pattern when the maximum radiation is steered to $\theta_0 = 85^o and\ \phi_0 = 83.1^o$. The approximate size is $8cm$ by $5\ cm$ for RX/TX array. The resulting antenna gain is $G_A = 21.3dB$. 5 rows along z-axis are fed by 5 phase locked DDS to have $T_{lz} = 2.04\ ns$, whereas TTDs are utilized for 8 elements placed along x-axis to obtain $T_{lx} = 0.2436\ ns$. The maximum time delay over aperture, $T_{fill} = 8.2ns$. Multiple pulses are used as explained in 4.7.3. The silent duration between consecutive pulses, $T_g = 250\mu s$, whereas $\tau = 1000\mu s$. Therefore, duration of the ± pulse pair, $T_p = 2500\mu s$. Here, we choose number of the coherent pulse pairs, $N_{\_} = 8$. These 8 pulse pairs form a burst, and then 24 non-coherent bursts are used in radar. The radar range equation gives the SNR in the presence of the noise as in the Eq-4.62. Energy of the transmitted waveform, $E_{ot} = 2\ P_t\tau$ where $2\ P_t = 10W$. The energy ratio, $r_E =$

28.68 . Transmitter loss is $L_t = 2dB$ and the atmospheric loss is $L_a = 0.096\,dB$. The radial distance to the target is assumed to be $R_0 = 2km$ and the noise energy to be $k\,T_s = 9.16\,x\,10^{-18}\,mJ$. The RCS of the target is considered $\sigma_s = 0.1\,m^2$ and its radial length $L_{tg} = 1m$ with the aforementioned velocity, $v_{tg} = -25.72\,m/s$. This velocity is chosen due to maximize the improvement due to velocity matched Doppler filters. The SNR improvement factor has its maximum value, $I_{N\_} = 8.533$, with the optimum values of v_{tg} and T_p. The Doppler frequency is 2.6 kHz. In order to have lower beat frequency after dechirping, time delay for LO in RX side is $T_{LO} = 13.276\,\mu s$. Then, $f_{bo} = 200kHz$. According to Nyquist theory, the sampling frequency for IF signal must be equal to or greater than $2f_{bo}$. By using $T_{LO} \geq 0$, we can lower the requirement on the sampling frequency, however, it can cause aliasing in frequency domain in case there is a target which is closer than the expected range. Nevertheless, presence of the single target and the LO time delay in RX side are considered for lowering the sampling frequency requirement.

$$SNR = \frac{E_{ot}}{r_E\ k\,T_s} \cdot \frac{G_A^2\ \sigma_s\ \lambda_o^2\ L_t\,L_a}{(4\pi)^3\,R_o^4} = \frac{D_1 \cdot\ L_x}{I_{N\_} \cdot\ G_i\ \cdot G_{div}} \qquad 4.62$$

Probability of the detection P_D and the probability of the false alarm P_{FA} can be used to express the detectability factor $D_1 = \frac{ln(P_{FA})}{ln(P_D)} - 1$. During coherent integration process, the target should remain within same range resolution portion. The total longitudinal distance occupied by the target is determined by not only the radial extent of it, which is 1 m, but also the distance travelled during the coherent integration time, $CTI^{FDA} = 22.26ms$, so that $\Delta R_o \geq L_{tg} + \left|v_{tg}\right| CTI^{FDA}$. Decorrelation time $T_{ctg} \cong 100ms$ is calculated as in [54]. For 24 bursts being utilized, the frame time $FRT^{FDA} = 24 * CTI^{FDA} \cong 534.3\,ms$ can be found. This means that the target can be decorrelated $n_{ctg} = \frac{FRT^{FDA}}{T_{ctg}} \cong 5$ times. After using 24 bursts, one detection is tried. That process will be called cumulative detection step (CDS). As one repeats the CDS n_s^{FDA} times, the cumulative probability of the false alarm P_{cfa} and detection P_{cd} will be higher than P_d and P_{fa} as given in the Eq-4.63.

$$P_{cd}^{FDA} = 1 - (1 - P_d)^{n_s^{FDA}}$$
$$P_{cfa}^{FDA} = 1 - \left(1 - P_{fa}\right)^{n_s^{FDA}} \quad 4.63$$

The probability of the detection and false alarm can be obtained by using Eq-4.62 as $P_d = 0.8346$ for $P_{fa} = 0.5\ x\ 10^{-6}$. Then by repeating the CDS by $n_s^{FDA} = 2$ times, one can show that $P_{cd}^{FDA} = 0.9727$ and $P_{cfa}^{FDA} = 10^{-6}$ from the Eq-4.63. $SNR^{FDA} = 16.8\ dB$ in FDA frame time. General diagrams for frequency vs time within a chirp were given on the Figure 4.22 and Figure 4.23 for positive and negative slopes in LFM pulse respectively. In both figures, only one target was considered. FDA modulated reflected waveforms for both pulses were also on the figures. The vertical axis for reflected signal is amplitude instead of the angular frequency. They are given on the same figure in order to show the relation between frequency bandwidth of the signal that is reflected back from the target and the instantaneous frequency of the transmitted chirp. The times of the maximum of $sinc$ like reflected signal are not equal for positive and negative slope pulses. Moreover, RF signal's frequency differs. The total frequency bandwidth impinged on the target can be calculated by using time bandwidth (TBW), as in the figures. $4\ dB$ energy equivalent TBW is $T_{nnz}/2$ for this example which has an envelope like $sinc$ function. Then, $\Delta f_{oFDA} \cong \left|\mu_f\right| T_{nnz}/2 \cong 98.9 MHz$. Due to the target's radial extent, the decorrelation frequency is $f_c \cong c/(2L_{tg}) = 150 MHz$ for the SW I target, which is greater than the frequency bandwidth. Therefore, there is no intra-pulse modulation in FD. The total detection duration would be $T_{rv}^{FDA} = n_s^{FDA}\ x\ FRT^{FDA} = 2\ x\ 534.3\ ms \cong 1068\ ms$ in this application.

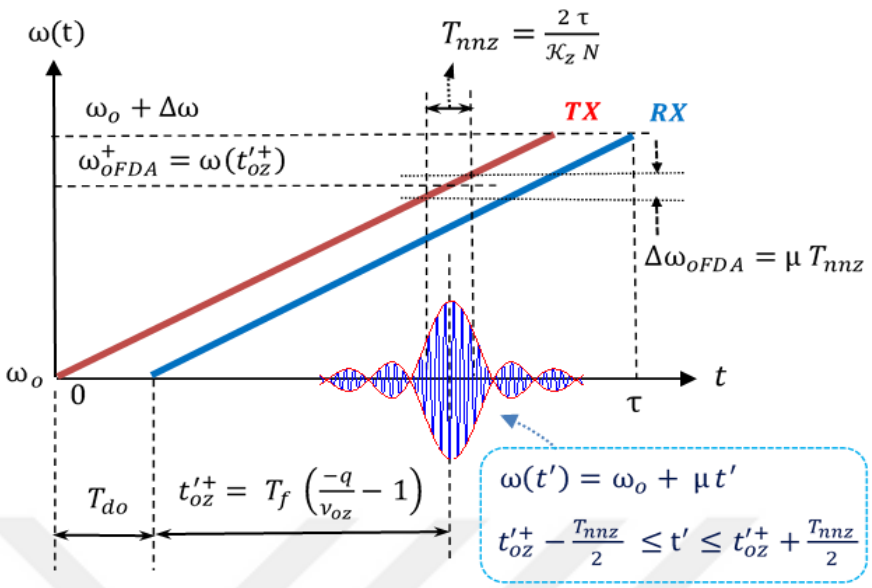

Figure 4.22. Frequency of RF signal and IF waveform for a particular target for positive slope

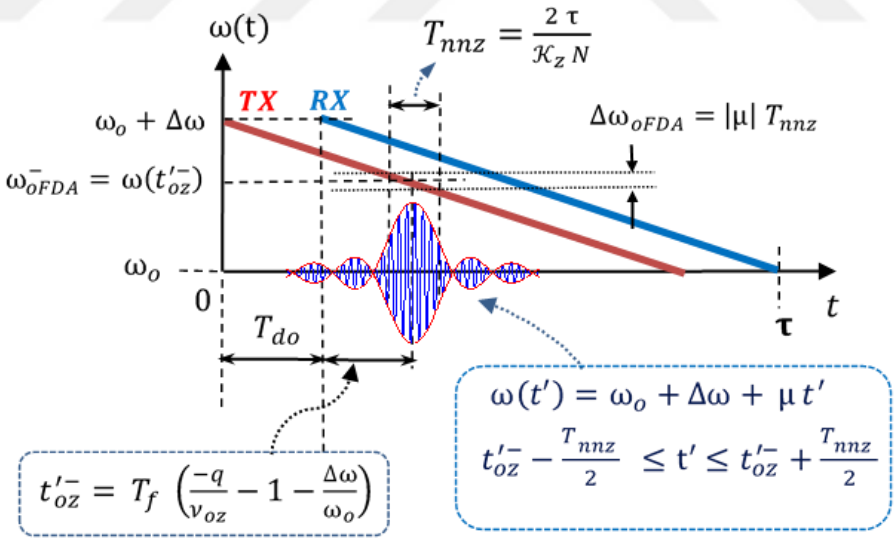

Figure 4.23. Frequency of RF signal and IF waveform for a particular target for negative slope

4.8.5 Comparison between the LFMCW FDA Radar and an equivalent LFMCW PA

In this section the comparison between the proposed planar radar and an equivalent phased array radar which uses LFMCW. For fair comparison, parameters of the PA equivalent are determined first. Antenna arrays are composed of same number of elements for both TX and RX and same type of antennas. In order to have similar amount of frequency bandwidth occupied by LFMCW-FDA for a point target, $\Delta f^{PA} = 95.296\ MHz$ is chosen. Number of the ± slope coherent LFM pulse pair used in PA remains same, $N_{-} = N_{-}^{PA} = 8$. However, number of non-coherent bursts is decreased, $n_{-}^{PA} = 2$. For comparison only one CDS is used in both radars, $n_s = n_s = 1$. The number of the frequency agility steps between two consecutive bursts is $N_{div}^{PA} = 2$. Then, $G_i^{PA} = 2.7dB$ and $G_{div}^{PA} = 6.35\ dB$ are obtained. Whereas the LFMCW FDA scans the all of the interested space within single pulse due to the self-scanning nature, same space must be scanned by changing PA's phase shifters. 36 beam position were selected for scanning the same space, as FDA does. Therefore, energy ration r_E, vanishes in the Eq-4.62 for PA, because all of the pulse energy is transmitted to intended angular location. That yields $P_d = 0.9708$ and $P_{fa} = 10^{-6}$. However, it requires more time to visit all 36 beam locations. The total frame time for a single beam location is $FRT^{PA} = WFT^{PA} = 44.53\ ms$, so overall scan time or revisit time with PA is $T_{rv}^{PA} = 36\ x\ WFT^{PA} = 1603\ ms$ with $SNR^{PA} = 23.65\ dB$ which is higher than FDA whose $SNR^{FDA} = 16.8\ dB$. But the revisit time in FDA is $T_{rv}^{FDA} = 534.3\ ms$.

For this particular scenario, the displacement of the target during the detection would be $13.75\ m$ and $41.35\ m$ for the proposed LFMCW FDA and PA radars respectively. Although, SNR is lower in LFMCW FDA, faster detection would be one of advantages of it especially for tracking targets which have high RCS.

$$E_{oT}^{FDA} = E_{oin} \;\; N_{-}^{FDA} \;\; n_{-}^{FDA} \;\; n_{s}^{FDA} = 384 \, E_{oin}$$
$$E_{oT}^{PA} = E_{oin} \;\; N_{-}^{PA} \;\; n_{-}^{PA} \;\; n_{s}^{PA} \;\; N_{b} = 576 \, E_{oin} \qquad 4.64$$

Energy-time product of both cases could also be compared. Output power of the chirp will be assumed constant for both radars. Because duration of the pulse is also constant, number of pulse used in both cases could be compared in order to energy-time product comparison. Energy transmitted to space for a positive and negative pulse pair is same for both which is called as $E_{oin} = E_{ot}$. Total energy calculations for both applications are given below. Whereas 384 pulse pairs are used in FDA, 576 pulse pairs are transmitted in PA. Therefore, the energy needed in FDA is less than in the PA equivalent. This is another advantage for the LFMCW FDA radar. This is valid for this example, generalization of this conclusion may be invalid for other FDA and PA comparisons.

4.8.6 Conclusion and Discussion

In this chapter, design steps and the critical points of the proposed LFMCW based planar array was presented in detail. Starting from the derivation of the transmitted field for a far-field observer was done in order to obtain the received field representation that reflects from the target. Both transmitted and received fields were illustrated for the examples with the chosen radar parameters. Coverage diagrams and radiation pattern for different cases revealed the abilities of the proposed transmitter to be used in the radar applications with the raster scanning beam formations. In order to progress step by step in this research topic, the PA receiver was deployed that makes easier the DF processes as well. Also, it is preferable in order to increase the receiver antenna gain which is vital for this example. Because, dwell time gets smaller, as the LFMCW-FDA scans the whole space very fast within only a millisecond for the given example. That causes the decrease in the received energy which should be compensated by antenna gains. This weak point was

overcome by applying non-coherent bursts that are composed of the periodic coherent positive and negative slope pulse pairs. The performance of the radar examples is compared under certain circumstances with the given target properties. The fast scanning feature makes the proposed LFMCW based planar FDA preeminent against the equivalent PA radar in target tracking applications, because the target's displacement is less during the detection process. The need for less energy-time product in the proposed radar, which is delivered to the radars, is another advantage. Although, it cannot be generalized to all of the FDA/PA comparisons, this advantage was observed and presented in this study. The utilization of the proposed array by observing and presenting some superiorities with given simulation results have been shown, in order to make the LFMCW based FDA concept more complete.

There are still open points in planar FDA concept that can be worked on. A proper receiver method should be studied, for the sake of the wholeness of the concept. Deploying a linear PA instead of the planar one as the receiver would be good starting point. It would decrease the cost and complexity of the receiver. One could decide the one angle by using this linear array. The other angle and distance to the target could be decided by using the procedure given in the previous chapter. Designing a FDA as receiver that is eligible to work with FDA transmitter would be even better research topic. Implementation of this array and obtaining real measurement result are always concept-proving studies. Advantages of the FDA in multipath environment and the target RCS characteristic have been shown by measurements conducted by Dr. Cetintepe, when the linear array was used. Behavior of the planar FDA could be investigated as well, whereas the target RCS characteristic will be investigated in the next chapter.

CHAPTER 5

TARGET RCS CHARACTERISTIC IN PLANAR LFMCW-FDA RADAR

In the previous section, a novel method is proposed and analyzed. The proposed planar LFMCW based FDA radar is also evaluated by presenting a realistic radar with a SW I type target. Some superiorities are illustrated in terms of target displacement during tracking and energy radiated by the radar. It is also one of the advantage of it, that total time to detect a thread is shorter with the LFMCW-FDA, as the revisit time is shorter in the proposed scenario. Therefore, that limits the time which the target can realizes the radar operating around and may also take countermeasure.

Although, the concept of LFMCW based FDA is rather novel topic, it has been already shown that it is a fruitful research area. Some hidden advantages have been revealed by [3], [4], [5], [11]. In 2014, Dr. Cetintepe and Prof. Dr. Demir showed that the classical FDA and the LFMCW based FDA outperforms its equivalent phased array rival in terms of the target RCS characteristic and "multipath characteristic over ground plane" in [2], and [1]. These works were deployed a linear antenna array for both the classical FDA and LFMCW-FDA. Designing a planar LFMCW FDA or classical FDA is different process and there are a lot of differences between their precursor and themselves. In this section, the target's radar cross-section (RCS) characteristic will be investigated by using the planar LFMCW-FDA transmitter presented in the previous section.

The organization of this section is as follows. Firstly, a brief description of the RCS and its history in the literature are given. Then, the approach focused on in this work will be introduced with a general solution. This general solution will be narrowed down to realistic canonical examples. This results will be compared with the

equivalent PA radar. Finally, results and performance will be evaluated and this section will be concluded.

5.1 Radar Cross-Section (RCS)

The term radar cross-section (RCS) is an important measure of how much reflective surface would be equivalent to the target for radar application. However, it does not have to be strictly related to the signal reflected back from the target. There are different approaches to RCS which may depend on the radar applications. Some radars try to detect the backscattered energy from the target only, it is called as monostatic radar. In this one, the transmitter and the receiver are collocated. The second one may be defined as that the direction of the reflection or scattering is same as the incidence direction. That one is called as forward-scatter RCS. The final one contains the all of the cases that are not enclosed by the aforementioned two. The bi-static RCS is a useful measure that may be used for the radar whose transmitter and receiver are not collocated. [55]

RCS is measure of ratio between incident power density and reradiated power density by the target towards receiver. Although, the scattered field may be radiated in any direction, only part of reradiated power toward the receiver position is interested. Backscattered field does not vary much with respect to the angle that EM field is incident from, when the target has a simple shape, i.e. a point scatterer or homogenously fabricated sphere. However, most targets have more complex shape and structure than these simple ones. When there is no symmetry along every line that can be drawn from volumetric center to outward direction, RCS is a function of the frequency as well as the angle that power incidents on the target. RCS, σ, can be written as in the Eq-5.1 , [56]. Dependency on incidence and scattering angles can also be shown in the equation. Since, monostatic radar is considered in this study, incidence and scattering angles are same.

$$\sigma_s(\theta_s, \phi_s, \theta_i, \phi_i) = \lim_{R\to\infty} 4\pi R^2 \frac{|E^s(\theta_s, \phi_s, \theta_i, \phi_i)|^2}{|E^i(\theta_s, \phi_s, \theta_i, \phi_i)|^2} \quad 5.1$$

Supposing a radar transmits energy towards a scatterer, incident power density is $\frac{P_t G_t}{4\pi R^2}$, where P_t is transmitted power from the radar. G_t is gain of the transmitter.

$$P_r = \frac{P_t G_t}{4\pi R^2} \cdot \frac{\sigma_s}{4\pi R^2} A_e \quad 5.2$$

5.2 Reflected power from a point scatterer

RCS fluctuation can cause that target may be invisible to the radar from certain angle of arrival, since the received power, that is proportional to the reflected power in the Eq-5.2, may not reach the target detection threshold. How much the target RCS fluctuates, also depends on the type of the radar itself. Since different spectral components are used at the same time in radars based on the frequency diverse arrays (FDAs), they may have less fluctuation in RCS with respect to the incidence angle. For linear antenna array, this advantage has been shown in [3] both theoretically and experimentally. This behavior will be investigated in this study for a planar LFMCW based FDA radar. The planar array given in the previous section is utilized as transmitter. However, an omnidirectional receiver is assumed to be used, as the reflected average power is considered to examine the target RCS characteristic. At the beginning, the received power will be given in the presence of the point scatterer whose backscatter RCS is constant for any angle. Moreover, it will be assumed that it is constant all over the frequency spectrum deployed.

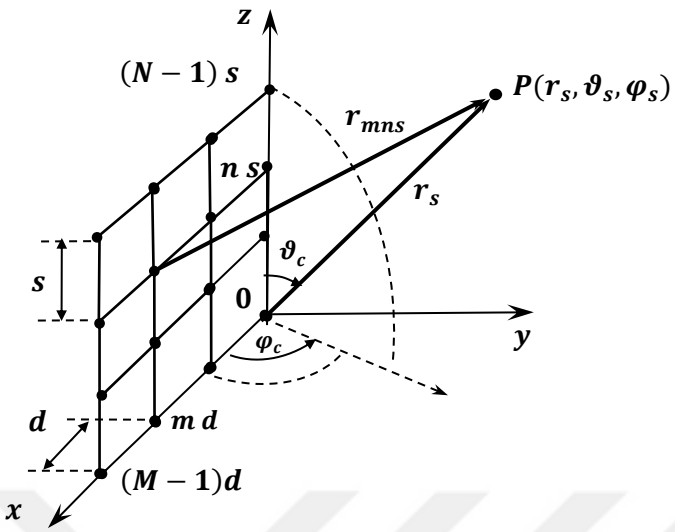

Figure 5.1. Planar LFMCW FDA transmitter with a point scatterer at the far-field point, $\boldsymbol{P(r_s, \vartheta_s, \varphi_s)}$

The planar TX array is illustrated on the Figure 5.1. Each point represents a transmit antenna, whose vector radiation pattern, $\overline{\boldsymbol{f_e}}(\theta, \phi | f_c)$, can be assumed as omnidirectional or directional pattern. Pattern of the practical antenna is frequency dependent, however, the element pattern is assumed to constant over frequency band in this example. Each element is excited by the voltage given in the below equation which is the LFMCW chirp. As it was given as previous sections, every antenna element has its own latency on the same chirp. The true time delay (TTD) for the mn^{th} element is given as $T_{mn} = mT_{lx} + nT_{lz}$, where $T_{lz} \gg T_{lx}$ or $T_{lx} \gg T_{lz}$ for the proper function of the proposed radar.

$$V_{in}(t) = \ P(t)\, e^{j\left[w_0 t + \frac{\mu}{2} t^2\right]} \qquad 5.3$$

$$\boldsymbol{E_t}(\boldsymbol{r},t) = \overline{f_e}(\theta,\phi\,|f_c)\sum_{m=0}^{M-1}\sum_{n=0}^{N-1}P(t-t_{mn})\frac{1}{r_{mns}}e^{j\left[w_0(t-t_{mn})+\frac{\mu}{2}(t-t_{mn})^2\right]} \quad 5.4$$

where

$$\begin{cases} \mu = 2\pi\dfrac{\Delta f}{T} & : the\ radian\ slope \\ w_0 = 2\pi\left(f_c - \dfrac{\Delta f}{2}\right) & : start\ angular\ frequency\ of\ the\ LFMCW\ \ signal \\ P(t) & : unit\ rectangular\ pulse\ over\ time\ in\ [0,T] \\ \overline{f_e}(\theta,\phi|f_c) & : the\ vector\ pattern\ of\ antenna\ elements \end{cases}$$

$$t_{mn} = T_{mn} + \frac{r_{mn}}{c} = T_{mn} + \frac{|\,\boldsymbol{r_s} - \hat{\boldsymbol{a}}_{\boldsymbol{x}} md - \hat{\boldsymbol{a}}_{\boldsymbol{z}}\, ns\,|}{c} \quad 5.5$$

The total transmitted electric field can be written by taking summation along x and z axes as in the Eq-5.4. The distance between mn^{th} element and the point scatterer is r_{mns}. The total time delay of the electric field that incident on the scatterer, which transmitted from mn^{th} element, is given as t_{mn}. This delay contains the total TTD of the excitation and the time that the field propagates towards the scatterer. The incident power would be reradiated by the target RCS, σ. Therefore, the scattered power density per unit solid angle can be found by scaling reflected power by $1/4\pi R^2$. Since electric field density is proportional to the square root of the power, one can multiply the incident electric field with $\sqrt{\sigma/(4\pi R^2)}$ to find the reradiated electric field. The reflected field would induce voltage of a receiver antenna that is located at the origin proportional to the square root of its effective aperture, A_{eff}. The voltage due to reflection from the point scatterer located $P(r_s,\theta_s,\phi_s)$ is given in the Eq-5.6. The term $1/4\pi$ is also included into A in this equation.

$$v_{rxs}(\boldsymbol{r_s},t) = A\sqrt{\sigma}\sqrt{A_{eff}}\sum_{m=0}^{M-1}\sum_{n=0}^{N-1}P(t-t_{mns})\frac{1}{r_{mns}\,r_s}e^{j\left[w_0(t-t_{mns})+\frac{\mu}{2}(t-t_{mns})^2\right]} \quad 5.6$$

Total delay of the signal transmitted from mn^{th} element and reflected back to the origin is t_{mns} in the Eq-5.7. The two way propagation path in free space that it takes is $r_{mns} + r_s$, where T_{mn} is the total TTD of the excitation on the corresponding antenna element.

$$t_{mns} = T_{mn} + \frac{r_{mns} + r_s}{c} \tag{5.7}$$

5.3 General representation of the reflected power from a group of point scatterers

The target RCS is dependent on the material, surface shape and the size of it. Practically, targets are much more complex than the point scatterer. Therefore, it is essential to expatiate upon this work for realistic example by considering multiple point scatterers instead of a single one as the target. In other words, RCS fluctuation is expected to be more significant, then a comparison with phased array radar can be done. This example may not represent all possible types of the targets, however, this is still a reliable and adequate starting point for comparison. The group is located on a sphere around the far field point $P_c(r_c, \theta_c, \phi_c)$ and radius of $\boldsymbol{\delta r_i}$. With such a shape it is possible that the overall reflection can vary with respect to look angle. In this subsection, the received voltage is formulized in presence of only a single point scatterer on the aforementioned sphere surface as in the Eq-5.8 by using the Eq-5.6.

$$v_{rxi}(\boldsymbol{r_i}, t) = A\sqrt{\sigma_i}\sqrt{A_{eff}} \sum_{m=0}^{M-1}\sum_{n=0}^{N-1} P(t - t_{mni}) \frac{1}{r_{mni}\, r_i} e^{j\left[w_0(t-t_{mni}) + \frac{\mu}{2}(t-t_{mni})^2\right]} \tag{5.8}$$

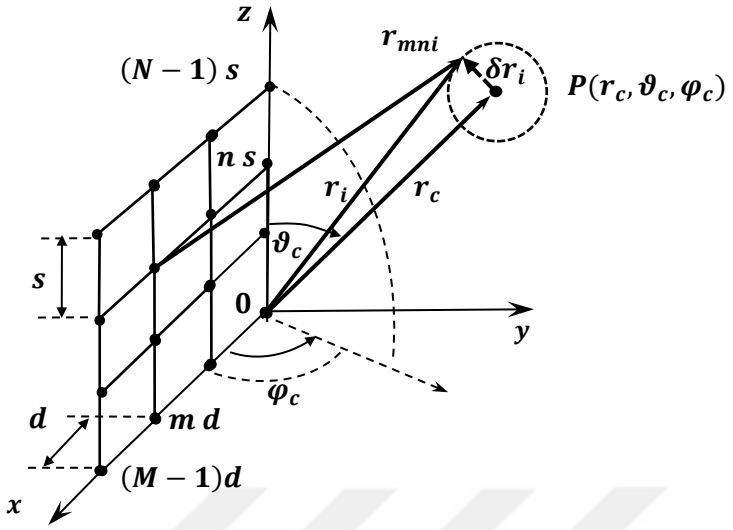

Figure 5.2. Planar LFMCW FDA transmitter with a group point scatterers around the far-field point, $\boldsymbol{P(r_s, \vartheta_s, \varphi_s)}$

$$t_{mni} = T_{mn} + \frac{r_{mni} + r_i}{c} = mT_{lx} + nT_{lz} + \frac{|\,\boldsymbol{r_c} - \boldsymbol{r'_{mn}} + \boldsymbol{\delta r_i}|}{c} + \frac{|\,\boldsymbol{r_c} + \boldsymbol{\delta r_i}|}{c} \quad 5.9$$

The total delay of the signal that is transmitted from mn^{th} element and reflected back from the i^{th} scatterer at the origin is t_{mni}. Vector representation could be helpful for further calculation at this point, and $r_{mni} = |\,\boldsymbol{r_c} - \boldsymbol{r'_{mn}} + \boldsymbol{\delta r_i}|$, where $\boldsymbol{r'_{mn}} = md\hat{a}_{x'} + ns\,\hat{a}_{z'}$**.** With the definition of the u_x and u_z given in the Eq-5.10, one can write r_{mni} and r_i as in the Eq- 5.11 & 5.12 respectively. Since, $r_c \gg |-mdu_x - nsu_z + \hat{a}_{rc} \cdot \boldsymbol{\delta r_i}|$**,** small part can be ignored for amplitude terms for far field targets. By applying similar approach to the Eq-5.13, r_i can be taken as r_c for amplitude terms. That cannot be applied for phase terms.

$$u_x = \hat{a}_{\boldsymbol{r}} \cdot \hat{a}_{\boldsymbol{x'}} = \sin\theta_c \cos\phi_c \quad , \quad u_z = \hat{a}_{\boldsymbol{r}} \cdot \hat{a}_{\boldsymbol{z'}} = \cos\theta_c \quad 5.10$$

$$r_{mni} \approx \begin{cases} r_c - mdu_x - nsu_z + \hat{a}_{\boldsymbol{rc}} \cdot \boldsymbol{\delta r_i} & , \quad for\ phase\ terms \\ r_c & , \quad for\ amplitude\ terms \end{cases} \qquad 5.11$$

$$r_i \approx \begin{cases} r_c + \hat{a}_{\boldsymbol{rc}} \cdot \boldsymbol{\delta r_i} & , \quad for\ phase\ terms \\ r_c & , \quad for\ amplitude\ terms \end{cases} \qquad 5.12$$

Substituting the r_{mni} and r_i values given in the Eq-5.11 & 5.12 into the Eq-5.9, one can get the general formula for the time delay as in the following equation.

$$t_{mni} = mT_{lx} + nT_{lz} + \frac{2r_c}{c} - m\frac{du_x}{c} - n\frac{su_z}{c} + \frac{2\,\hat{a}_{\boldsymbol{rc}} \cdot \boldsymbol{\delta r_i}}{c} \qquad 5.13$$

On the surface of the sphere, K number of scatterers are assumed to be located with their corresponding local angular positions. This local coordinate system whose origin is center point, P_c, of the far field sphere, will be explained when it is needed in the next subsection.

Time representation in the equations, t, has a time reference of the transmitter. For the sake of the simplicity, it is better to use retarded time which is delayed by the propagation of the wave in two ways. The time that the filed is transmitted and scattered back to the receiver, $2r_c/c$. This delay is obvious in the Eq-5.13. By letting this delay combine with the time, they form the retarded time $t' \triangleq t - 2r_c/c$. Moreover, $t'_{mni} \triangleq t_{mni} - 2r_c/c$ shall be defined. The overall summation of the received voltage can be written as in the Eq-5.14. Due to aperture delays are much less than the unit rectangular pulse duration, τ, $P\left(t' - t'_{mni}\right)$ can be simplified to $\left(t'\right) \cong P\left(t' - t'_{mni}\right)$.

$$v_{rx}(\sum \boldsymbol{r_i}, t) = A\sqrt{A_{eff}} \sum_{i=0}^{K-1}\sum_{n=0}^{N-1}\sum_{m=0}^{M-1} P(t' - t'_{mni}) \frac{\sqrt{\sigma_i}}{r_c^2} e^{j\left[w_0(t'-t'_{mni}) + \frac{\mu}{2}(t'-t'_{mni})^2\right]} \qquad 5.14$$

The phasor term in the above equation could be derived further in order to have a generalized formula for the total received voltage. By substituting Eq-5.13 into the Eq-5.14, the phasor becomes as in the Eq-5.15.

$$\begin{aligned} w_0(t'-t'_{mni})+\frac{\mu}{2}(t'-t'_{mni})^2 &= \left(w_0t'+\frac{\mu}{2}t'^2\right)\ \dots \\ &-(w_0+\mu t')\left[\, m\left(T_{lx}-\frac{du_x}{c}\right)+n\left(T_{lz}-\frac{du_z}{c}\right)+2\,\frac{\hat{\mathrm{a}}_{\boldsymbol{rc}}\cdot\boldsymbol{\delta r_i}}{c}\,\right]\dots \\ &+\frac{\mu}{2}\left[\, m^2\left(T_{lx}-\frac{du_x}{c}\right)^2+n^2\left(T_{lz}-\frac{du_z}{c}\right)^2+4\left(\frac{\hat{\mathrm{a}}_{\boldsymbol{rc}}\cdot\boldsymbol{\delta r_i}}{c}\right)^2\,\right]\dots \\ &+\mu mn\left[\left(T_{lx}-\frac{du_x}{c}\right)\left(T_{lz}-\frac{du_z}{c}\right)+2\,\frac{\hat{\mathrm{a}}_{\boldsymbol{rc}}\cdot\boldsymbol{\delta r_i}}{c}\left(\frac{T_{lx}}{n}-\frac{du_x}{nc}+\frac{T_{lz}}{m}-\frac{du_z}{mc}\right)\right] \end{aligned} \tag{5.15}$$

$$\begin{aligned} \frac{\pi}{1000}\ \approx\ &\frac{\mu}{2}\left[\, m^2\left(T_{lx}-\frac{du_x}{c}\right)^2+n^2\left(T_{lz}-\frac{du_z}{c}\right)^2+4\left(\frac{\hat{\mathrm{a}}_{\boldsymbol{rc}}\cdot\boldsymbol{\delta r_i}}{c}\right)^2\,\right]\dots \\ &+\mu mn\left[\left(T_{lx}-\frac{du_x}{c}\right)\left(T_{lz}-\frac{du_z}{c}\right)+2\,\frac{\hat{\mathrm{a}}_{\boldsymbol{rc}}\cdot\boldsymbol{\delta r_i}}{c}\left(\frac{T_{lx}}{n}-\frac{du_x}{nc}+\frac{T_{lz}}{m}-\frac{du_z}{mc}\right)\right] \end{aligned} \tag{5.16}$$

The part of the phasor that given in the Eq-5.16 can be omitted, since they are small enough. With the aforementioned assumptions and the derivation one can obtain the final form of the generalized formula for total received voltage from a group of scatterers as in the following equations. Furthermore, it is possible to write all three summations separately.

$$\begin{aligned} v_{rx}(\textstyle\sum \boldsymbol{r_i}, t) = \frac{A}{r_c^2}\,&\sqrt{A_{eff}}\ P(t')e^{j\left(w_0t'+\frac{\mu}{2}t'^2\right)} \\ &\sum_{i=0}^{K-1}\sqrt{\sigma_i}\ e^{-j(w_0+\mu t')2\,\frac{\hat{\mathrm{a}}_{\boldsymbol{rc}}\cdot\boldsymbol{\delta r_i}}{c}}\sum_{m=0}^{M-1}e^{jm\gamma_x}\sum_{n=0}^{N-1}e^{jn\gamma_z} \end{aligned} \tag{5.17}$$

where

$$\gamma_x = (w_0 + \mu t')\left(T_{lx} - \frac{du_x}{c}\right) \quad 5.18$$

$$\gamma_z = (w_0 + \mu t')\left(T_{lz} - \frac{du_z}{c}\right) \quad 5.19$$

5.4 Canonical example with dumbbell type scatterers

RSC characterization is expanded by giving a canonical example. RCS fluctuation with respect to the angle of the arrival of the field will be illustrated in this part of the work. Two point scatterers are considered as a target and build a bit more complex RCS. They are separated by the distance, l. The midpoint between them is assumed to be an origin of the local coordinate system, that can be seen on the Figure 5.3. Since, P_c is a generally defined point which may differ the location of the target, the local coordinate system must be defined with respect to global coordinate system shown on the figure. One can define that system however that is possible. In this study, definition of the selected conversion is as follows. y_s axis of the local coordinates is always in same direction with the unit vector in outward radial direction in global system at the center point of the scatterers, $\hat{a}_{\boldsymbol{rc}}$. Other axes are defined in accordance with the y_s axis and right hand rules. Unit vectors of the local coordinate system, $(\hat{a}_{\boldsymbol{xs}}, \hat{a}_{\boldsymbol{ys}}, \hat{a}_{\boldsymbol{zs}})$ are given here in terms of global ones $(-\hat{a}_{\boldsymbol{\phi c}}, \hat{a}_{\boldsymbol{rc}}, -\hat{a}_{\boldsymbol{\theta c}})$ at the given mid-point respectively. RCS of the point scatterers are σ_0 and σ_1, both are assumed to be equal to σ for further calculations. Vectors $\boldsymbol{\delta r_0}$ *and* $\boldsymbol{\delta r_1}$ are given in the Eq-5.20, magnitude of them is $\frac{l}{2}$ and their directions are opposite to each other. They can be written in terms of local coordinates as given in the equation.

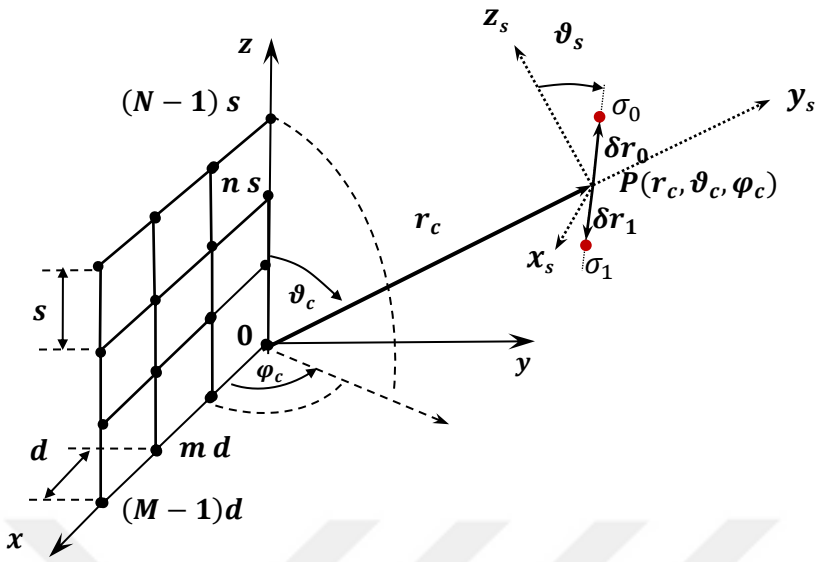

Figure 5.3. Planar LFMCW FDA transmitter with a pair of point scatterers around the far-field point, $\boldsymbol{P(r_c, \vartheta_c, \varphi_c)}$

$$\boldsymbol{\delta r_0} = -\boldsymbol{\delta r_1} = \frac{l}{2}\left(\sin\theta_s \cos\phi_s\, \hat{a}_{xs} + \sin\theta_s \sin\phi_s\, \hat{a}_{ys} + \cos\theta_s\, \hat{a}_{zs}\right) \tag{5.20}$$

In general formulation, there is the term "$\hat{a}_{\boldsymbol{rc}} \cdot \boldsymbol{\delta r_i}$". Since, the local coordinates are derived from the global coordinates and $\hat{a}_{\boldsymbol{rc}} = \hat{a}_{\boldsymbol{ys}}$. Therefore, the dot product can be found as in the Eq-5.21. And $K = 2$, because there are only two point scatterers on the sphere with radius $l/2$.

$$\hat{a}_{\boldsymbol{rc}} \cdot \boldsymbol{\delta r_0} = -\hat{a}_{\boldsymbol{rc}} \cdot \boldsymbol{\delta r_1} = \frac{l}{2}\sin\theta_s \sin\phi_s \tag{5.21}$$

By substituting the RCS values and Eq-5.21 into the general formula that is given in the Eq-5.17, one obtains the Eq-5.22. The effect of the rotating around the center point can be seen on the equation.

$$v_{rx}(\sum \boldsymbol{r_i}, t) = \frac{A}{r_c^2}\sqrt{A_{eff}}\ P(t')e^{j\left(w_0 t' + \frac{\mu}{2}t'^2\right)}\sqrt{\sigma} \left(e^{-j\gamma_s} + e^{+j\gamma_s}\right) \sum_{m=0}^{M-1} e^{jm\gamma_x} \sum_{n=0}^{N-1} e^{jn\gamma_z} \quad 5.22$$

where,

$$\gamma_s = (w_0 + \mu t')\ \frac{l}{c}\sin\theta_s \sin\phi_s \quad 5.23$$

5.4.1 Average Received Power

The total received voltage has been found in the previous section. However, it is important to determine the average power received from the reflected field in order to characterize the target RCS. The power is directly proportional to the absolute square of the voltage. By integrating received voltage over the pulse duration, τ, and then taking time average, one finds the average received power as in the Eq-5.24. The term, received power, is being used here, because this study focuses on a monostatic radar example. Average received power implies the average of the power reflected from the scatterer, which impinged on the receiver antenna on the origin. Therefore, efficiency and gain of the antenna, and gain of the receiver will be assumed to be constant over the operational frequency bandwidth. Only first reflection is considered as the reflected power in this study. Secondary reflection from a point scatterer that occurs due to the scattered field from the other one, is not in the scope of this work.

$$P_{avg} = \frac{1}{\mathrm{Z}_o \tau}\int_{\tau} |v_{rx}(\sum \boldsymbol{r_i}, t)|^2 dt = \frac{1}{\mathrm{Z}_o \tau}\int_{\tau} v_{rx}(\sum \boldsymbol{r_i}, t) * v_{rx}^*(\sum \boldsymbol{r_i}, t) dt \quad 5.24$$

By substituting the received voltage expression into the Eq-5.24, one would get the form as in the Eq-5.25. The part "$e^{-j\gamma_s} + e^{+j\gamma_s}$" that came to effect due to the dumbbell scatterer, is real valued and equal to " $2\cos\gamma_s$ " with Euler's formula.

$$P_{avg} = \frac{1}{\tau} A^2 |\sigma| A_{eff} \frac{1}{r_c^4} \int_{\tau} P(t') \left(e^{-j\gamma_s} + e^{+j\gamma_s}\right)^2 \sum_{m=0}^{M-1} \sum_{m'=0}^{M-1} e^{j(m-m')\gamma_x} \sum_{n=0}^{N-1} \sum_{n'=0}^{N-1} e^{j(n-n')\gamma_z} \, dt \tag{5.25}$$

After interchanging the order of the summations and the time integral, multiplication of complex numbers will give the following form.

$$P_{avg} = \frac{1}{\tau} A^2 |\sigma| A_{eff} \frac{1}{r_c^4} \int_{\tau} P(t') \sum_{m=0}^{M-1} \sum_{m'=0}^{M-1} \sum_{n=0}^{N-1} \sum_{n'=0}^{N-1} \left(2e^{j\left((m-m')\gamma_x + (n-n')\gamma_z\right)} + e^{j\left((m-m')\gamma_x + (n-n')\gamma_z + 2\gamma_s\right)} + e^{-j\left((m-m')\gamma_x + (n-n')\gamma_z + 2\gamma_s\right)}\right) dt' \tag{5.26}$$

$$\begin{aligned} \nu_0 &= (m-m')\left(T_{lx} - \frac{du_x}{c}\right) + (n-n')\left(T_{lz} - \frac{su_z}{c}\right) \\ \nu_1 &= (m-m')\left(T_{lx} - \frac{du_x}{c}\right) + (n-n')\left(T_{lz} - \frac{su_z}{c}\right) + \frac{2l \sin\theta_s \sin\phi_s}{c} \\ \nu_2 &= -(m-m')\left(T_{lx} - \frac{du_x}{c}\right) - (n-n')\left(T_{lz} - \frac{su_z}{c}\right) - \frac{2l \sin\theta_s \sin\phi_s}{c} = -\nu_1 \end{aligned} \tag{5.27}$$

Then, one can define following 3 variables ν_0, $\nu_1, and\ \nu_2$, in order to ease the representation. Also, interchanging the orders of time integral and summations can be applied. Substituting those variables into above equation, P_{avg} can be written as:

$$P_{avg} = \frac{1}{\tau} A^2 |\sigma| A_{eff} \frac{1}{r_c^4} \sum_{m=0}^{M-1} \sum_{m'=0}^{M-1} \sum_{n=0}^{N-1} \sum_{n'=0}^{N-1} \int_{\tau} \underbrace{P(t')}_{1, t' \in [0,\tau]} \left(2e^{-j\nu_0(w_0 + \mu t')} + e^{-j\nu_1(w_0 + \mu t')} + e^{j\nu_1(w_0 + \mu t')}\right) dt' \tag{5.28}$$

Integral of the unit rectangular pulse, $P(t')$, with $e^{-j\mu t'}$ term can be calculated as the $sinc$ function. Finally, average power can be written as in the Eq-5.29. Because

of the fact that $\nu_1 = -\nu_2$, resultant exponential terms combined together to form the term $\cos(w_c \nu_1)$ in this equation. Although, further simplifications in average power calculation are possible, nevertheless, it will be found with computational methods by using MATLAB©.

$$P_{avg} = A^2 |\sigma| A_{eff} \frac{2}{r_c^4} \sum_{m=0}^{M-1} \sum_{m'=0}^{M-1} \sum_{n=0}^{N-1} \sum_{n'=0}^{N-1} \left(e^{-jw_c \nu_0} \left(\frac{\sin(\pi \Delta f \nu_0)}{\pi \Delta f \nu_0} \right) + \cos(w_c \nu_1) \left(\frac{\sin(\pi \Delta f \nu_1)}{\pi \Delta f \nu_1} \right) \right) \quad 5.29$$

5.4.2 Average Received Power with PA

Target RCS characterization of the LFMCW-FDA will be evaluated and compared with the equivalent PA example in terms of the RCS fluctuation with respect to the incidence angle of the radar signal. Therefore, average received power of the reflected signal is needed also for the phased array radar. Same number of antenna and positions for antennas in transmitter are utilized in the equivalent example for fair comparison. The illustration of the PA and a far-field target would be same as the one in Figure 5.1. Because the focus is the RSC fluctuation here, it is appropriate to use a single omnidirectional receiver antenna as in the LFMCW-FDA. The transmitted electric field with MxN antennas along x and z axes respectively can be written as in the Eq-5.30. Phase differences between each consecutive elements along x and z axes are $\Delta\Phi_x$ and $\Delta\Phi_z$ respectively. The inter-element displacements are assumed to be same as the LFMCW example.

$$\boldsymbol{E_t^{PA}}(\boldsymbol{r}, t) = \overline{f_e}(\theta, \phi \,|f_c) \sum_{m=0}^{M-1} \sum_{n=0}^{N-1} P(t - t_{mn}) \frac{1}{r_{mn}} e^{j[w_c t' + m(k_c d u_x - \Delta\Phi_x) + n(k_c s u_z - \Delta\Phi_z)]} \quad 5.30$$

One could also find the reflected field as it was done before. The field scattered back with $\frac{\sigma_s}{4\pi R^2}$. The reflected field would excite voltage on the receiver terminal. This

voltage conversion can be shown by effective antenna aperture. Same efficiency values are also assumed here. All these effects are buried into A again in the formulas. Therefore, one can write the received voltage as in the Eq-5.31.

$$v_{rx}^{PA}(\boldsymbol{r},t) = A\sqrt{\sigma}\sqrt{A_{eff}}\sum_{m=0}^{M-1}\sum_{n=0}^{N-1}\frac{a_{mn}}{r_{mn}}\, e^{j[w_c t' + m(k_c d u_x - \Delta\Phi_x) + n(k_c s u_z - \Delta\Phi_z)]} \qquad 5.31$$

These summations can be calculated as digital $sinc$ functions for uniform excitation i.e. $a_{mn} = 1 \;\; for\; all\; m\; and\; n$. In order to implement the effect of multiple point reflector another summation must be included. The received voltage due to a single scatterer can be included by using this form $\frac{\sqrt{\sigma_i}}{\sqrt{4\pi r_c}}\, e^{-j2\pi\, 2\frac{\hat{\mathbf{a}}_{\boldsymbol{rc}}\cdot\boldsymbol{\delta r_i}}{\lambda_c}}$ as in the previous section. Therefore, the total received power can be found as in the Eq-5.32. Furthermore, average power can be found as in the Eq-5.33, by applying $P_{avg} = \frac{|V|^2}{Z_o}$. The $digital\; sinc$ functions have their maximum values for PA, because maximum power radiation direction is tilted to the center point of the scatterers by using the corresponding phases.

$$v_{rx}^{PA}(\boldsymbol{r},t) = A\sqrt{A_{eff}}\; MN\sum_{i=0}^{K-1}\sqrt{\sigma_i}\, e^{-j2\pi\, 2\frac{\hat{\mathbf{a}}_{\boldsymbol{rc}}\cdot\boldsymbol{\delta r_i}}{\lambda_c}} \frac{\sin\left(\frac{M}{2}(k_c d u_x - \Delta\Phi_x)\right)}{M\sin\left(\frac{1}{2}(k_c d u_x - \Delta\Phi_x)\right)}\;\frac{\sin\left(\frac{N}{2}(k_c s u_z - \Delta\Phi_z)\right)}{N\sin\left(\frac{1}{2}(k_c s u_z - \Delta\Phi_z)\right)} \qquad 5.32$$

$$P_{avg} = A^2|\sigma|A_{eff}M^2N^2\frac{1}{r_c^4}\sum_{i=0}^{K-1}\sum_{i'=0}^{K-1}e^{-j2\pi\beta_{ii'}} \underbrace{\left[\frac{\sin\left(\frac{M}{2}(k_c du_x - \Delta\Phi_x)\right)}{M\sin\left(\frac{1}{2}(k_c du_x - \Delta\Phi_x)\right)}\right]^2}_{=1}\underbrace{\left[\frac{\sin\left(\frac{N}{2}(k_c su_z - \Delta\Phi_z)\right)}{N\sin\left(\frac{1}{2}(k_c su_z - \Delta\Phi_z)\right)}\right]^2}_{=1} \quad 5.33$$

General form of $\beta_{ii'}$ is as following formula.

$$\beta_{ii'} = \frac{2\hat{\boldsymbol{a}}_{\mathbf{rc}} \cdot (\boldsymbol{\delta r_i} - \boldsymbol{\delta r_{i'}})}{\lambda_c} \quad 5.34$$

For the Dumbbell target couple, all possible values for $\beta_{ii'}$ are given as in the Eq-5.35. After substituting this into the Eq-5.33, final P_{avg} with PA can be shown as in the Eq-5.36 with the fact that maximum radiation direction is on the center point of the scatterers.

$$\begin{aligned} \beta_{00'} = \beta_{11'} = 0 \\ \beta_{01'} = -\beta_{10'} = 2\frac{l}{\lambda_c}sin\theta_s sin\phi_s \end{aligned} \quad 5.35$$

$$P_{avg} = A^2|\sigma|A_{eff}M^2N^2\frac{2}{r_c^4}\overbrace{\left(1+\cos\left(4\pi\frac{l\sin(\theta_s)\sin(\phi_s)}{\lambda_c}\right)\right)}^{Constant\ and\ Fluctuating} \quad 5.36$$

Average received power by PA is given in the Eq-5.36. With the fact that cosine function can be between 1 and -1, so that maximum of the average power is $P_{avg} = A^2|\sigma|A_{eff}M^2N^2\frac{4}{r_c^4}$. It is obvious in the formula that this value is fluctuating between its maximum and zero with respect to the incidence angle.

5.4.3 Comparison of the Average Received Power

One of the advantage of the LFMCW-FDA is its self-scanning behavior that makes possible to steer the beam corresponding angle with respect to the time within a chirp. It radiates its power to whole region of interest within single LFM pulse, which can be a huge section of the space depending on the design parameters. Consequently, the more space the LFMCW-FDA scans, the lower average power incidents on a single far-field point in the region of interest. Assuming constant average transmitted power, gain of the antenna array and duration of the chirp, as the scanned space increases, the duration that beam is tilted to the far field point decreases. Therefore, the average received power would be lower as a result of the faster scan with larger scanned space. On the other hand, the PA's average received power does not change for the same far-field point. Because, the usage of the PA is radically different from the other. The maximum radiation direction does not change within a pulse duration in the PA case. The beam is directed to the aforementioned point by using phase shifter throughout the pulse duration.

Scanned space in LFMCW-FDA is determined by the design of the transmitter as it was given in the previous section of this study. Once the transmitter was built, the scanned angles can be controlled by the chirp properties. With the higher bandwidth deployed for the chirp, enclosed space gets larger. Therefore, one could find the relation between the average received power and the chirp bandwidth.

Value of the P_{avg} is fluctuating between zero and $A^2|\sigma|A_{eff}M^2N^2\frac{4}{r_c^4}$ with respect to the incidence angle for the phased array radar. Because the expression has DC term and also cosine function as AC term. However, direct interpretation is not possible for the LFMCW-FDA case given in the Eq-5.29 yet. The DC and AC terms are used for the constant and fluctuating part of the received power with respect to incidence angle respectively. First, we need to define one equality that helps the determination of the DC part of the average received power by the LFMCW-FDA. The part that is

not related to incidence angle in the Eq-5.29 can be calculated as the DC part by letting $a_{(m-m\prime)(n-n\prime)} = e^{-jw_c\nu_0}\left(\frac{\sin(\pi\Delta f\nu_0)}{\pi\Delta f\nu_0}\right)$.

$$\sum_{m=0}^{M-1}\sum_{m'=0}^{M-1}\sum_{n=0}^{N-1}\sum_{n'=0}^{N-1} a_{(m-m\prime)(n-n\prime)} = \sum_{\bar{m}=-(M-1)}^{M-1}\sum_{\bar{n}=-(N-1)}^{N-1}(M-|\bar{m}|)(N-|\bar{n}|)a_{\bar{m}\bar{n}} \tag{5.37}$$

$$P_{avg}^{DC} = A^2|\sigma|A_{eff}\frac{2}{r_c^4}\sum_{\bar{m}=-(M-1)}^{M-1}\sum_{\bar{n}=-(N-1)}^{N-1} e^{-jw_c\left(\bar{m}\left(T_{lx}-\frac{du_x}{c}\right)+\bar{n}\left(T_{lz}-\frac{su_z}{c}\right)\right)} (M-|\bar{m}|)(N-|\bar{n}|)\left(\frac{\sin\left(\pi\Delta f\left(\bar{m}\left(T_{lx}-\frac{du_x}{c}\right)+\bar{n}\left(T_{lz}-\frac{su_z}{c}\right)\right)\right)}{\pi\Delta f\left(\bar{m}\left(T_{lx}-\frac{du_x}{c}\right)+\bar{n}\left(T_{lz}-\frac{su_z}{c}\right)\right)}\right) \tag{5.38}$$

$$P_{avg}^{DC} = A^2|\sigma|A_{eff}\frac{2}{r_c^4}\sum_{\bar{m}=-(M-1)}^{M-1}\sum_{\bar{n}=-(N-1)}^{N-1}(M-|\bar{m}|)(N-|\bar{n}|)\left(\frac{\sin\left(\pi\Delta f\left(\bar{m}p\pi+\bar{n}q\pi\right)\right)}{\pi\Delta f(\bar{m}p\pi+\bar{n}q\pi)}\right) \tag{5.39}$$

Prerequisite of that the beam is directed to the center of the point scatterers is having $w_i\left(T_{lx}-\frac{du_x}{c}\right) = p\pi$ and $w_i\left(T_{lz}-\frac{su_z}{c}\right) = q\pi$ where $p, q \in \mathbb{Z}$, and w_i is instantaneous center frequency. By substituting this into the Eq-5.38, one can obtain simpler form of the DC part of the average received power as in the Eq-5.39. As it can be interpreted from the formula, DC part is getting lower when the occupied frequency bandwidth is increased. That

is the effect of the larger scanned space, which is explained above. On the other hand, this value is constant and given in the Eq-5.40 for the equivalent PA, because of the fixed maximum radiation direction.

$$P_{avg}^{DC} = A^2|\sigma|A_{eff}M^2N^2\frac{2}{r_c^4} \tag{5.40}$$

Table 5.1 Array Parameters of an Example Planar Radar for RCS characterization

Parameter	*Value*	Parameters	*Value*
M	8	Δf	0%, 0.25%, 0.5%, 1%
N	5	l_s	1.4 m
f_c	16.65GHz	d	$\frac{\lambda_c}{2}$
τ	1ms	s	$\frac{\lambda_c}{2}$
T_{lx}	0.243 nsec	T_{lz}	2.04 nsec
θ	93.9^o	ϕ	83.57^o
θ_s	90^o	ϕ_s	$\epsilon\ [0^0, 180^0]$

5.4.4 Simulation and Results with the Dumbbell Target

Average power received in the presence of the planar LFMCW-FDA and PA transmitters have been calculated and compared. However, simulations in MATLAB would make deeper investigation possible. Also it makes easier to compare the results with plots of the average power fluctuations with respect to incidence angle with different bandwidths of the chirp. For the sake of the full coverage of the all aspects in the proposed planar LFMCW-FDA, same structure given in the previous section will be considered in the simulations, whose parameters are given on the

Table 5.1. For this transmitter, four different bandwidths values will be considered. As the zero bandwidth among the simulation scenarios, and that means beam is directed to the corresponding angle, a meaningful location for the center of the Dumbbell target would be determined by null bandwidth case. This angle is found as $\theta = 93.9^o$ and $\phi = 83.57^o$. This example can be applied any point enclosed by the scan of the transmitter, but for the sake of continuum, the center frequency is assumed to be constant for each scenario as it is in the previous sections.

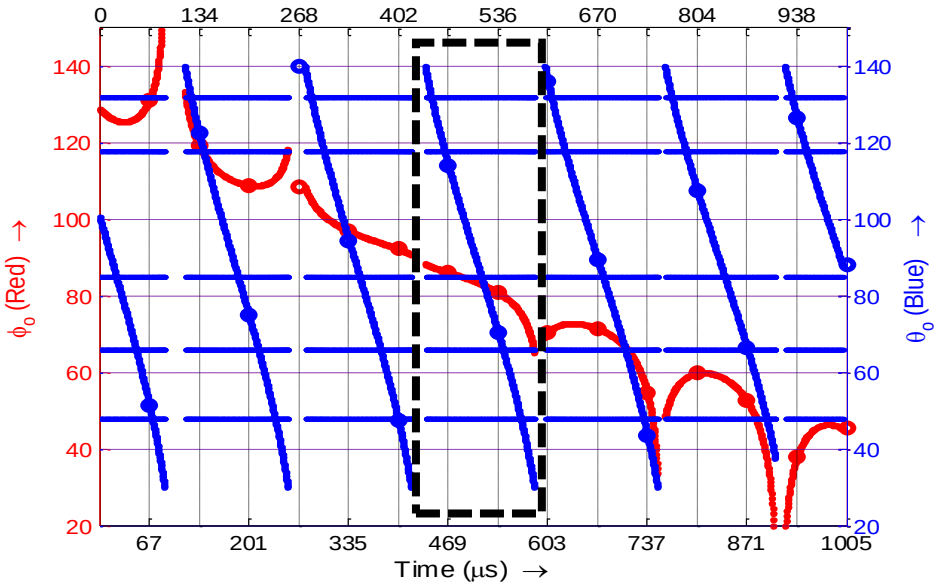

Figure 5.4. The general coverage diagram of the transmitter of the planar radar example corresponding piecewise frame of LFM signal

Because all space is covered by this transmitter, during the most of the pulse duration, the maximum radiation is not directed to angle of the aforementioned target location. For RSC investigations, it is more adequate to investigate effect of the bandwidth by considering the fact that dwell time is limited by bandwidth of the chirp. On the Figure 5.4, the main beam radiation direction with respect to time is given. There is only one far field point, which is considered to be the target location.

This point belongs to the small portion of the scan as illustrated on the figure. Corresponding bandwidth is only about 16% of the total bandwidth of the chirp. Therefore, there is no impact of the chirp bandwidth on the received average power graph anymore, when the chirp bandwidth exceeds this value. This affect is investigated by using the chirp with different bandwidths in this section. Different fractional bandwidths, such as 0%, 0.25%, 0.5%, and 1%, are considered for the given radar example. For the center frequency, $f_c = 16.65GHz$, the fractional bandwidths coincide with $0\,Hz$, $41.625MHz$, $83.25MHz$, and $166.5MHz$ respectively. Corresponding angular section that is steered and scanned by the maximum radiation direction changes as well as the average received power. These angular sections, that the radar visit, are defined as $(\theta_o, \phi_o) \in ([114^o, 74.38^o], [85.48^o, 80.95^o])$ for 1% fractional bandwidth. These values have been chosen particularly on account of the fact that the group of point scatterers located at the point, $(\theta, \phi) = (93.9^o, 83.57^o)$, is within scanned region. Indeed, it is on the middle of the scanned region, as the center frequency is selected on purpose. Received power fluctuation is given in the Figure 5.5 with different bandwidth deployments. It can be seen on the Figure 5.5-a, the power fluctuation is nothing but we have with PA example, when the bandwidth is zero. As the bandwidth is increased, radar starts to scan around the target. That property is illustrated as a remarkable feature of the LFMCW in previous section that contains the evaluation of radar scan like the *fixational eye movement* and this characteristic has been shown as an advantage to target detection. The increasing bandwidth ends up with significantly less fluctuation, especially higher values of ϕ_s than 30^o. This may be an outstanding advantage of the proposed radar in terms of the target RCS characteristic. This substantiates the previous findings for linear LFMCW-FDA radar study in [3] and [1]. As might have been expected, the simulation results show that mean value of the average received power vs the incidence angle graph is getting lower. That might be claimed as a drawback. However, the radar scans all region of interest within only one pulse duration. The degradation in SNR value can be

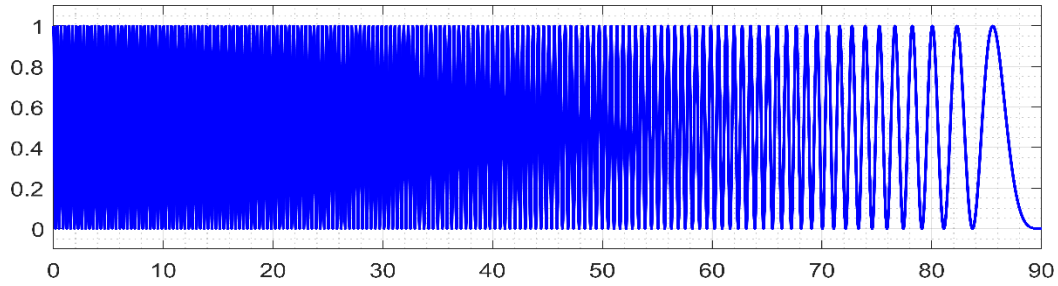

(a) Bandwidth 0% and PA

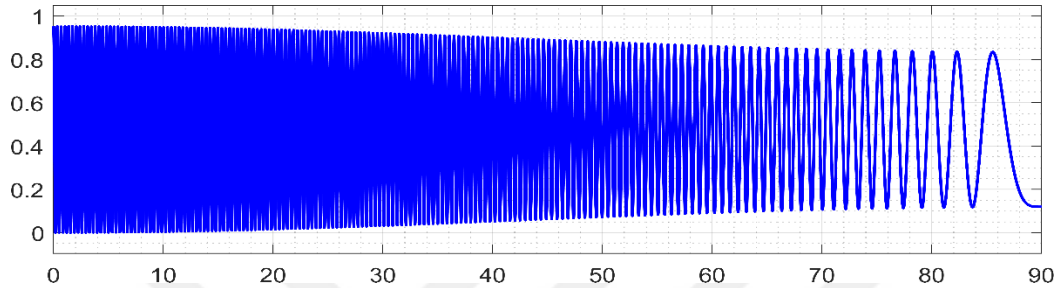

(b) Bandwidth 0.25%

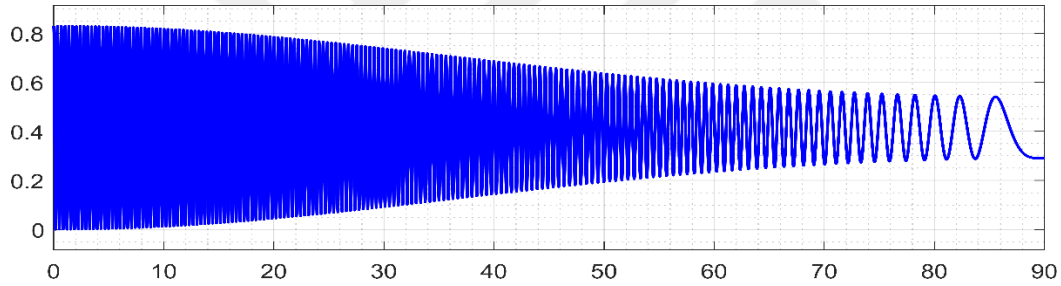

(c) Bandwidth 0.5%

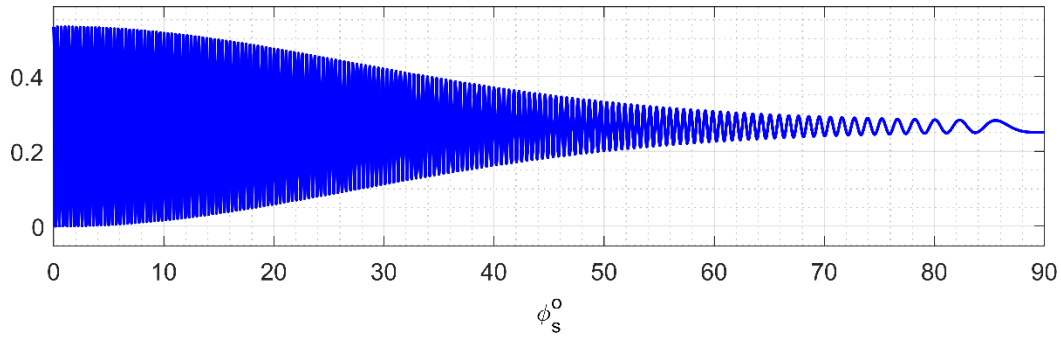

(d) Bandwidth 1.0%

Figure 5.5. Average Received Power reflected from Dumbbell targets w.r.t the incidence angle

compensated by applying procedure described as in the previous section with a realistic radar example. By applying multiple coherent positive and negative pulse

pairs which form non-coherent bursts, the probability of detection can be increased while probability of the false alarm still low.

5.5 Canonical Example with the 4 and 6 Targets on a rod

As the target's shape gets more complex, overall reflected power would be expected to fluctuate more. Therefore, same investigation as with the Dumbbell target is repeated with higher number of scatterers that are located on the rod that is illustrated on the Figure 5.6. The calculation steps are not different than the ones for the Dumbbell Target example. Therefore, the same procedure can be applied to find the average received power reflected from a group of 4 scatterers placed along a rod. Displacement between consecutive point scatterers is assumed to be constant and equal to l, so that $|\delta r_0| = 3|\delta r_1| = 3|\delta r_2| = |\delta r_3| = 3l/2$. Then, "â$_{\boldsymbol{rc}} \cdot \boldsymbol{\delta r_i}$" values can be found as in the Eq-5.41, that are in terms of the aspect angles, (θ_s, ϕ_s) and l.

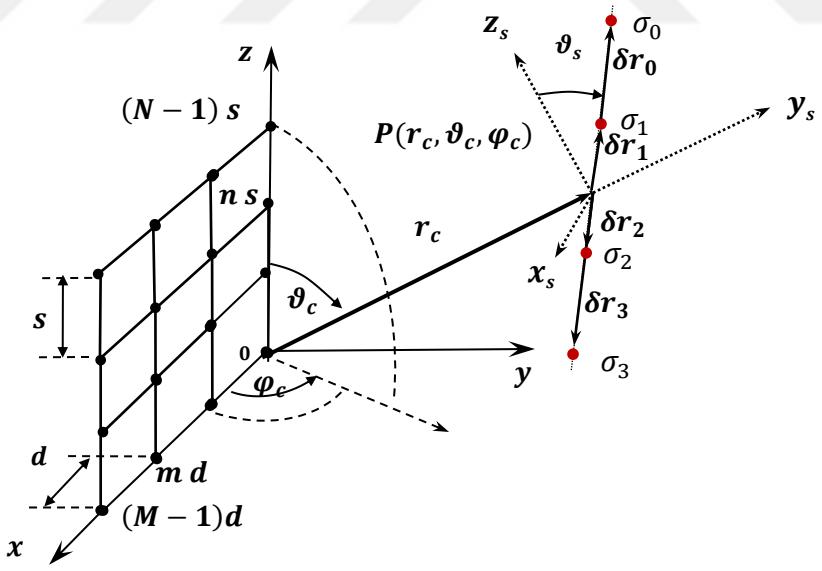

Figure 5.6. Planar LFMCW FDA transmitter with a group of 4 point scatterers on a rod around the far-field point, $\boldsymbol{P(r_c, \vartheta_c, \varphi_c)}$

$$\frac{\hat{a}_{\boldsymbol{rc}} \cdot \boldsymbol{\delta r_0}}{\mathbf{3}} = \hat{a}_{\boldsymbol{rc}} \cdot \boldsymbol{\delta r_1} = -\hat{a}_{\boldsymbol{rc}} \cdot \boldsymbol{\delta r_2} = -\frac{\hat{a}_{\boldsymbol{rc}} \cdot \boldsymbol{\delta r_3}}{\mathbf{3}} = \frac{l}{2}\sin\theta_s \sin\phi_s \qquad 5.41$$

$$P_{avg} = \frac{1}{\tau}A^2|\sigma|A_{eff}\frac{1}{r_c^4}\int_{\tau} P(t')\sum_{m=0}^{M-1}\sum_{m'=0}^{M-1}\sum_{n=0}^{N-1}\sum_{n'=0}^{N-1} \left(4e^{j\nu_0} + 3e^{j\nu_1} + 3e^{-j\nu_1} + 2e^{j\nu_2} + 2e^{-j\nu_2} + e^{j\nu_3} + e^{-j\nu_3}\right)dt' \qquad 5.42$$

$$\begin{aligned}
\nu_0 &= (m-m')\left(T_{lx} - \frac{du_x}{c}\right) + (n-n')\left(T_{lz} - \frac{su_z}{c}\right) \\
\nu_1 &= (m-m')\left(T_{lx} - \frac{du_x}{c}\right) + (n-n')\left(T_{lz} - \frac{su_z}{c}\right) + \frac{2l\sin\theta_s\sin\phi_s}{c} \\
\nu_2 &= (m-m')\left(T_{lx} - \frac{du_x}{c}\right) + (n-n')\left(T_{lz} - \frac{su_z}{c}\right) + \frac{4l\sin\theta_s\sin\phi_s}{c} \\
\nu_3 &= (m-m')\left(T_{lx} - \frac{du_x}{c}\right) + (n-n')\left(T_{lz} - \frac{su_z}{c}\right) + \frac{6l\sin\theta_s\sin\phi_s}{c}
\end{aligned} \qquad 5.43$$

Then, one can define following variables ν_0, $\nu_1, \nu_2, and\ \nu_3$ as in the Eq-5.43, in order to ease the representation. Also, interchanging the orders of time integral and summations would make easier to handle the equation. Applying same steps and substituting those variables into the Eq-5.42, the P_{avg} can be written as in the following form as in the Eq-5.44. The resulting average received power reflected from a rod like scatterer group can be seen on the Figure 5.7 with respect to the incidence angle ϕ_s. Because, one could observe the maximum fluctuation by rotating this angle while $\theta_s = 90^o$, or vice-versa. The Figure 5.7-(a) shows the RCS fluctuation with respect to aspect angle of the PA competitor which is equivalent to the LFMCW-FDA with zero bandwidth. As it is in the previous example, there are many nulls in the RCS plot that causes miss of the target for the corresponding aspect

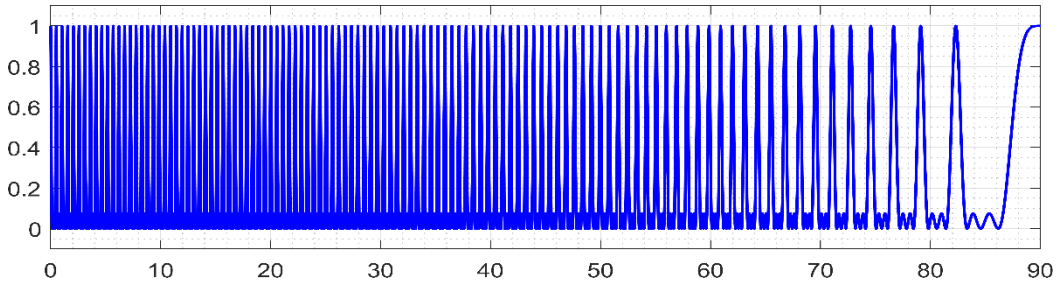

(a) Bandwidth 0% and PA

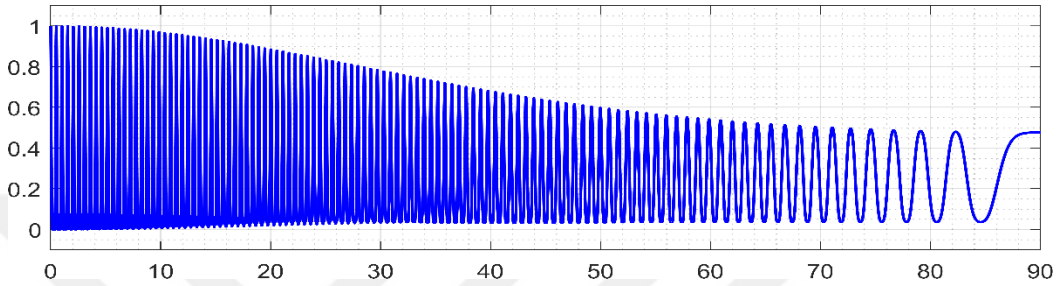

(b) Bandwidth 0.25%

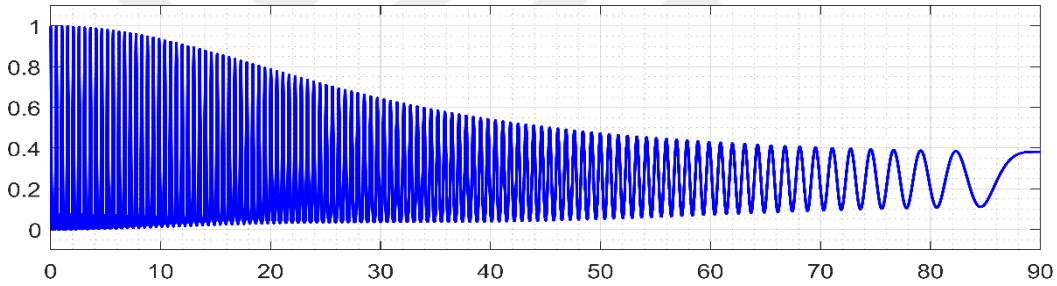

(c) Bandwidth 0.50%

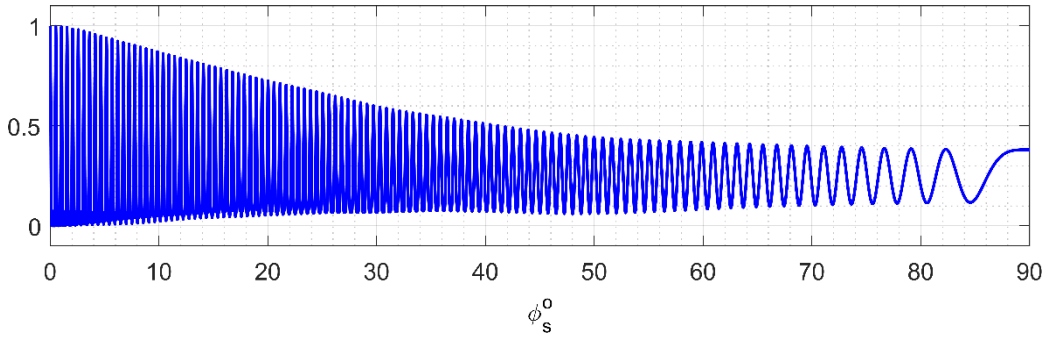

(d) Bandwidth 1.00%

Figure 5.7. Average Received Power reflected from a group of 4 point scatterers w.r.t the incidence angle

angles. As the fractional bandwidth is increased to 0.25%, 0.50%, and 1.00%, simulation results can be seen on the Figure 5.7 (b), (c), and (d) respectively. Similar effects are also observable in this example too. With the increased bandwidths, not only less nulls but also smoother fluctuation characteristics are obtained. Because of the increased the field-of-view by the wider bandwidth usage, aspect angle-averaged received power is decreasing in this canonical example as well.

$$P_{avg} = A^2|\sigma|A_{eff}\frac{1}{r_c^4}\sum_{m=0}^{M-1}\sum_{m'=0}^{M-1}\sum_{n=0}^{N-1}\sum_{n'=0}^{N-1}\left(e^{-jw_c\nu_0}\left(4\frac{\sin(\pi\Delta f\nu_0)}{\pi\Delta f\nu_0}\right)\right.$$
$$+6\cos(w_c\nu_1)\left(\frac{\sin(\pi\Delta f\nu_1)}{\pi\Delta f\nu_1}\right)+4\cos(w_c\nu_2)\left(\frac{\sin(\pi\Delta f\nu_2)}{\pi\Delta f\nu_2}\right) \quad 5.44$$
$$\left.+2\cos(w_c\nu_3)\left(\frac{\sin(\pi\Delta f\nu_3)}{\pi\Delta f\nu_3}\right)\right)$$

5.6 Conclusion and Discussion

In this chapter, advantage of using the LFMCW based planar FDA in terms of target RCS characteristics was revealed and discussed. The path has been taken as follows. Firstly, the proposed array was considered as transmitter. After finding transmitted field representation, the back scattered power was calculated with $\frac{\sigma}{4\pi R^2}$. Received voltage expression was found by assuming the single omnidirectional antenna whose effective aperture, A_{eff}, is assumed to be constant within the chirp's frequency band. This voltage expression is used for finding average power. These steps were repeated in case of presence of the multiple scatterers around a far field point. This generalized average power expression was used for determining the average power reflected from different target combinations. In order to show the target RCS characteristic, two point scatterers which are separated by the distance l were considered instead of single point scatterer. According to simulation results, average received power is fluctuating with the term $1+\cos\left(4\pi\frac{l\sin(\theta_s)\sin(\phi_s)}{\lambda_c}\right)$ that is equal

to zero many times as the incidence angle changes. Having zero average power for certain incidence angles is unwanted behavior of any radar. That may cause undetectable threading target in air surveillance applications. On the other hand, less nulls are observed on simulations obtained with the LFMCW based planar array. Furthermore, the wider frequency bandwidth utilized, the less fluctuations takes place in the average received power vs incidence angle plots. One can consider that the incidence angle is stochastic. Therefore, the probability of having null on the receiver antenna terminal would be much less, when the LFMCW-FDA is utilized. This Dumbbell type target assumption is extended to the group of four scatterers placed along an imaginary rod. Inter-element displacement of the four scatterers is assumed to be l and uniform for this example. The target RCS characteristic of the LFMCW-FDA is better that the PA equivalent like the previous target combination. Albeit, the average received power drops to zero with the FDA radar, there are much less visit to zero in the resultant power vs incidence angle graphs than the case with the PA radar. However, the DC part of the average received power is less in the FDA. It is because of the scanned sector is increasing with the increasing bandwidth of the LFM chirp. On the other hand, only constant region defined by the main beam is scanned during one pulse duration. The decrease in the received energy is because of the larger scanned space and distributed energy towards those directions. That is nothing but a trade-off. It has been also shown by [40], [41] that there is an advantage to have spatial modulation within a single pulse duration for resolving multiple targets with the MIMO radar utilizing LFM pulse. Our findings in the target RCS characteristics with naturally spatial modulated LFMCW-FDA are consistent with the previous researches also.

5.6.1 Future Work

Including also multiple reflection paths between the point scatterers could be a good study object that makes the simulation condition closer to real life situation. Building the setup and validating the concept by taking measurements are always considered

as milestone in the literature. Also, this investigation could be enlarged to the classical planar FDA that proposed by [34], [37]. Although example with group of multiple scatterers is adequate start point for the RCS characteristic comparison, that could be extended to a realistic target model.

CHAPTER 6

CONCLUSION

The concept of FDA has been investigated by many researchers for the last two decades. In this study, a relatively novel LFMCW based FDA concept is investigated in order to discover its benefits more. Reliability of this concept has been proved by the previous studies with both analytical and experimental findings. This study tries to fill the different gaps in the LFMCW based FDA literature, and accomplishes to show them with simulation.

In the Chapter 2, an LFMCW based linear FDA is deployed to form a radar with an omnidirectional receiver antenna. Main motivation of this chapter is to define realistic direction finding (DF) method by using the aforementioned radar setup. Therefore, it is possible to evaluate its the range resolution and the angle resolution. Derivation of the transmitted field is given here as a background for next steps. Properties of the transmitted field are illustrated, which is vital for defining the DF procedure. Resulting transmitted field has an envelope like sinc function whose null-to-null time duration can be considered as dwell time for the radar. In order to resolve two target that lie along same angle, one could not use time domain signal. Because, the range resolution could be in the range of kilometers for time domain detection. Therefore, frequency domain processing is essential for this radar, that shows outstanding performance. However, time domain processing is useful for angle resolution. In this study, a sliding window frame of the time domain signal is taken as input for fast Fourier transform (FFT). Window width is equal to half of the sinc function's null-to-null time and sinc like envelope is considered as weighting coefficient for FFT process. Because of the need for the space time adaptive processing (STAP) in FDA applications, one further processing to recover the location of the target is applied. Simulation results, which are in line with the expectations in DF application, are obtained wıth 16 element linear array.

An impressive state of art MIMO example is chosen for comparison. That study claimed and showed with simulations that there is an advantage to use spatially modulation to improve both range and angle resolution, [41]. The similarities between the LFMCW based FDA and the MIMO rival are illustrated. It is seen that the LFMCW based FDA has the feature of the spatial modulation due to its nature, that makes its angle and range resolutions better. Even though, there is more flexibility to choose type of spatial modulation with the MIMO radar, accomplishments in resolving targets are observed with the LFMCW based FDA.

Another novel development contributed by this study is building a planar array that exploits the advantages of the LFMCW-FDA concept. There are studies of LFMCW-FDA implementation with only linear arrays, that can accomplish 2D scanning. In this study, the planar FDA is proposed with design steps and essential steps. The transmitted field formulations are derived for the given array structure. Raster scan is possible by using much larger true time delay (TTD) along one axes of the array plane. Each parameter must be determined very carefully to obtain proper radiation pattern that scans the region of interest without revisiting any direction within single LFM pulse. Resulting radiation pattern is changing with respect to time, distance and angle, therefore, STAP is needed. The envelope of the transmitted field in time domain is multiplication of two sinc functions that can be arranged separately. With the fact that TTDs along one axis is much grated than the other, one of the sinc function's null-to-null time is much less than other one. Half of the smaller null-to-null time one can be considered as dwell time. The dwell time is also direction dependent because the velocity of the change of radiation direction is angle dependent as well. All details are presented in the Chapter 4 with the radiation pattern and the waveforms in time domain, that shows the coverage diagram of the proposed array. The given example covers $\theta \sim 38^o \rightarrow 143^o$ and $\phi \sim 30^o \rightarrow 134^o$ with 8×5 elements along x and z axis respectively. A radar is formed by using this transmitter with the PA receiver that makes angle of arrival estimation (AoA) possible. Because of the short dwell time, high receiver antenna gain is preferred. Also, in order to increase cumulative probability of detection and

decrease the cumulative probability of false alarm, 24 non-coherent bursts that are comprised of 8 coherent positive and negative slope pulse pairs are used. Furthermore, LFM pulse with positive and negative slope make possible to determine the velocity of the target. Reasonable performance of the radar is shown by analytical calculations. These results are compared with the equivalent PA competitor under certain circumstances. Less target displacement is observed during the detection made by the LFMCW based planar radar. That may be outstanding advantage for the air surveillance radars when targets with high RCS are expected. Although it can be generalized to all FDA/PA comparisons, it is observed that the LFMCW-FDA needs less energy to accomplish same duty as the PA radar.

In the Chapter 5, the RCS characteristic of the novel planar array is investigated. Starting from the transmitted field, scattered fields are calculated. The omnidirectional receiver antenna captures the reflected fields by the single far field point scatterer. To reveal the RCS characteristic, a bit more complex target shape is constructed. A group of scatterers on a surface of an imaginary sphere comprises the target for the generalized formulations. It is shown that LFMCW-FDA using single tone signal is equivalent to the PA concept particularly for the target RCS characteristic. A dumbbell target is assumed for the further analysis, that are separated by 1.4 m. Change in the average received power with respect to incidence angle is illustrated with different fractional bandwidths which are 0%, 0.25%, 0.5%, and 1%. These bandwidths are selected to visit only around the target not the whole region defined in the previous chapter. Therefore, main beam scans only small portion like the spatial modulation desired with MIMO array in Chapter 2. Received average power changes with respect to incidence angle plots show the decreasing number of nulls as the LFMCW FDA utilizes wider bandwidth. That is an advantage, which may significantly decrease the probability of miss of target for certain angles. Moreover, smoother RCS fluctuation is desired for the radar applications, that is also observed with the proposed radar. Then, four identical point scatterers placed along an imaginary rod is considered in order to bring more complexity to target. Similar superiorities are observed for this canonical example as well.

The LFMCW based FDA concept has already been shown as reliable and low-cost approach with comparable performance as the conventional radars. This study focuses on its different aspects to claim and prove that it benefits in DF and 2D angular scanning applications with smoother RCS fluctuation. This relatively novel concept can be investigated more to be among the state of art concepts. Firstly, implementation of DF application would present more solid findings for the literature. A receiver design for planar FDA array is another open point. A linear PA receiver, which finds one AoA by digital beamforming techniques, could be deployed with the DF algorithms explained in Chapter 2 that can estimate the other AoA. Therefore, burden of receiver planar PA would decrease. Primary reflections form point targets are taken into account in the RCS derivations. Although that is adequate for comparison, more realistic target shapes that include secondary reflections as well would be another future work object. Also, this investigation could be enlarged to the classical planar FDA that proposed by [34], [37].

REFERENCES

[1] C. Cetintepe and S. Demir, "Examination of target RCS characteristics in FDA radars," *IEEE Antennas Propag. Soc. AP-S Int. Symp.*, pp. 1754–1755, 2014, doi: 10.1109/APS.2014.6905203.

[2] C. Cetintepe and S. Demir, "Multipath characteristics of frequency diverse arrays over a ground plane," *IEEE Trans. Antennas Propag.*, vol. 62, no. 7, pp. 3567–3574, 2014, doi: 10.1109/TAP.2014.2316292.

[3] Ç. Çetintepe, "Analysis of Frequency Diverse Arrays for Radar and Communication Applications," Ph.D. Dissertation, Dept. of Electrical and Electronics Eng., Middle East Technical University, Ankara, November, 2015.

[4] T. Eker, S. Demir, and A. Hizal, "Exploitation of linear frequency modulated continuous waveform (LFMCW) for frequency diverse arrays," *IEEE Trans. Antennas Propag.*, vol. 61, no. 7, pp. 3546–3553, 2013, doi: 10.1109/TAP.2013.2258393.

[5] T. Eker, "A conceptual evaluation of frequency diverse arrays and novel utilization of LFMCW," Ph.D. Dissertation, Dept. of Electrical and Electronics Eng., Middle East Technical University, September, 2011.

[6] M. C. Wicks, "A brief history of waveform diversity," *IEEE Natl. Radar Conf. - Proc.*, no. 1, 2009, doi: 10.1109/RADAR.2009.4977142.

[7] J. W. Garnham and J. R. Roman, "Why and what is waveform diversity, and how does it affect electromagnetics?," *IEEE Int. Symp. Electromagn. Compat.*, pp. 0–3, 2007, doi: 10.1109/ISEMC.2007.41.

[8] A. M. Yao, N. Anselmi, and P. Rocca, "A novel planar frequency diverse

array design approach for far-field wireless power transmission," *2017 IEEE Antennas Propag. Soc. Int. Symp. Proc.*, vol. 2017-Janua, no. 3, pp. 1807–1808, 2017, doi: 10.1109/APUSNCURSINRSM.2017.8072946.

[9] E. Fazzini, M. Shanawani, A. Costanzo, and D. Masotti, "Focusing RF-on demand by logarithmic frequency-diverse arrays," *2020 IEEE Wirel. Power Transf. Conf. WPTC 2020*, pp. 76–79, 2020, doi: 10.1109/WPTC48563.2020.9295603.

[10] J. Xiong and W.-Q. Wang, "Sparse reconstruction-based beampattern synthesis for multi-carrier frequency diverse array antenna," in *2017 IEEE International Conference on Acoustics, Speech and Signal Processing (ICASSP)*, Mar. 2017, vol. 57, no. 2, pp. 3395–3398, doi: 10.1109/ICASSP.2017.7952786.

[11] M. Secmen, S. Demir, A. Hizal, and T. Eker, "Frequency Diverse Array Antenna with Periodic Time Modulated Pattern in Range and Angle," in *2007 IEEE Radar Conference*, 2007, pp. 427–430.

[12] S. Karadağ, Ş. Demir, and A. Hızal, "Space scanning FMCW-based two-dimensional frequency diverse array radar," *J. Eng.*, vol. 2019, no. 20, pp. 6452–6456, Oct. 2019, doi: 10.1049/joe.2019.0388.

[13] P. Antonik, M. C. Wicks, H. D. Griffiths, and C. J. Baker, "Multi-mission multi-mode waveform diversity," *IEEE Natl. Radar Conf. - Proc.*, pp. 580–582, 2006, doi: 10.1109/RADAR.2006.1631858.

[14] P. Antonik, M. C. Wicks, H. D. Griffiths, and C. J. Baker, "Frequency diverse array radars," *IEEE Natl. Radar Conf. - Proc.*, pp. 215–217, 2006, doi: 10.1109/RADAR.2006.1631800.

[15] M. C. Wicks and P. Antonik, "Method And Apparatus For A Frequency Diverse Array," *U.S. Pat. 2006/0 252 377 A1*, 2006.

[16] M. C. Wicks and P. Antonik, "Frequency Diverse Array With Independent

Modulation Of Frequency, Amplitude, And Phase," *US 7319427 B2*, 2008.

[17] P. Antonik, "An Investigation of a Frequency Diverse Array," Ph.D. dissertation, Dept. of Electronic and Electrical Eng., University College London, April, 2009.

[18] J. Farooq, M. A. Temple, and M. A. Saville, "Application of frequency diverse arrays to synthetic aperture radar imaging," *2007 Int. Conf. Electromagn. Adv. Appl. ICEAA'07*, pp. 447–449, 2007, doi: 10.1109/ICEAA.2007.4387334.

[19] J. Farooq, M. A. Temple, and M. A. Saville, "Exploiting frequency diverse array processing to improve SAR image resolution," *2008 IEEE Radar Conf. RADAR 2008*, pp. 8–12, 2008, doi: 10.1109/RADAR.2008.4721083.

[20] J. Farooq, "Frequency diversity for improving synthetic aperture radar imaging," Ph.D. dissertation, Air University, Air Education and Training Command, Air Force Institute of Technology, March, 2009.

[21] Jingjing Huang, Kin-Fai Tong, and C. J. Baker, "Frequency diverse array with beam scanning feature," in *2008 IEEE Antennas and Propagation Society International Symposium*, Jul. 2008, pp. 1–4, doi: 10.1109/APS.2008.4619415.

[22] J. Huang, C. Baker, and K. F. Tong, "Frequency diverse array: Simulation and design," *Loughbrgh. Antennas Propag. Conf. LAPC 2009 - Conf. Proc.*, no. November, pp. 253–256, 2009, doi: 10.1109/LAPC.2009.5352422.

[23] J. Huang, "Frequency Diversity Array : Theory and Design," Ph.D. dissertation, Dept. of Electronic and Electrical Eng., University College London, September, 2010.

[24] T. Higgins and S. D. Blunt, "Analysis of range-angle coupled beamforming with frequency-diverse chirps," in *2009 International Waveform Diversity and Design Conference*, Feb. 2009, no. Onr 31, pp. 140–144, doi: 10.1109/WDDC.2009.4800333.

[25] P. F. Sammartino and C. J. Baker, “The Frequency Diverse Bistatic System,” *2009 Int. Waveform Divers. Des. Conf. Proceedings, WDD 2009*, no. 2, pp. 155–159, 2009, doi: 10.1109/WDDC.2009.4800336.

[26] P. F. Sammartino and C. J. Baker, “Developments in the frequency diverse bistatic system,” *IEEE Natl. Radar Conf. - Proc.*, no. 4, pp. 9–13, 2009, doi: 10.1109/RADAR.2009.4976937.

[27] P. F. Sammartino, C. J. Baker, and H. D. Griffiths, “Frequency diverse MIMO techniques for radar,” *IEEE Trans. Aerosp. Electron. Syst.*, vol. 49, no. 1, pp. 201–222, 2013, doi: 10.1109/TAES.2013.6404099.

[28] P. F. Sammartino, C. J. Baker, and H. D. Griffiths, “Range-angle dependent waveform,” *2009 Int. Waveform Divers. Des. Conf. Proceedings, WDD 2009*, vol. 49, no. 2, pp. 155–159, 2013, doi: 10.1109/RADAR.2010.5494568.

[29] A. M. Jones and B. D. Rigling, “Frequency diverse array radar receiver architectures,” in *2012 International Waveform Diversity & Design Conference (WDD)*, Jan. 2012, pp. 211–217, doi: 10.1109/WDD.2012.7311296.

[30] A. M. Jones, “Frequency Diverse Array Receiver Architectures,” M. Sc. Thesis, Dept. of Electrical Eng. and Computer Science, Wright State University, November, 2011.

[31] A. M. Jones and B. D. Rigling, “Planar frequency diverse array receiver architecture,” in *2012 IEEE Radar Conference*, May 2012, pp. 0145–0150, doi: 10.1109/RADAR.2012.6212127.

[32] A. Turhaner, “Implementation of direction finding with frequency diverse array,” M.Sc. Thesis, Dept. of Electrical and Electronics Eng.,Middle East Technical University, July, 2017.

[33] A. Turhaner, S. Demir, and A. Hizal, “Monopulse direction finding for linear frequency modulation based frequency diverse array,” in *2017 IEEE Radar*

Conference (RadarConf), May 2017, pp. 0089–0094, doi: 10.1109/RADAR.2017.7944177.

[34] R. Cetiner, A. Hizal, and R. F. Tigrek, "Narrow band wide angle scanning circular frequency diverse array radar," in *2017 European Radar Conference (EURAD)*, Oct. 2017, vol. 2017, no. CP728, pp. 231–234, doi: 10.23919/EURAD.2017.8249189.

[35] A. Akkoc, E. Afacan, and E. Yazgan, "Investigation of Planar Frequency Diverse Array Antenna in Concentric Circular Geometry," in *2019 11th International Conference on Electrical and Electronics Engineering (ELECO)*, Nov. 2019, pp. 651–654, doi: 10.23919/ELECO47770.2019.8990521.

[36] R. Cetiner, S. Demir, and A. Hizal, "Range and angle measurement in a linear pulsed Frequency Diverse Array radar," in *2017 IEEE Radar Conference (RadarConf)*, May 2017, no. 8, pp. 0064–0067, doi: 10.1109/RADAR.2017.7944172.

[37] R. Çetiner and A. Hizal, "Narrow band space scanning two-dimensional linear frequency diverse array radar," *J. Eng.*, vol. 2019, no. 21, pp. 8146–8150, 2019, doi: 10.1049/joe.2019.0695.

[38] Y. Zhou, W. Wang, Z. Chen, Q. Zhao, Y. Deng, and R. Wang, "A novel high-resolution and wide-swath SAR imaging mode using frequency diverse planar array," *Proc. Eur. Conf. Synth. Aperture Radar, EUSAR*, vol. 2021-March, pp. 1052–1056, 2021.

[39] S. Saeed, I. M. Qureshi, W. Khan, S. Saleem, and A. Salman, "Frequency Offset Selection based adaptive 3D Beamforming in Planar Frequency Diverse Array.," *RAEE 2019 - Int. Symp. Recent Adv. Electr. Eng.*, pp. 0–5, 2019, doi: 10.1109/RAEE.2019.8887034.

[40] S. D. Blunt, P. McCormick, T. Higgins, and M. Rangaswamy, "Spatially-modulated radar waveforms inspired by fixational eye movement," in *2014*

IEEE Radar Conference, May 2014, pp. 0900–0905, doi: 10.1109/RADAR.2014.6875719.

[41] P. Mccormick, M. Rangaswamy, S. D. Blunt, and T. Higgins, "Physical emission of spatially-modulated radar," *IET Radar, Sonar Navig.*, vol. 8, no. 9, pp. 1234–1246, Dec. 2014, doi: 10.1049/iet-rsn.2014.0057.

[42] M. I. Skolnik, *Introduction to Radar Systems*, 3rd ed. New York: McGraw Hill Education, 2001.

[43] D. O. North, "An Analysis of the Factors which Determine Signal/Noise Discrimination in Pulsed-Carrier Systems," *Proc. IEEE*, vol. 51, no. 7, pp. 1016–1027, 1963, doi: 10.1109/PROC.1963.2383.

[44] H. A. Said, A. E. El-Henawey, and A. A. El-Kouny, "Design and realization of an efficient VLIC architecture for a linear frequency modulation (LFM) pulse compression in pulsed radars using FPGA," in *2013 Africon*, Sep. 2013, no. Icaicte, pp. 1–7, doi: https://doi.org/10.1109/IEEESTD.2020.9310748.

[45] E. Ahissar and A. Arieli, "Seeing via Miniature Eye Movements: A Dynamic Hypothesis for Vision," *Front. Comput. Neurosci.*, vol. 6, no. OCTOBER 2012, pp. 1–27, 2012, doi: 10.3389/fncom.2012.00089.

[46] M. Rolfs, "Microsaccades: Small steps on a long way," *Vision Res.*, vol. 49, no. 20, pp. 2415–2441, Oct. 2009, doi: 10.1016/j.visres.2009.08.010.

[47] J. Cui, M. Wilke, N. K. Logothetis, D. A. Leopold, and H. Liang, "Visibility states modulate microsaccade rate and direction," *Vision Res.*, vol. 49, no. 2, pp. 228–236, Jan. 2009, doi: 10.1016/j.visres.2008.10.015.

[48] S. Blunt, M. Cook, J. Jakabosky, J. De Graaf, and E. Perrins, "Polyphase-coded FM (PCFM) radar waveforms, part I: implementation," *IEEE Trans. Aerosp. Electron. Syst.*, vol. 50, no. 3, pp. 2218–2229, Jul. 2014, doi: 10.1109/TAES.2014.130361.

[49] S. Blunt, J. Jakabosky, M. Cook, J. Stiles, S. Seguin, and E. Mokole,

"Polyphase-coded FM (PCFM) radar waveforms, part II: optimization," *IEEE Trans. Aerosp. Electron. Syst.*, vol. 50, no. 3, pp. 2230–2241, Jul. 2014, doi: 10.1109/TAES.2014.130362.

[50] B. Lewis and F. Kretschmer, "Linear Frequency Modulation Derived Polyphase Pulse Compression Codes," *IEEE Trans. Aerosp. Electron. Syst.*, vol. AES-18, no. 5, pp. 637–641, Sep. 1982, doi: 10.1109/TAES.1982.309276.

[51] G. Turin, "An introduction to matched filters," *IEEE Trans. Inf. Theory*, vol. 6, no. 3, pp. 311–329, Jun. 1960, doi: 10.1109/TIT.1960.1057571.

[52] H. Rohling and C. Möller, "Radar waveform for automotive radar systems and applications," *2008 IEEE Radar Conf. RADAR 2008*, no. 1, pp. 13–16, 2008, doi: 10.1109/RADAR.2008.4721121.

[53] Khan and Power, "Doppler processing for coherent 'chirp' radars," in *Proceedings of Canadian Conference on Electrical and Computer Engineering CCECE-94*, 1994, no. 3, pp. 767–770 vol.2, doi: 10.1109/CCECE.1994.405864.

[54] T. S. Edrington, "The Amplitude Statistics of Aircraft Radar Echoes," *IEEE Trans. Mil. Electron.*, vol. 9, no. 1, pp. 10–16, Dec. 1965, doi: 10.1109/TME.1965.4323170.

[55] "IEEE Recommended Practice for Radar Cross-Section Test Procedures," Dec. 2020. doi: https://doi.org/10.1109/IEEESTD.2020.9310748.

[56] P. Blacksmith, R. E. Hiatt, and R. B. Mack, "Introduction to radar cross-section measurements," *Proc. IEEE*, vol. 53, no. 8, pp. 901–920, 1965, doi: 10.1109/PROC.1965.4069.